STARS

Electronic Theses and Dissertations, 2004-2019

2006

Additive Lithography Fabrication And Integration Of Micro Optics

Mahesh Pitchumani

University of Central Florida

Part of the Electromagnetics and Photonics Commons, and the Optics Commons

Find similar works at: https://stars.library.ucf.edu/etd

University of Central Florida Libraries http://library.ucf.edu

Showcase of Text, Archives, Research & Scholarship

ADDITIVE LITHOGRAPHY
FABRICATION AND INTEGRATION OF MICRO OPTICS

by

MAHESH PITCHUMANI
B.Sc.University of Mumbai 1994
M.Sc University of Mumbai 1997
M.Tech Devi Ahilya University 1999

A dissertation submitted in partial fulfillment of the requirements
for the degree of Doctor of Philosophy
in the College of Optics and Photonics
at the University of Central Florida
Orlando, Florida
U.S.A.

Spring Term
2006
Major Professor Eric G. Johnson

ABSTRACT

Optical elements are the fundamental components in photonic systems and are used to transform an input optical beam into a desired beam profile or to couple the input beam into waveguides, fibers, or other optical systems or devices. Macroscopic optical elements are easily fabricated using grinding and polishing techniques, but few methods exist for inexpensive fabrication of micro optical elements. In this work we present an innovative technique termed Additive Lithography that makes use of binary masks and controlled partial exposures to sculpt photoresist into the desired optical surface relief profile.

We explore various masking schemes for fabricating a variety of optical elements with unprecedented flexibility and precision. These masking schemes used in conjunction with the additive lithographic method allows us to carefully control the photoresist exposure and reflow processes for fabricating complex aspheric lens elements, including aspheric elements whose fabrication often proves highly problematic. It will be demonstrated that employing additive lithography for volume sculpting followed by controlled reflow can also allow us to fabricate refractive beam shaping elements. Finally we will discuss the dry etching techniques used to transfer these optical elements into the glass substrate. Thus the additive lithography technique will be demonstrated as an inexpensive, high throughput and efficient process in the fabrication of micro optical elements.

Dedicated
To my Parents

ACKNOWLEDGMENTS

I would like to thank my advisor Dr. Eric. G. Johnson for giving me the opportunity to work on this project and various other projects and for his support, trust and patience during the years of my PhD. His dedication and hard work in facilitating this research work and providing the necessary tools has made this work possible and pleasurable. I would also like to thank my committee members Dr. Jim Moharam, Dr. Aravinda Kar and Dr Louis Chow for serving on my committee.

I would like to thank my colleagues and friends from the Micro Photonics Lab both past and present especially Waleed Mohammed and Pradeep Srinivasan who have always found time to discuss various aspects of my research. I would like to thank my friends from CREOL Martina Atanassova, Supraja Murali, Alok Mehta, Chang Ching Tsai, Mohamed Salem and George Siganakis for always being there for me when I needed them and enriching my life during my stay here. I would like to thank Heidi Hockel for her help with proof reading my dissertation at such short notice.

Last but not the least I am eternally thankful to my parents and my brother without whose efforts, sacrifice, patience, and trust in me this endeavor would not have been possible.

TABLE OF CONTENTS

LIST OF FIGURES

LIST OF TABLES

LIST OF ACRONYMS/ABBREVIATIONS

CGH   Computer Generated Hologram

DOE   Diffractive Optical Element

DOF   Depth of Focus

ECR   Electron Cyclotron Resonance

GRIN   Graded Index

HEBS   High Energy Beam Sensitive

IC   Integrated Circuit

MOB   Micro Optical Bench

NA   Numerical Aperture

PAC   Photo Active Compound

PEB   Post Exposure Bake

RMS   Reticle Management System

RIE   Reactive Ion Etching

ICP   Inductively Coupled Plasma

RF   Radio Frequency

CHAPTER 1: INTRODUCTION

The development of the optical fiber gave birth to the era of optical communications. This led to subsequent development of semiconductor lasers and detectors fabricated using the preexisting and highly mature technology in the IC industry. The drive then was to reduce the losses in these systems so as to achieve cheaper long haul networks with fewer amplifiers. Optical fibers with losses as low as 0.2 dB Km-1 at the zero dispersion 1.55 μm wavelengths were reported. Light from a laser had to go through bulk beam coupling elements that helped launch it into a fiber. The initial devices that performed this function were Graded Index (GRIN) lenses. These devices were expensive to fabricate and package; and the insertion losses though low were still substantial. In 1979 Yariv and his coworkers demonstrated the integration of Lasers, Detectors and transistors on a single chip. Thus monolithic integration could be performed using well known IC technology, thus reducing the overall cost of these devices and "Integration" became a key concept driving the industry [1-8].

The size of the beam coming out of a laser diode is about the size of the stripe about 10-20 μm thus requiring optical devices in the far field that were a couple of hundred microns in diameter. The size being so small traditional fabrication methods could not be used for their fabrication. The essential nature of optical elements that perform beam shaping or coupling being analog, these had to be replaced by their multilevel diffractive counterparts so as to employ binary IC fabrication techniques. The initial optical devices were binary diffractive lenses with low efficiency. More efficient multilevel diffractive

elements were then demonstrated using the 2N fabrication technique involving multiple masking and etching steps [1, 2]. Use of IC fabrication techniques enabled the fabrication of hundreds of elements on a single wafer thus reducing the cost of the individual devices. They still needed to be packaged with the laser diode and fiber [3-5]. The price for increased efficiency was paid in complexity of fabrication using this process.

The need for these devices was not restricted to optical communications as a number of technologies for metrology, sensing, materials processing etc evolved, thus driving the market towards higher levels of integration and better techniques for fabrication. Gray Scale lithography and Half tone lithography evolved allowing for fabrication of truly analog optics in single exposure processes [1, 2]. The flip side of these techniques was the expensive fabrication process of the mask itself. Other techniques such as photoresist reflow were suggested for the fabrication of simple lens elements. Though it provided a cheaper alternative there was little control on the shape of the fabricated elements and was restricted to the fabrication of aspheric lenses. Other direct writing techniques such as E-beam writing, laser writing, ion beam milling have also been developed. These techniques are very flexible and allow for fabrication of very complex analog profiles on the photoresist but are usually very slow and are not suited for high throughput applications. A few of the above techniques will be discussed in more detail in the coming sections.

1.1 Amplitude masking technique
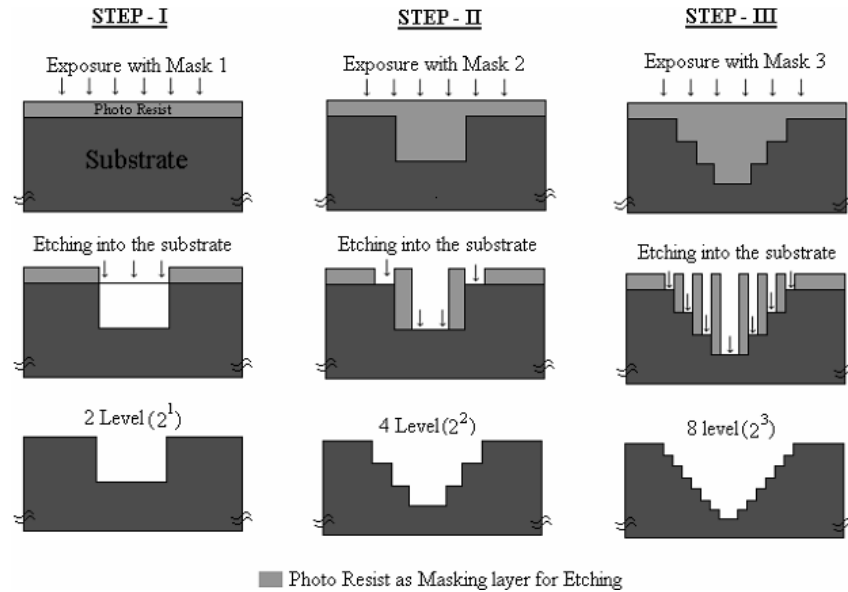
Figure 1-1 2N technique for micro optic fabrication using binary amplitude mask

Fabricating of multilevel diffractives using amplitude masks involves at least N masking patterns for creating 2N levels [8-12]. The wafer is coated with photoresist and then exposed with the 1st pattern leaving a binary pattern on the photoresist after developing. This is then etched into the substrate. The wafer is again coated with photoresist and the 2nd pattern is aligned to the 1st etched pattern on the photoresist and exposed, developed and the wafer etched. The process is repeated 3 times for an 8 level diffractive 4 times for a 16 level diffractive and so on, Figure 1-1. The major problem with this technique is pattern to pattern alignment required with each mask pattern, the accuracy of which is defined by the exposure tool used and the previous processing performed on the wafer. Another problem is that the technique is time consuming since a set of processes have to be repeated for each masking pattern.

1.2 Gray Scale and Half tone lithography

Gray scale masking and half toning involve modulating the intensity by controlling the local transmission of the mask [13-19]. A gray scale mask is fabricated by implementing a continuously varying optical density on HEBS glass using an electron beam patterning or high resolution printing methods, Figure 1-2-(a) [13-15]. The optical density has to be matched to the response of the specific photoresist to be used. This limits the flexibility of the fabricated mask. This technique can provide very smooth surface profiles but the masks are fairly expensive to fabricate and the micro optic fabrication is bounded by the design parameters of the mask.
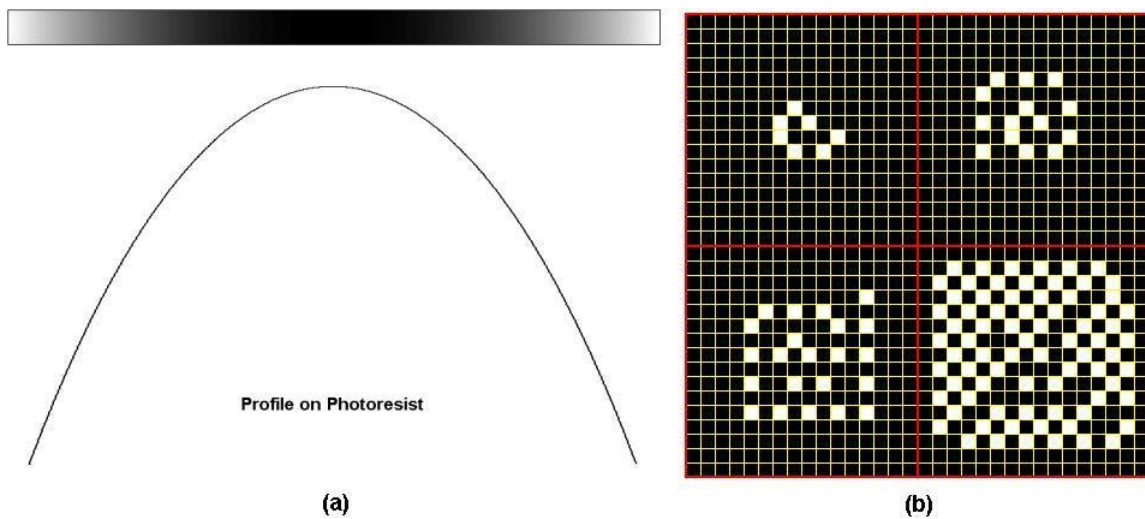
Figure 1-2 a. Gray scale mask and resulting profile on the photoresist. b. Half tone mask with pixels and sub pixel transmission control to create analog profiles.

In half tone lithography each pixel is further divided into multiple levels and the amplitude transmittance of these pixels is controlled by the sub levels in the pixel by creating required transparent sublevels, Figure 1-2-(b) [17, 18]. The mask is usually a

standard amplitude mask written with a very fine address unit. This increases the write time and the tolerance and hence the mask is again expensive to fabricate. It also has the drawback of edge scattering, which contributes to a noisy image on the wafer thus leading to roughness in the analog surface.

1.3   <u>Phase Masking technique</u>

The phase masking technique works mainly on a stepper. The principal again is to create the required analog intensity profile on the substrate but here the properties of the stepper are exploited to achieve this goal [20]. A stepper prints by imaging features on the mask onto a substrate. The mask spectrum gets filtered in the pupil plane and the surviving spatial frequencies interfere at the substrate to provide the image. If the object is smaller than the resolution limit of the stepper then the 0th order alone survives the pupil filtering leaving us with a dc intensity and no image. The phase mask delivers analog intensity on the wafer by locally modulating the 0th order intensity.

A 'π' phase mask with 50% duty cycle provides zero power in the 0th order. But if the duty cycle is varied the 0th order power will not be zero anymore. A phase mask uses a 1-D or 2-D phase grating with a period below the resolution of the stepper on the mask and the 0th order power is modulated by locally modulating the duty cycle of this grating. The mask fabrication is fairly inexpensive as compared to Gray Scale or Half tone lithography but still costlier than the amplitude masks used in the 2N technique. Though the need of a stepper may seem as a disadvantage the nature of the fabrication process is

such that very old steppers working at higher wavelengths are perfect for micro optic fabrication. Some of these steppers can be bought for almost the cost of new and specialized mask aligners while providing much more features than most aligners.

1.4 Direct writing

Direct electron beam or laser patterning of the photoresist has also been employed to fabricate smooth profiles on the photoresist which can subsequently be etched into the substrate [21, 23]. This is usually performed by using a photoresist like PMMA and writing a function pixel by pixel with very precise dose control and stage motion control. This technique can be used to fabricate nearly any optical function on the photoresist surface but at the disadvantage of large write times. Fabricating high aspect ratio structures using these techniques can be extremely time consuming and very difficult and thus they work much better for low aspect ratio structures.

1.5 Photoresist Reflow

In photoresist reflow thick pillars of photoresist are fabricated using standard lithography on an aligner or a stepper [24-29]. The wafer is then baked in a convective oven at a temperature above the glass transition temperature of the photoresist. The surface tension of the photoresist causes the surface to change shape so as to minimize the energy thus leading to aspheric surfaces. Though the fabricated surfaces are perfectly analog this method can be used only to fabricate aspheric lenses.

6

1.6   <u>Molding and Embossing</u>

Embossing and Molding techniques start with a master, which then can be replicated onto a soft polymer thus replacing either the lithography step or sometimes even the etching step. These technologies today can reproduce patterns as small as tens of nanometers but they still need the master which has to be fabricated using the techniques mentioned earlier. Some techniques of directly molding the glass at high temperatures with binary patterns as the master have also been demonstrated [30].

Other novel methods for fabrication of micro optical elements have been suggested and demonstrated [31-34]. There are tradeoffs involved in each of the above mentioned techniques either in cost or in quality. The 2N is a cheaper fabrication technique at the cost of lower efficiency and higher fabrication time of the optical elements while the Phase Mask technique is slightly more expensive but delivers perfectly analog surfaces. The Gray Scale and Half tone techniques are much more expensive than Phase masks while providing the same quality and direct writing techniques are very low throughput techniques not suited for bulk manufacturing.

In this dissertation we present additive lithography as an alternative technique for the fabrication of multilevel and pseudo analog optical surfaces using amplitude masking patterns and dose control. The entire optical element is fabricated on the photoresist in a single process which might involve multiple successive exposures followed by developing and etching. This eliminates the need for multiple coat-alignment-exposure-etching processes. The use of amplitude masks makes this process inexpensive and the

fabrication can be performed on a stepper or on an aligner, though a stepper is the ideal fabrication tool since alignment is automatic and highly accurate. We will discuss the design of these optical elements in the Chapter 2 and present the additive lithographic process in Chapter 3. In Chapter 4 we will present the photoresist reflow process and its limitations and discuss schemes using the additive pre-sculpting process to overcome these limitations. In the subsequent chapters we will discuss the fabrication of various optical elements using the additive technique and transfer etching of these structures into the fused silica glass substrates.

CHAPTER 2: OPTICAL DESIGN

Miniaturizing is a passionately pursued goal in all the fields and in optics the developments in micro Diffractive Optical Elements (DOE) has rendered it possible to have Micro Optical Benches (MOB). DOE changes an input wavefield by means of diffraction thus rendering the required output field and it can do so in ways that many a times cannot be achieved using traditional refractive and reflective optics. DOEs of current interest are designed for use with monochromatic light. Typical DOEs can have either continuous microreliefs or multilevel microreliefs (Binary Optics) with features ranging from submicron to millimeter dimensions and relief amplitudes of a few microns.

Bulk optical lenses can focus or collimate an optical beam but there are very few techniques available for the fabrication and integration of scaled down versions of these refractive lenses for use in micro-optics. These techniques are fairly new and weren't available until more than a decade back. Very thin Diffractive elements can help achieve the same objective. The initial lenses were simple amplitude zone plates. They then evolved into binary and then multilevel phase elements that provide higher efficiencies. These elements are very attractive in the field of microoptics especially in the optical MEMS industry, as they can be batch fabricated along with other elements onto a single substrate. These techniques can also be employed in the fabrication of various other beam shaping DOEs that perform more complex phase transformations to the input field to render the required output field. These elements are useful in a variety of applications such as communications, materials processing, bio-photonics, etc.

In this chapter we will discuss analytical and numerical techniques for designing these refractive and diffractive components and in the later chapters we will discuss the fabrication of these elements using additive lithography.

2.1 <u>Refractive and diffractive elements</u>

Transmittance of an optical element that performs phase modification on an input wavefield Ui (x,y) to give an output field Uo (x,y) can be written as [35,36]

$$t(x,y) = \frac{U_o(x,y)}{U_i(x,y)} = \frac{e^{i\phi_o(x,y)}}{e^{i\phi_o(x,y)}} = e^{i\phi_o(x,y)-\phi_i(x,y)} = e^{i\phi_d(x,y)} \qquad 2.1$$

This element modifies the phase of the wave and is represented by a phase function

$$\phi_d(x,y) = \phi_o(x,y) - \phi_i(x,y) \qquad 2.2$$

The transmittance of a refractive lens with focal length f is given as

$$t(x,y) = e^{i\frac{k(x^2+y^2)}{2f}} \qquad 2.3$$
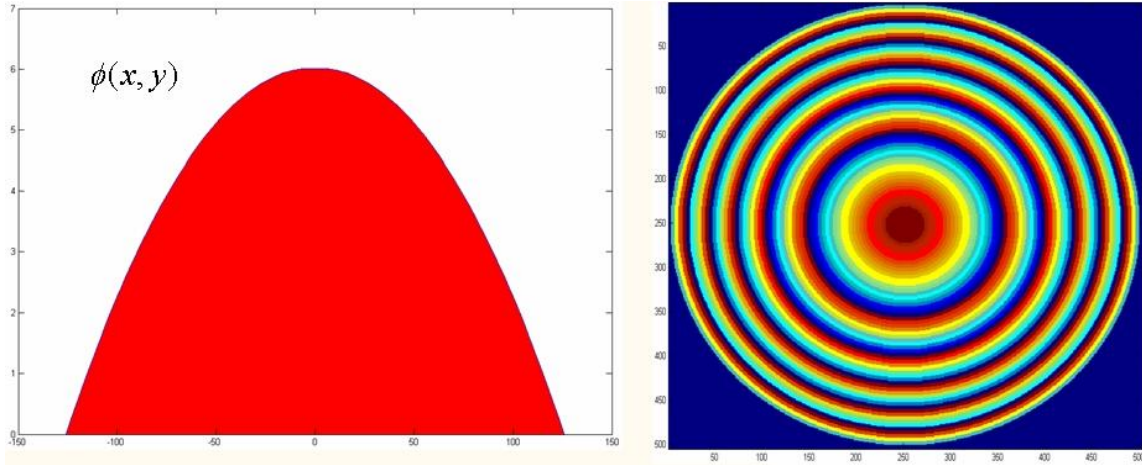
Figure 2-1 Surface profile of a refractive lens and its phase

As shown in Figure 2-1, this refractive lens can be broken down as integral multiple of 2π in phase. This transformation of a refractive lens into the corresponding diffractive-refractive structure is shown in Figure 2-1. This structure is still analog since the surface relief is continuous and smooth in each zone except at the zone boundaries. Thus the radius of the mth zone of the diffractive phase element is given as

$$r_m = (2m\lambda f)^{1/2} \qquad\qquad 2.4$$

and sag

$$h = \frac{\lambda}{n(\lambda)-1} \qquad\qquad 2.5$$

where n(λ) is the refractive index of the material at the design wavelength.
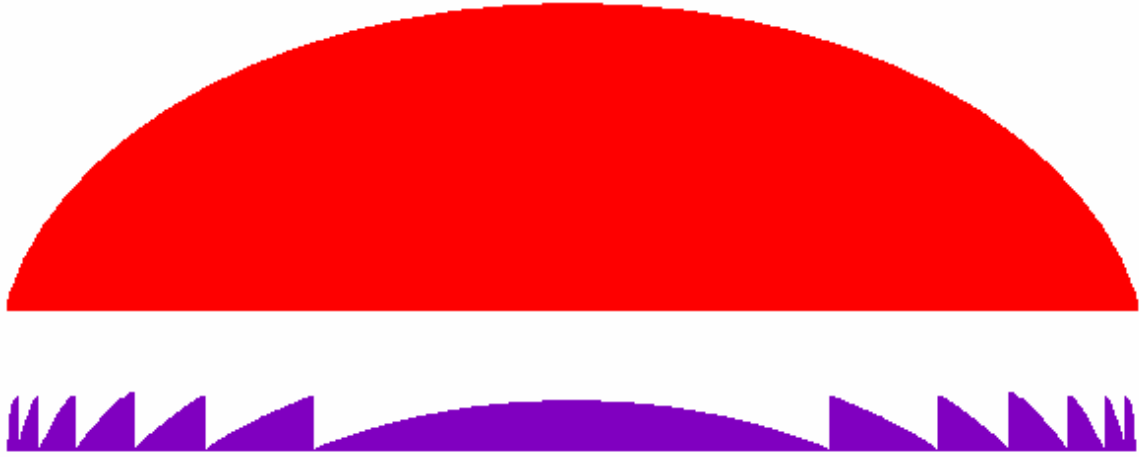
Figure 2-2 Diffractive lens as a mod (2π) breakup of refractive lens

It is evident that the zone period reduces as we go out from the center of the lens. We may think of these lenses as a plano-convex thick lens whose thickness has been reduced by breaking down the curved face in concentric rings. In Fresnel lenses the wavefront produced is in general not spherical but randomly ring stepped. The reason for this is that the refracted ray direction is controlled by means of groove slope and the thickness cannot be controlled with precision. Gabor plates, Kinkoforms or diffractive optical zone plates can produce spherical or flat wave fronts. It is clear that a zone plate is wavelength dependent and may not perform its function efficiently at wavelengths far from the design wavelength.

The phase function of a rotational symmetric diffractive lens with arbitrary profile can be expressed as

$$\phi(r) = 2\pi(a_2 r^2 + a_4 r^4 + ...) \qquad\qquad 2.6$$

The optical power of the diffractive lens in the pth diffraction order is given as

$$\Phi = \frac{1}{f_0} = -2a_2\lambda_0 p \qquad 2.7$$

where $\lambda 0$ is the design wavelength and $f0$ is the design focal length.

For a refractive lens the focal length fr is given as

$$f_r = \frac{1}{n(\lambda)-1}\frac{1}{c_1 - c_2} \qquad 2.8$$

where c1 and c2 are the curvatures of the two surfaces c=1/R where R is the radius of curvature of the surface.

For the diffractive lens discussed above the focal length would be

$$f_d(\lambda) = f_0\frac{\lambda_0}{\lambda} \qquad 2.9$$

Thus we see that a diffractive lens shows much larger wavelength dispersion as compared to a refractive lens.

The airy disk radius for a refractive lens is

$$r(\lambda) = 1.22\frac{\lambda f}{D} \qquad 2.10$$

and for a diffractive lens it is

$$r(\lambda) = 1.22\frac{\lambda_0 f_0}{D} \approx cons\tan t \qquad 2.11$$

All refractive optical elements can be reduced to their diffractive counterparts in a similar manner. Structures thus obtained are still analog, and the next step is to quantize them to multilevel structures to be able to fabricate them using amplitude masking schemes used in IC processing.

2.2 **Multilevel diffractive structures**

In a multilevel structure the period L is divided into N subperiods and each sublevel can be represented by a rect function centered at [36]

$$x = [\frac{L}{N}(l + \frac{1}{2})]$$

2.12
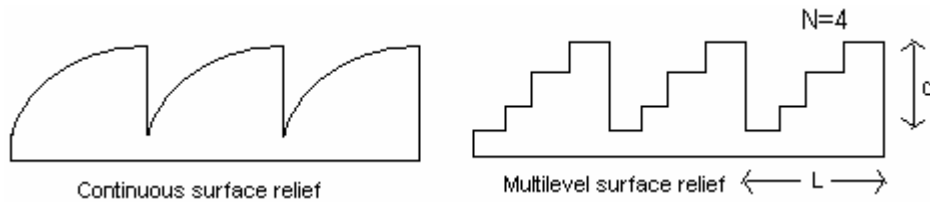
Figure 2-3 Analog surface and its multilevel quantized equivalent surface

Each subperiod introduces a phase shift

$$2\pi\phi_l = \frac{l\phi_0}{N}2\pi$$

2.13

where ϕ_0 is the largest phase shift of all subperiods.

The far field amplitude distribution of the N subperiods within the total period L can be written as

$$U(f_x) = \frac{1}{N} \sum_{l=0}^{N-1} \frac{Sin\left(\frac{\pi L f_x}{N}\right)}{\frac{\pi L f_x}{N}} e^{-i(2\pi L(l+(1/2))f_x)/N} e^{-i(2\pi l \phi_0/N)}$$ 2.14

where   fx = m / L.

The far field amplitude of the mth order can is given as

$$A_m = e^{-i(\pi m/N)} \frac{Sin\left(\frac{\pi m}{N}\right)}{\frac{\pi m}{N}} \frac{1}{N} \sum_{l=0}^{N-1} e^{-i(\pi(m-\phi_0)l)/N}$$ 2.15

The diffraction efficiency for the mth order is obtained to be

$$\eta_m^N(\phi_0 \to 1) = \left[\frac{Sin\left(\frac{m\pi}{N}\right)}{\frac{m\pi}{N}}\right]^2$$ 2.16

Increasing the number of levels approximates the continuous structures and hence a better diffraction efficiency is expected.
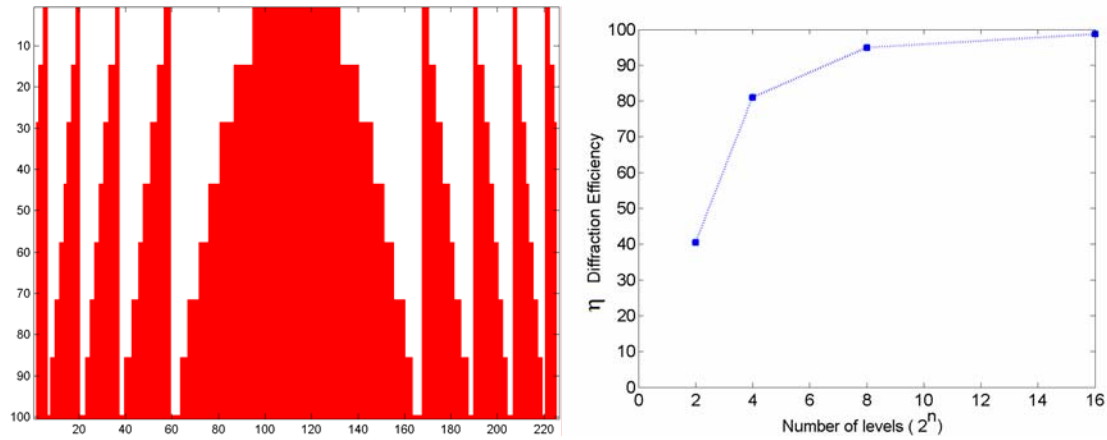
Figure 2-4 Quantization of the sag (phase) for a positive diffractive lens and diffraction efficiency as a function of the number of levels
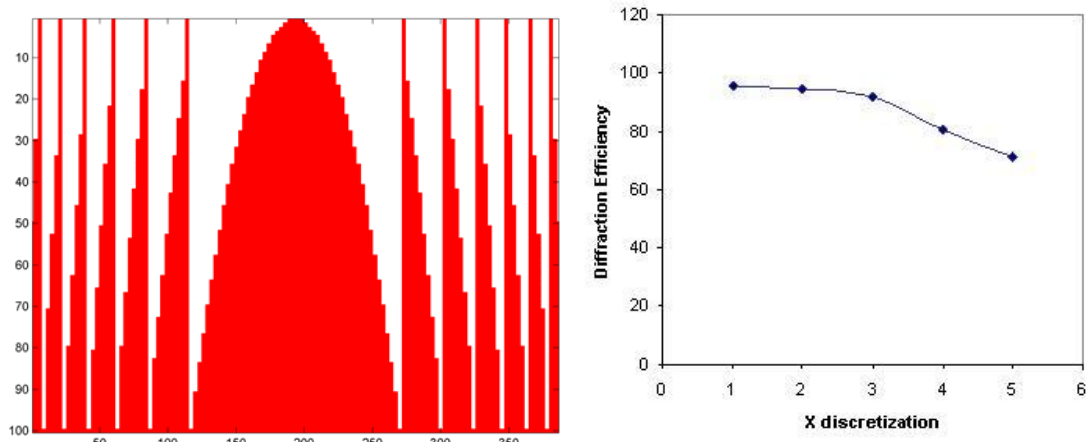
Figure 2-5 Quantization in the x direction for a positive diffractive lens, and diffraction efficiency as a function of the grid size.

Quantization to achieve a multilevel element could involve discretization along the height or along the width. These will lead to different masking schemes, discussed in Chapter 3. Figure 2-4 a shows the sag (phase) quantization of a analog positive lens. The heights of all the levels in the structure are equal. Figure 2-4 shows the corresponding diffraction efficiency for phase discretization as a function of the number of levels used to represent

16

the analog profile. It is seen that the efficiency is almost 95% for an 8-level element. Figure 2-5 shows the alternative quantization scheme where the lens is placed on a symmetric grid. The corresponding heights of the levels between the grid points in this scheme are not equal. Figure 2-5 also shows the diffractive efficiency of this quantization scheme as a function of the grid size and it is seen that for a grid size of 2 μm or smaller the diffraction efficiency is 95% or more.

2.3   Beam shaping elements

Beam shaping elements are used for manipulating the Gaussian beam output from lasers to obtain a desired intensity profile[37]. These elements are extensively used in the industry and for research and have a wide variety of applications in materials processing, optical communications, optical sensing, bio-photonics, etc. The problem of designing beam shaping optics is finding the phase function required to affect the transformation of the input beam to the desired output beam profile[36].

Let us assume a rotationally symmetric input wave with a phase function given by kψo(r). The phase of the light field after the DOE is then given as [36-39]

$$k\psi(r) = k\psi_o(r) + \phi(r) \qquad\qquad 2.17$$

where ɸ(r) is the phase function of the DOE that needs to be determined.

The ray inclination equation is then given as

$$\frac{d\psi}{dr} = \frac{\rho(r)-r}{\sqrt{l^2 +(\rho(r)-r)^2}} = \frac{\rho(r)-r}{l} \qquad 2.18$$

where the function ρ(r) is the mapping function that needs to be determined for affecting the transforming of the input beam to the desired far field intensity profile.

If we integrate equation 2.18 with respect to r and substitute into equation 2.17 the eikonal ψ thus obtained, we get the phase function of the DOE

$$\phi(r) = -\frac{kr^2}{2l} + \frac{k}{l}\int_0^r \rho(r)dr - k\psi_o(r) \qquad 2.19$$

The first term on the right hand side represents a spherical lens function and the second term represents the phase of the DOE.

Considering lossless beam shaping the total input energy is equal to the total output energy. This is written as

$$E_{in} = \int_0^r 2\pi I(r)rdr = E_{out} = \int_{\rho(0)}^{\rho(r)} 2\pi I(\rho)\rho d\rho \qquad 2.20$$

18

Considering a plane wave as the input to a DOE that provides an uniform annular beam at the focal plane at a distance 'f' from the DOE plane. On solving equation 2.20 and 2.19 we get the phase function of the DOE as

$$\phi(r) = -\frac{kr^2}{2f} + \frac{k\rho_1}{2fc}[cr(c^2r^2+1)^{\frac{1}{2}} + ln(cr + (c^2r^2+1)^{\frac{1}{2}})] \qquad 2.21$$

where c is given as

$$c = \frac{(\rho_2^1 - \rho_1^1)^{\frac{1}{2}}}{a\rho_1}$$ and ρ1 and ρ2 are the inner and outer radii of the annular output beam.

A toroidal lens focuses the input beam into a tightly focused ring such that ρ1 and ρ2 are nearly equal. Thus in the limit that 'c' tends to zero equation 2.21 becomes

$$\phi(r) = -\frac{kr^2}{2f} + \frac{k\rho_1 r}{2f} \qquad 2.22$$

Another element that can perform a similar function is a vortex lens defined by the phase function [168],

$$\psi(r,\theta) = m\,tan^{-1}(\frac{y}{x}) \qquad 2.23$$

19

2.4   Iterative Fourier Transform algorithm

In the previous sections we have seen analytical methods for obtaining the required phase of the optical element for a required far-field output. This is an inverse problem in that we are trying to find the input phase function for a given output intensity distribution [35,36]. For more complicated output profiles a much easier solution was presented by Gerchberg and Saxton and was originally applied to electron microscopy. Figure 2-6 shows the algorithm and it has been used widely in the fabrication of Computer Generated Holograms (CGH) [41].

```
┌─────────────────────┐
│ Randomize           │
│ -π/2 < φ < π/2       │
└─────────────────────┘
          │
          ▼
┌─────────────────────┐     ┌───┐     ┌─────────────────────┐
│ f₁ = a exp(jφ)      │ ──▶ │ ℑ │ ──▶ │ f₂ = b exp(jα)      │
│ |a|= input beam     │     └───┘     │                     │
└─────────────────────┘               └─────────────────────┘
          ▲                                      │
          │                                      ▼
┌─────────────────────┐     ┌───┐     ┌─────────────────────┐
│ f₂ = c exp(jφ)      │ ◀── │ ℑ⁻¹│ ◀── │ Output Intensity    │
│                     │     └───┘     │ Constraint (I)      │
│                     │               │ f₃ = I^{1/2} exp(jα)│
└─────────────────────┘               └─────────────────────┘
```

$$f_1 = a\ \exp(j\phi)$$
$$|a| = \text{input beam}$$
$$f_2 = b\ \exp(j\alpha)$$
$$f_2 = c\ \exp(j\phi)$$
$$f_3 = I^{1/2}\ \exp(j\alpha)$$
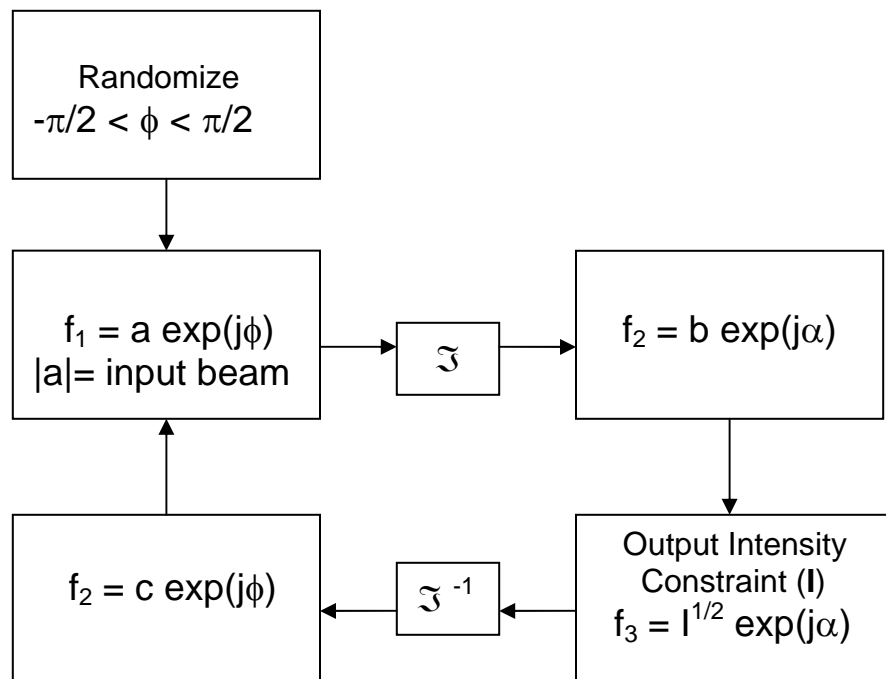
Figure 2-6 Gerchberg Saxton algorithm for DOE phase retrieval

The initial phase distribution can be a random guess. The constraint on the input plane is the amplitude distribution of the input laser beam. The phase mapping in the

reconstruction plane (far-field) is the actual phase mapping from the DOE. A fourier transform of the input random guess and the fixed amplitude distribution from the laser beam is performed to obtain the far field phase and amplitude. The constraint in this reconstruction plane namely the required amplitude distribution is then applied to the field obtained from the forward fourier transform. This field is then mapped back to the input DOE plane through an inverse fourier transform. The input plane constraints are again applied to the field and a forward fourier transform is performed. Thus a finite number of loops of forward and backward transforms are performed with the required constraints to obtain the phase of the input DOE that will provide the required output intensity profiles. The phase of a 9-spot fan out DOE obtained after 10 iterations is shown in Figure 2-7.
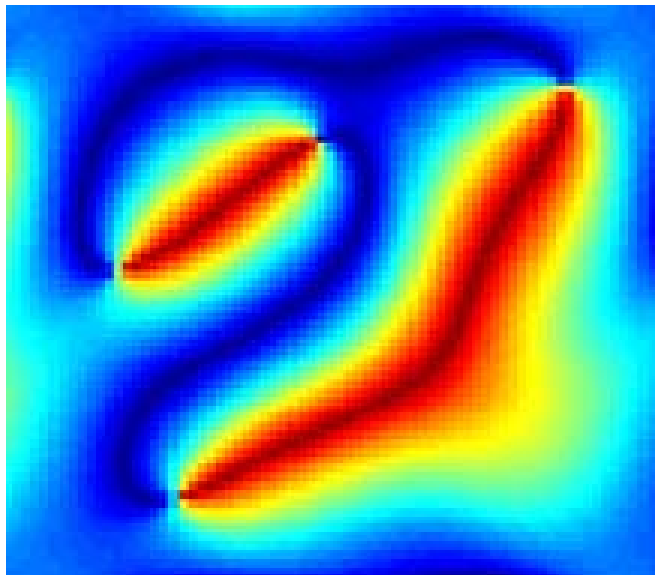
Figure 2-7 Phase of a 9-spot fan out DOE.

This technique falls under the broad category called the Method of Projections. The algorithm itself is very simple and efficient, but care has to be taken in the choice of constraints in the algorithm so that it does not converge automatically. This algorithm has been further investigated and improved over the years by many researchers.

CHAPTER 3: ADDITIVE LITHOGRAPHY

Microlithography has been extensively studied in the IC industry and is the process of choice for fabrication of micro optics [1-7]. The process usually starts by exposing a wafer coated with a photoactive polymer through a mask. This polymer is called the photoresist and it can be of two types namely positive and negative tone resists. In a positive photoresist exposed areas are etched away on developing in a solvent and in a negative photoresist exposed areas are left behind on developing in a solvent. The mask is a rigid quartz or soda lime plate with transparent aperture regions and opaque chrome regions. Exposure is performed either on a Mask aligner or on a projection system that images the mask object onto the substrate. Before we introduce additive lithography we will discuss the various exposure techniques and their advantages.

3.1   Exposure Techniques

Photoresists are made of a base resin, a Photo Active Compound (PAC) and a casting solvent. The purpose of the casting solvent is solely to allow spin coating a thin layer of the photoresist onto the substrate of choice. After the spin coating process, the substrate is subject to a soft bake to remove the solvents from the thin film. After the soft bake the photoresist is exposed to electromagnetic radiation of appropriate wavelength through a mask in contact with the substrate as with contact printing or imaging a mask onto the substrate as with projection printing. Other mask-less sequential exposure processes such as laser writing, e-beam writing or ion beam writing can also be used to write patterns on

the photoresist [42]. In the following sections we will discuss the contact and projection

printing techniques and their respective merits and demerits.

3.1.1 *Contact Printing*

Contact exposure, also known as shadow printing mode, is performed by placing a mask

in contact with a photoresist coated wafer and exposing with a collimated light source,

Figure 3-1. The mask and the wafer can be under pressure contact coupled with a vacuum

between them or they could be in a proximity printing mode where there is a separation

between the mask and the wafer. The patterns on the mask are reproduced on the

photoresist and the resolution of the process is defined by diffraction of light at the edge

of the transparent features on the mask, alignment of the wafer to the mask, non

uniformities of the wafer and debris between the mask and the wafer. Diffraction causes

sharp edges to become blurred thus reducing the resolution.
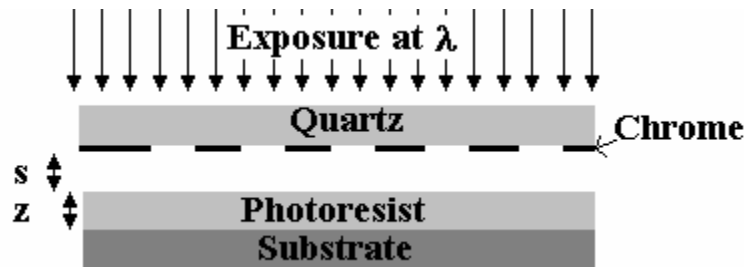
Figure 3-1 Contact printing mode

Diffraction is unavoidable in the case of contact printing as it will occur through the bulk

of the resist even if the mask substrate gap is zero. In the practical case, Fresnel

diffraction effects due to the gap, the thickness of the photoresist and the wavelength of the source used, limits the resolution. Thus the minimum feature size R, that can be resolved with the contact mode printing is obtained from Rayleigh resolution criteria and is given as [42]

$$\mathbf{R} = \frac{3}{2}\sqrt{\lambda\left(\mathbf{s} + \frac{\mathbf{z}}{2}\right)} \qquad\qquad 3.1$$

where, λ is the wavelength of the light used for exposure, s is the gap between the mask and the photoresist surface and z is the thickness of the photoresist. With an I-line (365 nm) source, a zero gap between the mask and substrate and a 500 nm thick photoresist layer, the minimum feature that can be printed using contact printing will be 453 nm. In practice though, a zero gap between the mask and the substrate over a four inch area is impossible to achieve. Thus with a 500 nm gap between the mask and the substrate, the minimum resolution decreases to 785 nm and with a 1000 nm gap the resolvable line width is 1013 nm.

Thus, for best resolution we need to make the gap between the substrate and the mask minimal and to use shorter wavelengths with thinner photoresist layers. The theoretical maximum resolution is seldom achieved with contact exposures. The required contact between the mask and the substrate usually contaminates the mask and may also cause permanent mask damage. The process of pulling a good vacuum between the substrate and the mask consumes valuable process time. Moreover it is harder to obtain good contact over a large substrate area. Thus contact printing is not an ideal technique for high throughput applications. Because the features on the mask need to be identical to

those printed on the photoresist, the fidelity of the mask features must be high. This increases the mask write time enormously and significantly increases the cost of mask fabrication.

3.1.2   *Projection Printing*

Projection printing was developed to alleviate the faults of contact printing. Figure 3-2 shows the important components of a projection lithographic tool.
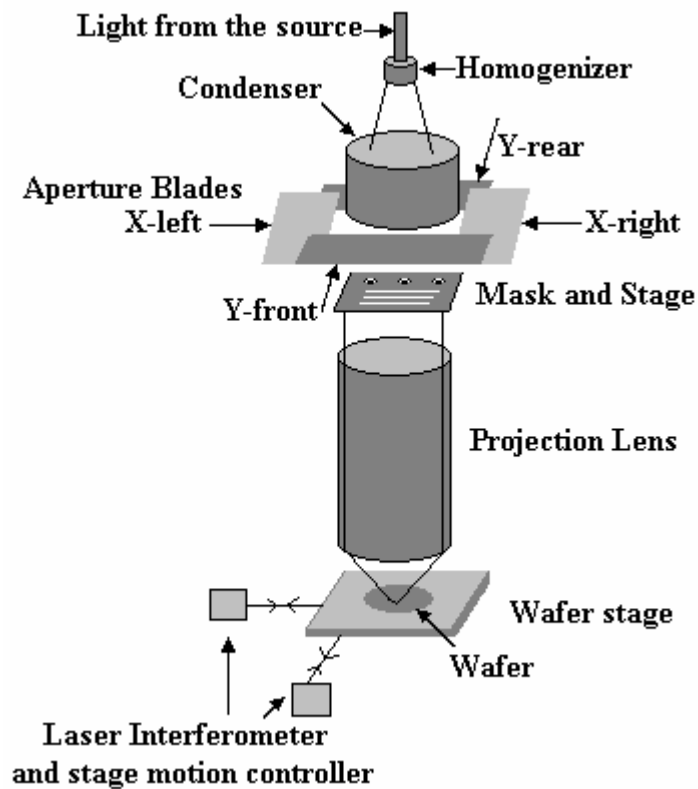
Figure 3-2 Schematic of a projection lithographic system

In projection printing a mask pattern is imaged onto a photoresist coated wafer [42,61]. The mask and the wafer are never in contact thus keeping the process clean with no mask or wafer damage. The first steppers had a xenon discharge lamp with filters to restrict the exposure illumination to wavelength of 436 nm (G-line). The NA of these systems was about 0.35 and the resolution was about 0.8-1 μm. This was followed by the introduction of the I-line steppers (365 nm) reducing the resolution to 0.35 μm. This was also followed by an increase in the NA of the system. Today's steppers can print features as small as 0.09 μm and use KrF (248 nm) and ArF (193 nm) excimer lasers. X-ray (1.1 nm) steppers today can print sub 50 nm features and align with 35nm accuracies. This is the state of the art for the electronics industry. However, in fabricating micro optical elements such as lenses, waveguides etc. the smallest features are well above the resolution limit for the G-line steppers and thus older and hence less expensive stepper technology can be employed.

The projection system consists of an illumination system, a lithographic lens assembly, a reticle alignment system, and a very precise wafer positioning system. It also has additional instrumentation for automatic alignment using global and local alignment schemes. The illumination system consists of a source with an aperture and a condenser lens. The condenser lens in the illuminator is designed such that the position of the light source is in its front focal plane. This type of illuminator configuration is called, Koehler illumination system. Other types of modified illumination schemes are used in newer lithographic systems for enhancing the resolution of the system. Typical modern lithographic projection systems use a combination of refractive lenses or a combination

of both refractive lenses and mirrors for imaging the mask patterns onto the wafer. This lens system projects either a 1:1 or a reduced image of the mask features onto the substrate plane. Reduction systems allow larger features on the mask thus making fabrication of the mask easier and cheaper. They are also more forgiving since any imperfections on the mask also get reduced at the image plane by the reduction factor of the system, usually 4X, 5X or 10X. In projection systems the mask is usually referred to as a 'reticle'. The wafer positioning system is a very important part of the stepper since it allows placing the wafer to within $\leq$ 50-100 nm accuracy thus allowing very accurate alignment. Repeatability and alignment accuracy is also controlled by alignment features called Reticle Management system (RMS) windows on the reticle that ensure that the reticle is placed at the exact same location every time the reticle is used. On a 5X reduction system a 100x100 mm (4x4 inch) mask would form a 20x20 mm image on the substrate, alternatively called the field size. Multiple fields or dies can be exposed on a single wafer. After each exposure the wafer is shifted to the next die position and the exposure is performed again. That is why these systems are referred to as wafer steppers.
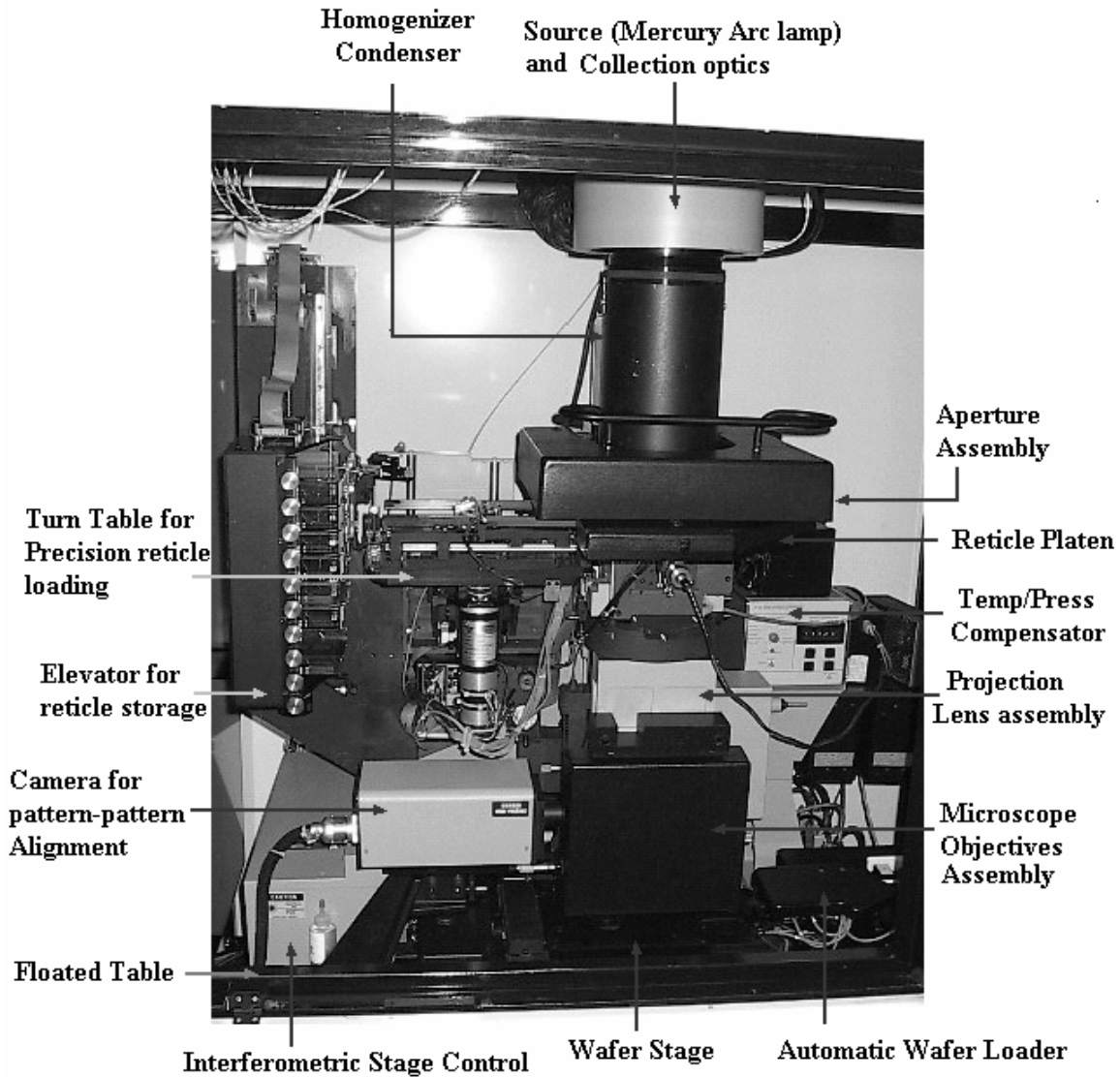
Figure 3-3 GCA 6300 G-line (436 nm) wafer stepper

Figure 3-3 shows the GCA 6300-C G-line stepper system in our lab and its important components. The source assembly is called the maximus. The source inside the maximus is a Mercury arc lamp operating at 350 Watts. The light output from the lamp is collected by an elliptical mirror assembly and focused onto the second foci where it is collected by four separate optical fiber bundles. These four bundles are then bunched together along the optical axis of the system. The numerical aperture of the source on our system is

NAs = 0.21. At the end of these fibers is a precision shutter that is used to control the exposure time and a small aperture that represents a point source. The maximus is equipped with an inline detector that monitors the power output of the lamp and sends a corresponding signal to an integrator. The integrator controls the shutter open time and adjusts it with respect to a programmed reference to ensure that the actual exposure energy is kept constant irrespective of changes to the lamp intensity over the lamp's lifetime. Our GCA system is setup to provide 150 mJ/(cm2sec) at the substrate plane. If the lamp power drops the exposure time is increased by the integrator automatically to ensure that the power delivered to the substrate is maintained at this reference value. This ensures repeatability of the exposure process. Instead of a 350 W lamp, a 1 kW or 2 kW mercury arc lamp can provide much higher power at the substrate thus increasing the throughput and is usually preferred in binary exposure processes used in IC fabrication. A high power lamp is detrimental to the additive lithographic process, because it depends on controlled partial exposures and some of the masking levels require very small exposure energies. The smallest consistent shutter open time on the GCA stepper is 5 msec using a 350W lamp thus leading to a ±12nm variation in level heights as will be shown in Chapter 5. Using a source with higher output power will increase this inaccuracy caused due to limitations in the shutter speed. This will result in lower tolerance in the fabricated profiles. Therefore a source with lower power is preferred for achieving higher fabrication tolerance.

The light output from the maximus is then filtered to transmit only the G-line (436 nm) and then homogenized and collimated to cover an area larger than 4″ x 4″. This output

light is partially coherent with a coherence factor σ = 0.6 on our GCA system. The coherence of the source, the numerical aperture of the projection lens system and wavelength of the source used for exposure will determine the resolution of the projection system. Other factors such as uniformity of the illumination and the aberrations of the projection lens assembly will also affect the resolution.

The size of the reticles used on the GCA stepper is 5″ x 5″. The region beyond the 4″ x 4″ area is used for supporting the reticle on the platen and for alignment features that ensure that the reticle is aligned on the platen for repeatability. Thus the required masking features have to be placed within this 4″ x 4″ area. In reality though, the patterns have to be placed within a 4″ diameter circle, because the projection lens pupil filters out patterns that lie outside this area on the reticle. Though the entire 4″ x 4″ area can be the exposure field, the actual field exposed on the substrate can be controlled through aperture control features available on the stepper. The GCA stepper is equipped with four blades placed before the reticle plane Figure 3-2. Each of these blades can be individually moved from one edge of the reticle to the other over a 100 mm distance. This allows us to open rectangular apertures over any region of the reticle for selectively imaging certain regions of the reticle. The other parts of the reticle are not illuminated and thus not imaged onto the wafer. This allows us to place multiple patterns on the same reticle and each pattern can be separately exposed with different exposure times.

Immediately after the apertures, is the reticle platen which performs the function of holding the reticle and is equipped with motors to align the reticle so as to eliminate any

X, Y and θ errors. This ensures that the center of the reticle is aligned with the axis of the system and multiple patterns on the same reticle or on multiple reticles can be easily overlaid with high accuracy and the process is repeatable. This is achieved with the help of RMS windows as shown in Figure 3-4. The RMS window on one side of the reticle is at the center along the x axis and on the other side is offset from the center by 11 mm. A LED source is used to shine light through the RMS windows. The detectors A-F detect the power going through the windows as shown in Figure 3-4. The reticle is aligned on the platen when the detectors are balanced such that detectors A=C, D=F and B=E.
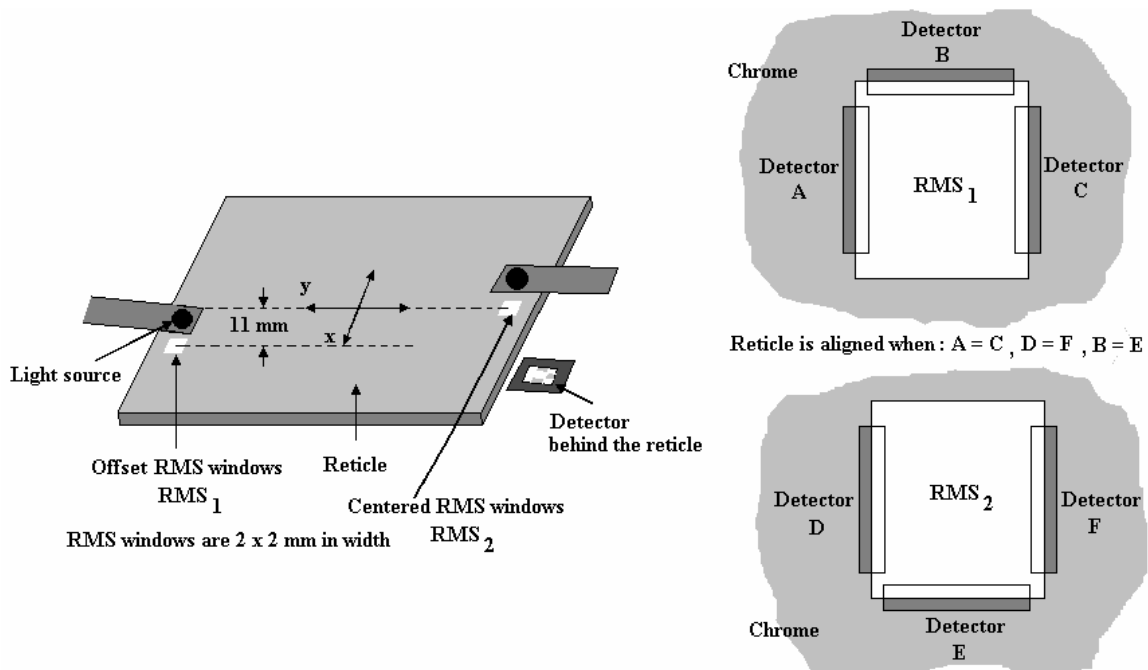
Figure 3-4 RMS windows on a reticle and alignment scheme

Below the reticle platen is the projection lens assembly that performs the function of imaging the reticle features onto the wafer plane. The GCA system performs a 5X reduction of the features and the numerical aperture of the lens system used is NA=0.35.

The substrate coated with photoresist is placed on this plane on a highly precise translation stage. A 4″ x 4″ (100 x 100 mm) reticle field on exposure through this lens is reduced to 0.8″ x 0.8″ (20 x 20 mm) die. The GCA stepper can accommodate substrates with 4″ diameter. Thus multiple dies can be exposed on the same substrate. The stage translates the substrate after every exposure to a new die position. The shutter is opened again to illuminate the reticle thus imaging the 5X reduced pattern onto the new die position on the substrate. The positioning precision of the wafer stage on the GCA stepper is ± 50 nm. Therefore alignment tolerance in the additive lithography process using multiple patterns on a single reticle and successive exposures without displacing the substrate is approximately ± 50 nm.

Apart from this the stepper is also equipped with features for automatic detection of the surface of the wafer through an auto focus feature and adjusting the surface of the wafer to be at best focus. This ensures high fidelity of the images transferred onto the photoresist since the image quality deteriorates very fast beyond the depth of focus of the system. The auto focus signal is also used to level the wafer so that the wafer is perpendicular with respect to the optical axis. A temperature and pressure monitor and compensator ensure that changes in temperature and pressure that can cause shifts in the image focus position and magnification are automatically compensated to maintain best focus and a constant 5X reduction. The entire assembly is floated on a compressed air table and placed in a temperature controlled enclosure to ensure optimum operating conditions and isolation from environment factors that may affect the system performance.

The resolution R and the depth of focus (DOF) in a projection system are given as [42]

$$R = \frac{k_1 \lambda}{NA} \qquad\qquad 3.2$$

$$DOF = \frac{k_2 \lambda}{NA^2} \qquad\qquad 3.3$$

where NA is the numerical aperture, k1 and k2 are characteristic constants of the specific lithographic process. In practical semiconductor lithography, k1 and k2 generally depend on the photoresist and process parameters, the type of the mask and the pattern being imaged, tool parameters such as aberrations in the lens system and coherence and uniformity of the source, requirements of the shape and allowed size range of the developed photoresist profile.

By eliminating the NA in the above equations we can write a relation between the DOF and the resolution R (feature size) as,

$$DOF = \frac{k_2}{k_1^2} \frac{R^2}{\lambda} \qquad\qquad 3.4$$

As can be seen from the above equation, larger feature sizes yield a larger DOF. This is an important parameter to remember when printing through thick photoresists with small features. As can be seen, shorter wavelengths and higher NA can help print smaller features.

We will introduce additive lithography in the following section and discuss the various masking schemes employed. We will also present the resulting photoresist profiles obtained from modeling the exposure-develop process using these masking schemes.

3.2   Introduction to Additive Lithography

In chapter 1, various methods for fabricating micro-optical elements were discussed and their advantages and disadvantages were highlighted. The alternative to these techniques termed "Additive Lithography" was developed for fabricating multilevel optical elements as part of this research. Exposure dose control is employed with multiple binary mask patterns designed for fabricating a specific multilevel optical element. Simple dose control helps in fabricating the same optical function for operation at various wavelengths. On the other hand a simple set of binary patterns chosen to represent a specific domain of optical functions can be combined with exposure dose variation for fabricating optical elements belonging to that specific domain. This method for photoresist sculpting can be further extended by combining them with other techniques such as reflow, for fabricating more complex analog beam shaping and focusing elements. The simplicity and the speed of the technique helps increases the throughput and/or decrease the cost of fabrication as compared to many of the current fabrication techniques mentioned earlier.

3.2.1 *Photoresist Contrast Curve*

Fabrication of multilevel structures on the photoresist using Additive lithography depends on partially developed photoresist achieved by partial exposure of the photoresist [43-47]. Photoresist sculpting is performed by using a set of binary amplitude mask patterns and simple exposure dose control. In order to do this it is necessary to understand the exposure response of the photoresist. This is given by the contrast curve of the photoresist, which is engineered to be nonlinear to improve the resolution for applications in the semiconductor industry. Usually a contrast curve is a plot of the fraction of the photoresist undeveloped as a function of exposure energy. Here we plot the fraction of the photoresist developed after exposure with respect to the exposure time since this curve has more meaning when we try to understand additive lithography and utilize it for the fabrication of diffractive optical elements. By making suitable transformations from time to energy we can easily obtain the traditional contrast curve for the photoresist.

The contrast curve for a general positive photoresist shows three regions, Figure 3-5,

1. A slow response region below a threshold time corresponding to threshold energy.

2. A fast rising region between the threshold and saturation; this could be linear or non linear depending on the photoresist (the figure shows linear region).

3. A saturation region where the photoresist is completely bleached.
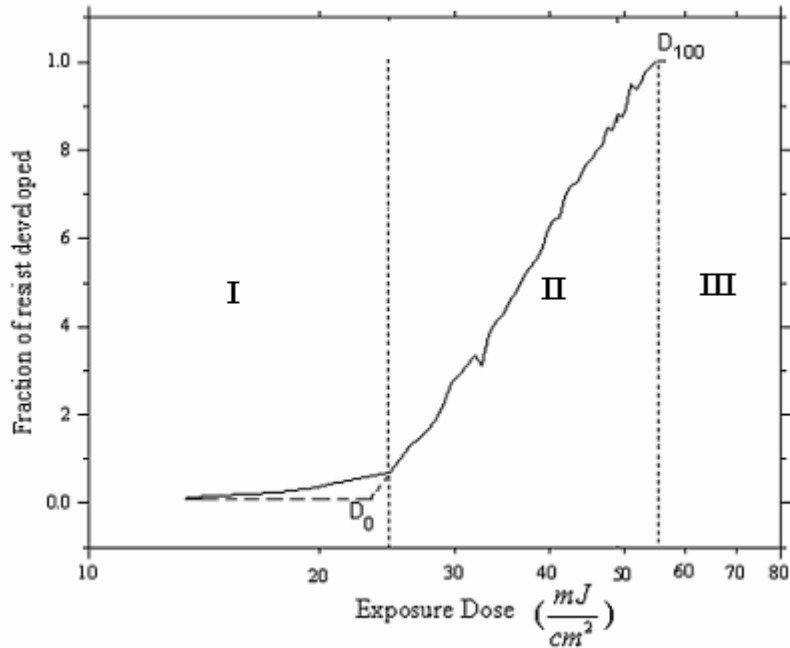
Figure 3-5 Contrast Curve for a positive photoresist.

Negative tone photoresist will have the opposite curve of that shown in Figure 3-5, but for additive lithography we will be discussing only positive photoresists. Additive lithography utilizes the 2nd region of this curve and depending on whether it is linear or non linear different masking and/or post processing techniques can be employed. Two types of masking schemes will be employed, namely entire domain in which each successive mask may further expose regions throughout the entire region and sub domain masking which splits up the regions into separate domains that may be completely non-overlapping or singularly overlapping such that each receives a separate exposure. These masking techniques are discussed at length in the following sections. For a photoresist with a linear working region both entire domain and sub domain masking techniques can be employed, but sub domain masking schemes are preferred for a photoresist with a non linear working region. Entire domain schemes can be utilized for non linear photoresists,

37

but the etching process will have to be morphed to correct for the irregularities obtained as a result of the non linear behavior of the photoresist. We will discuss the reasons for this in detail in the following sections.

As mentioned earlier the first step of the additive process is obtaining the photoresist response curve. This is done by generating an exposure array using a simple binary pattern and is easily performed by using the features available on the stepper. The process is shown in Figure 3-6. The height of the developed photoresist will increase with the exposure dose on the specific die. This is characterized to obtain the curves shown in Figure 3-7. The substrate used is Fused Silica. On a highly reflective substrate such as Silicon or Gallium Arsenide there will be back reflections leading to standing wave ripples in the contrast curve. These standing wave fluctuations in the response curve can be reduced by using top or bottom anti reflection coatings and post exposure processing as discussed in the previous chapter. The curves show the depth of the exposed pattern after developing as a function of the exposure time. This can be easily correlated to the exposure dose since the energy delivered to the substrate is known.
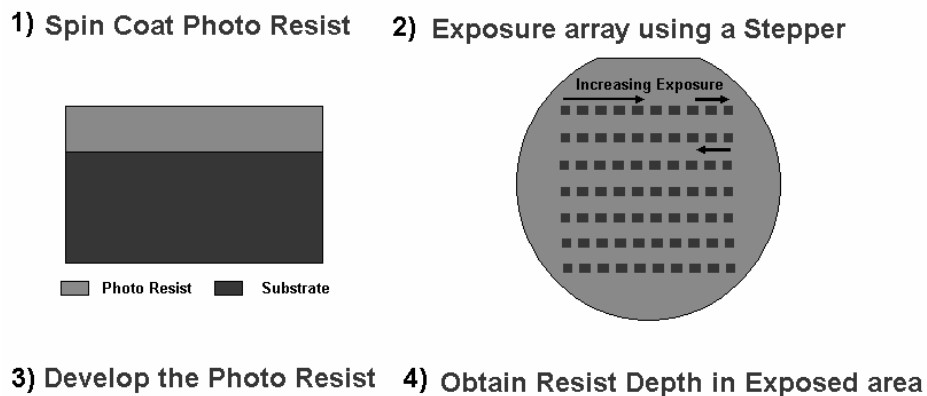
Figure 3-6 Process steps for obtaining the resist characteristic curve

38
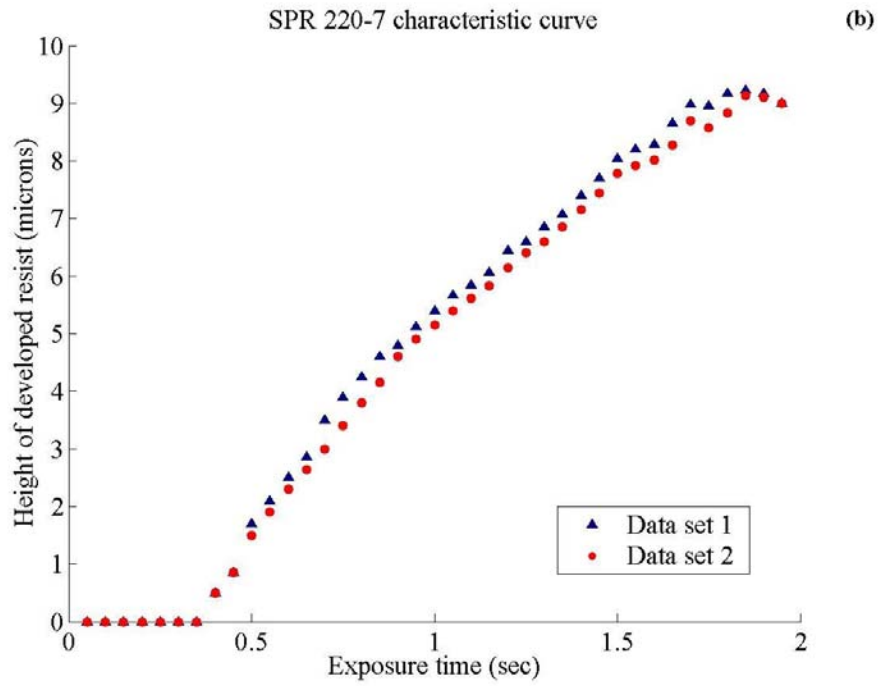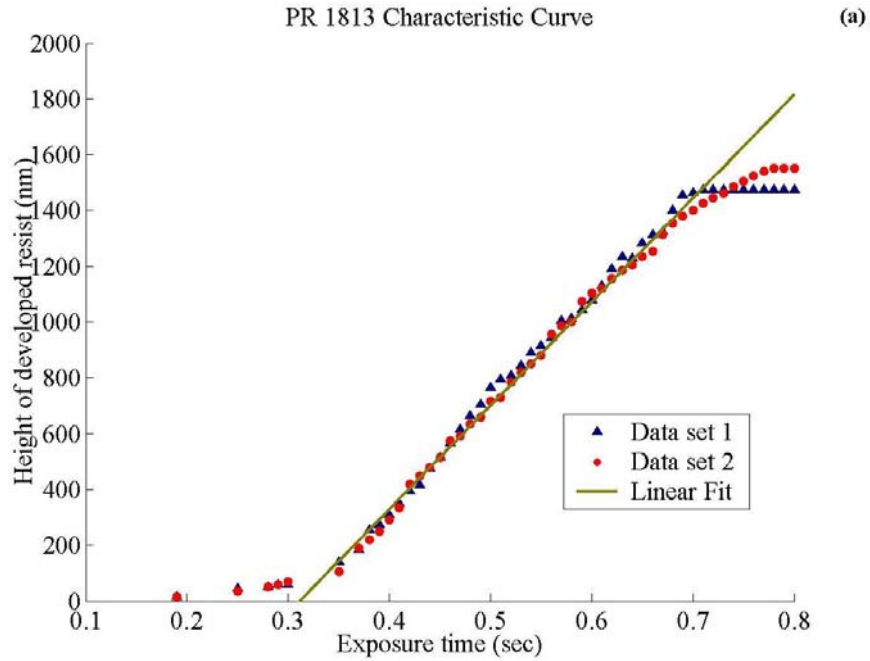
Figure 3-7 Contrast curve (a) S1813 (b) SPR 220-7, showing repeatability. Exposure at G-line (436 nm)

The stepper is equipped with an integrator that ensures that the energy delivered for the specific mask over the calculated time is kept constant in spite of the changes in the lamp intensity or other variables such as barometric pressure and temperature. This ensures a repeatable exposure process. The intensity of the bulb is monitored and the shutter open time is adjusted to compensate for the changes in the intensity of the lamp. A lower energy is preferred for additive lithography because this allows better shutter control. Below an exposure time of 0.01 sec the shutter open time may not be consistent which results in larger variations in the level heights. Thus a 350 W lamp source is better than a 1000 W lamp source because the exposure time is much larger, and one may obtain notably higher fabrication accuracies.

The energy received at the photoresist surface on the GCA 6300C stepper in our lab is 150 mJ/(cm2 s) which shows a saturation dose of 120 mJ/(cm2 s) for 1.55 μm coating of photoresist S1813 and 261 mJ/(cm2 s) for a 9 μm coating of SPR 220-7. It is also seen that the region of interest is linear for S1813 and is non linear for SPR220.

To show that the additive technique can be performed on an aligner the contrast curve was obtained on a Quintel mask aligner. The exposure at I-line (365 nm) is shown in figure 3-3. Aligners also have a mode for constant intensity so that the intensity at the surface is kept constant in spite of the changes to the intensity of the lamp over its life time. Though additive lithography can be performed on an aligner in a similar manner to that on a stepper, layer to layer alignment is not automatic. The first step therefore is to lay down alignment marks on the wafer and then each masking layer is aligned with

respect to these alignment marks. Most aligners do not allow large translations of the wafer or the mask and hence each masking level needs to be on a separate mask. This makes the process more expensive. In a stepper, all the masking patterns can be laid out on a single mask and by opening the apertures at the appropriate locations each pattern can be independently exposed. This reduces the cost of mask fabrication. The alignment on a stepper is automatic and hence overlay accuracy of 50-100 nm can be easily achieved on our stepper but on the aligner it is user defined and the best accuracy is usually 500 nm.
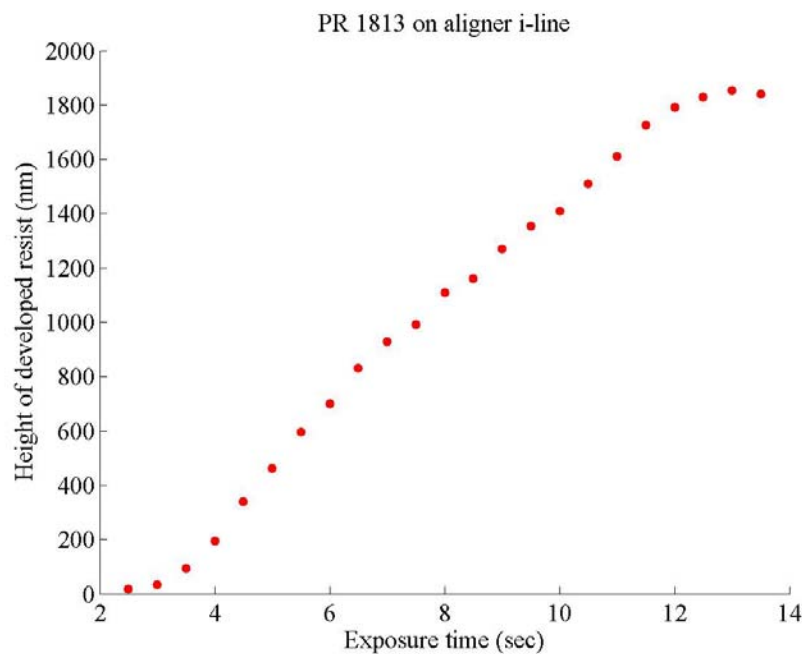
Figure 3-8 Contrast curve 1813 on aligner. Exposure at I-line (365 nm)

The response curve is very linear beyond threshold for thin photoresists since they have a low clear through exposure dose. But for thick photoresists that need higher doses the change in the absorption through the bulk over the exposure time leads to a non linear

curve. The difference between the exposed and unexposed absorption is also an important parameter in defining the linearity of the resist. The larger this difference the more pronounced is the non linearity. For S1813 this difference is much larger at I-line exposures than at G-line exposures, Figure 3-9. As expected the curve is non linear for I-line exposure Figure 3-8 compared to the G-line exposure Figure 3-7.
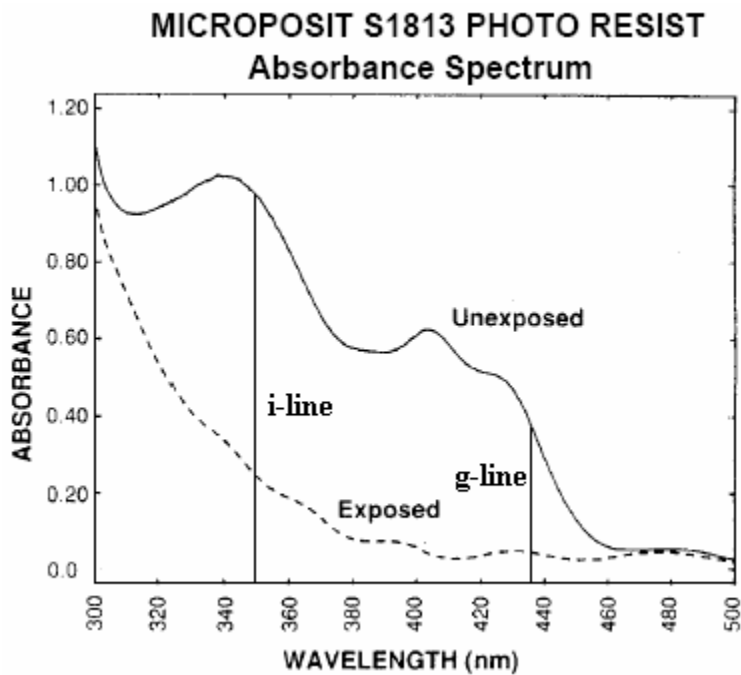
Figure 3-9 Absorbance spectrum of exposed and unexposed S1813 resist (Data provided in Shipley data sheets for S1800 photoresist)

The maximum die size that can be exposed on a stepper is 20 x 20 mm and this restricts the maximum aperture size of optical elements that can be fabricated using the stepper to 20 mm. For fabricating optical elements with an aperture size greater than 20 mm additive lithography can be performed on the aligner by using the photoresist characteristic curve at the I-line. The exposure energy delivered by the Quintel aligner in

our lab is 4.2 mJ/(cm2sec). Thus the clear through exposure for 1800 nm of S1813 is 52 mJ/(cm2sec). The minimum shutter open time on the aligner is 0.5 sec and it allows for time increments of 0.1 sec. Because of the shutter time limitation the aligner provides less flexibility and tolerance in the fabricating process. The etching process can be morphed as will be shown in Chapter 7 to compensate for these limitations in the exposure process.

From the curves we obtain the threshold or bias exposure time for the photoresist, corresponding to the inflection point. For the linear photoresist we can calculate the slope of the curve in the region of interest and for the non linear curve we can obtain a polynomial fit to the curve.

The linear fit for the 1813 curve in Figure 3-7(a) gives us the relations between the exposure time 't' and the required height 'h' as,

$$t = \frac{h + 1.155}{3.74} \qquad\qquad 3.5$$

The polynomial fit to the SPR curve in Figure 3-7(b) is,

$$t = -0.00255\,h^3 + 0.04491\,h^2 + 0.15526\,h - 0.00101 \qquad\qquad 3.6$$

The first step in the fabrication of multilevel elements using additive lithography is the biasing of the photoresist which is performed by exposing an open aperture of the size of the diffractive to be fabricated with the threshold exposure time at the inflexion point in

the response curve. The exposure time for the masking patterns is then calculated either from the slope or from the polynomial fit obtained for the curve.

3.2.2 *Entire Domain Masking*
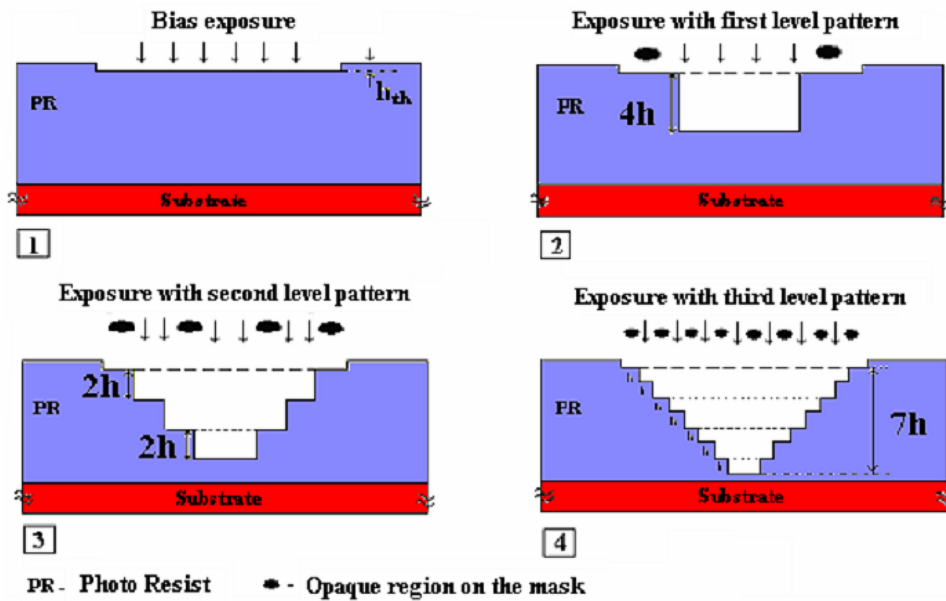
Figure 3-10 Additive lithography process using entire domain masking.

A refractive lens can be transformed into a multilevel diffractive structure using techniques discussed in Chapter 2. This multilevel structure can then be split into multiple masking patterns, addition of which would lead to the desired multilevel diffractive structure. For fabricating an 8 level diffractive we will need 3 masking patterns. The additive lithography process with these three mask patterns is shown in Figure 3-10. This masking scheme utilizes quantization of the height such that the level heights are all equal [43].
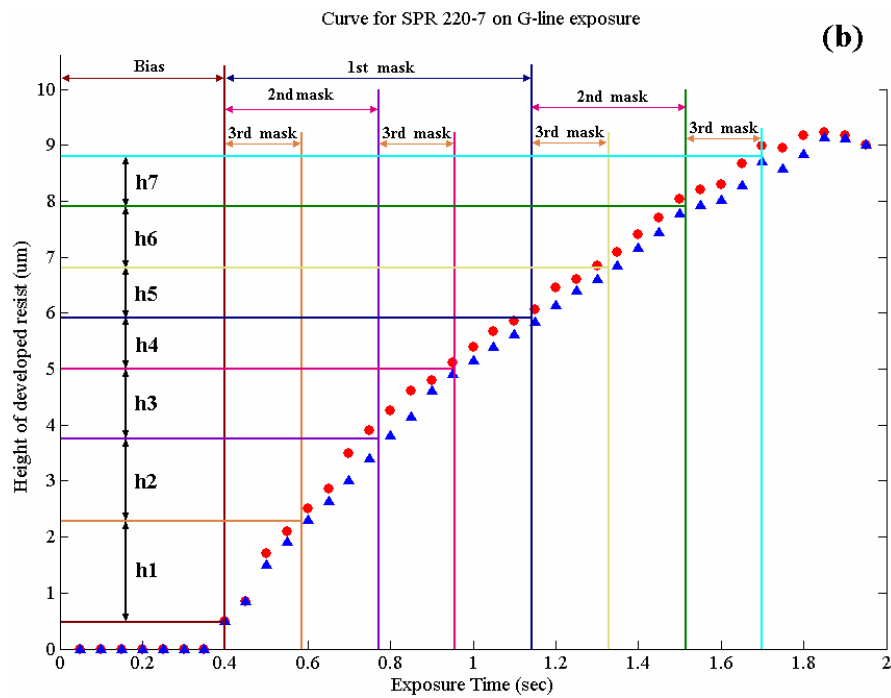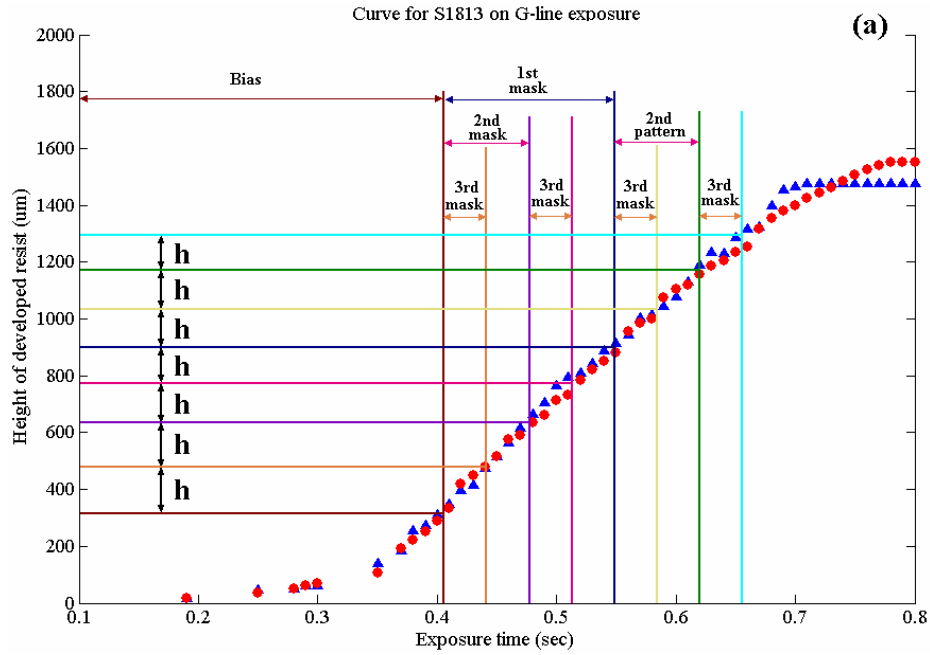
Figure 3-11 Addition of 3 mask patterns on (a) The linear curve for S1813 giving equal level heights. (b) The non linear curve for SPR 220-7 showing unequal level heights. The exposure of 2nd mask affects two points on the curve and 3rd mask pattern affects four points on the curve.

For the entire domain masking scheme these masking patterns extend over the entire aperture of the lens. Thus exposure through the 2nd mask after exposing with the 1st mask affects two points on the contrast curve as shown in Figure 3-10 and Figure 3-11. Similarly exposure through the 3rd mask pattern affects four points on the contrast curve. The exposure time for both these points is the same since they are part of the same mask pattern. The localized slope for the linear working region of S1813 is equal to the global slope of the curve. Therefore addition of exposures over different points due to exposures using multiple mask patterns leads to equal heights as is seen in Figure 3-11 (a). For a non linear working region as with SPR 220-7 the local slope of these different points affected by the same exposure are different. This leads to unequal level heights as can be seen from Figure 3-11 (b). Therefore photoresists with a linear response are preferred for employing such masking procedures. Thin photoresists usually show a linear response in the region of interest, but for thicker photoresists absorption and the resulting change in propagation characteristics for the bulk medium cause the response to be non linear. This can restrict the range and efficiency of optical elements we can fabricate. The solution to this problem is to correct the resulting height errors in the levels by using morphing schemes during the transfer etching process.

(a)

PAC concentration in the 1813 resist after exposure for 8 level diffractive lens

Height into the resist (um)

Distance from center of lens (um)

Unexposed region

(b)

Central zone of 8 level diffractive lens after developing on 1813 for 632.8 nm

Height into the resist after developing (um)

Distance from center of lens (um)
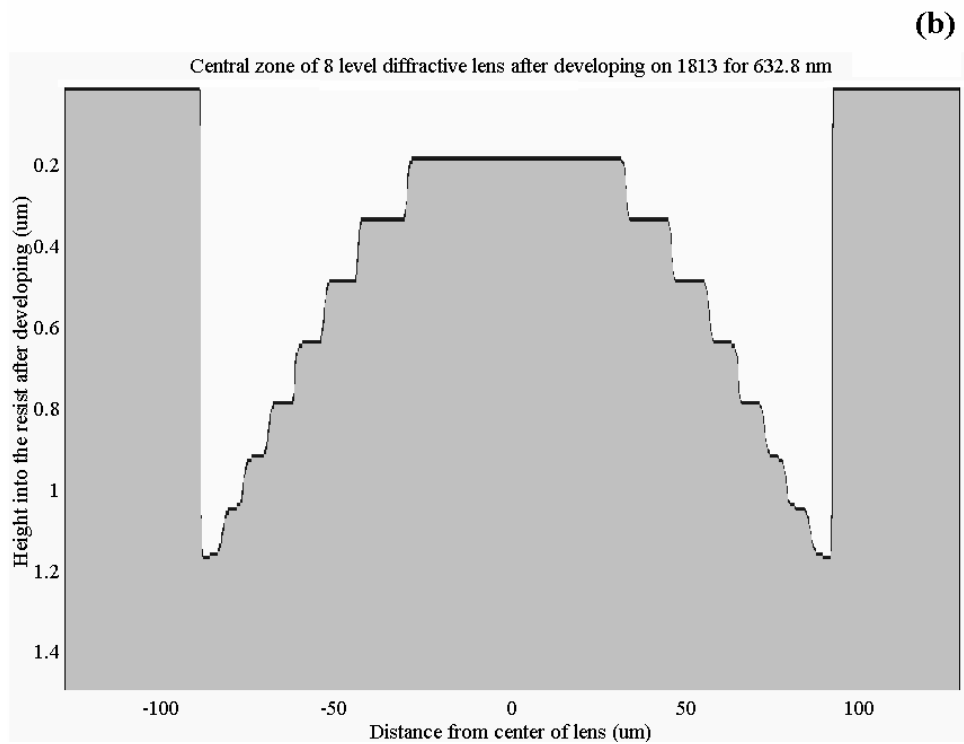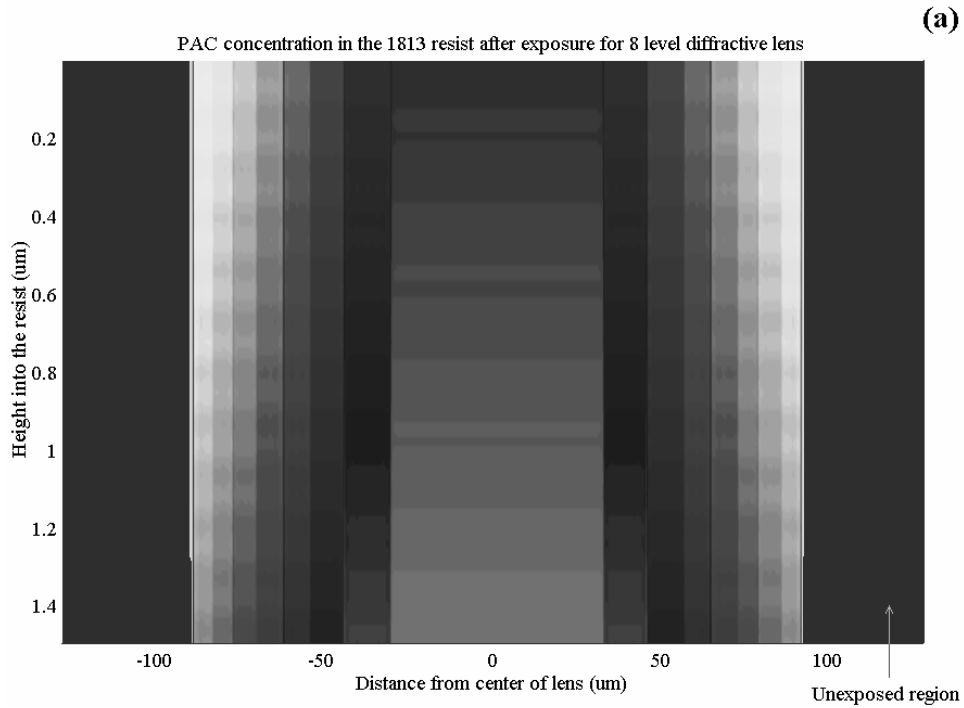
Figure 3-12 First zone of a 8 level diffractive lens using additive lithography for operation at 632 nm. Top: PAC concentration in resist after exposure. Bottom : Final profile on resist after developing.

Figure 3-10 shows the exposure through the first zone of a diffractive lens for operation at 632 nm split up into 8 levels. This involves three masks and an open bias exposure. The exposure modeling is discussed in Appendix A. The two dimensional PAC distribution for the rotationally symmetric diffractive lens, after exposure through all the masking patterns with the appropriate time calculated from the curve in Figure 3-7 (a) is shown in Figure 3-12 (a). For positive resists lower PAC concentrations, increases the dissolution rate in the developer solvent. After the exposures the substrate is immersed in a developer solution for an appropriate period of time. The photoresist is dissolved selectively in the developer solvent with a rate depending on the local PAC concentration after successive exposures with the three masking patterns thus evolving in the final 8 level structure in the resist as shown in Figure 3-12 (b).

Diffractive structures are wavelength dependent and altering one of the design parameters will lead to changes in the other mask parameters for some of the diffractive elements, e.g. lenses, see Chapter 2. Secondly the mask can be used for the fabrication of only one type of phase element. On the other hand, entire domain masking does allow us to use a fairly small number of mask exposures to describe complete elements, generally log2(N) exposures for an N-level element. Sub domain masking provides a greater degree of adaptability, and for example allows us to independently control the design parameters of diffractive elements as well as fabricate various optical functions belonging to a specific set, such as rotationally symmetric functions with a single set of mask patterns.

3.2.3 *Sub Domain Masking.*

It is possible to come up with a set of masking patterns that allow for either non-overlapping exposures or singularly overlapping exposures. For a specific class of diffractive or refractive elements we can generate a basis set of patterns that will allow us to fabricate any element of the group by simple exposure dose control. The process then eliminates the need for linearity in the additive region and thus any photoresist can be employed for fabricating diffractives belonging to that class [44].

Non orthogonal basis set

The individual patterns of the set overlap but only at one specific point on the contrast curve and thus do not need linearity. But the range of elements that can be fabricated using this set is limited.

Consider the class of rotationally symmetric elements such as positive or negative lenses. Circular masking apertures with successively increasing diameters can be used to fabricate these elements. Transparent apertures will allow us to fabricate negative lenses and opaque apertures will allow us to fabricate positive lenses, figure 3-6.
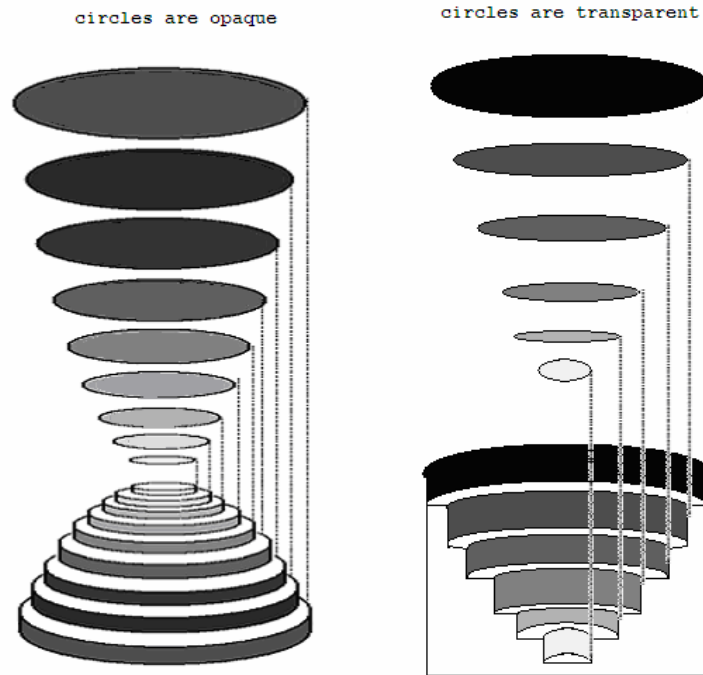
Figure 3-13 Sub domain non orthogonal basis set for rotationally symmetric micro optic elements. Left : positive lens with opaque circles Right: Negative lens with transparent circles.

Orthogonal basis set

An orthogonal set of basis patterns provides maximum flexibility in terms of fabrication. The individual patterns of the set do not overlap in space and thus each exposure is independent of other exposures. The class of rotationally symmetric elements can be represented by a set of concentric rings with incremental diameters. It is possible to fabricate any rotationally symmetric micro optic element using this technique, figure 3-7.
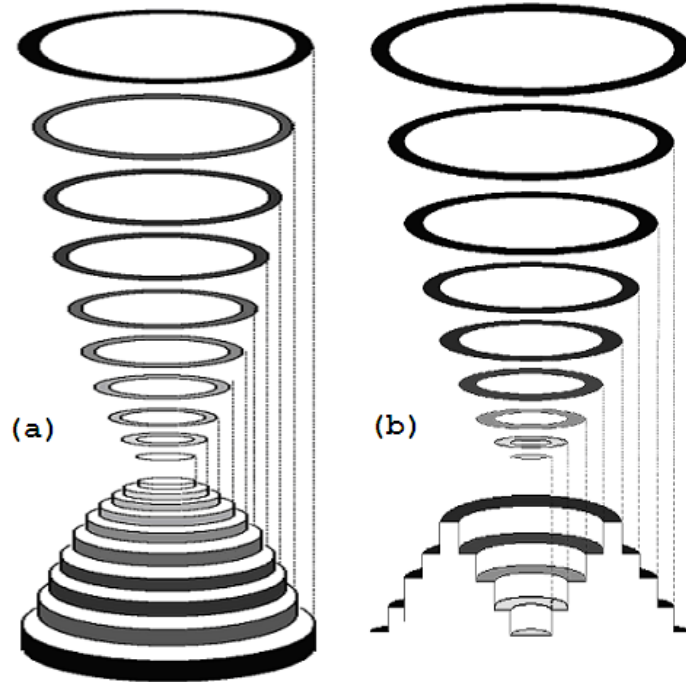
Figure 3-14 Additive lithography using sub domain orthogonal basis set of rings for rotationally symmetric micro optic elements. a) positive lens b) toroidal lens.

A rotationally symmetric optical function $\phi(r)$ can be written as

$$\phi(r) = \exp\left[i\,k\,d(r)\,(n-1)\right]$$
<div align="right">3.7</div>

where d(r) is the height of the photoresist at the position r and n is the refractive index of medium.

The height of the photoresist to be developed off at the position r is then given as

$$h(r) = H - d(r)$$
<div align="right">3.8</div>

where H is the total height of the diffractive or refractive to be fabricated. The problem now is to calculate the time required to sculpt this height h(r).

Thus the optical function $\phi(r)$ can be written in terms of the exposure time as

$$\phi_p = \exp\left[i\ k\ (n-1)\left\{H-\left(\tau_p\ A\right)\right\}\right]$$ 3.9

where τp is the exposure time corresponding to a height hp(r) for the pth ring and is calculated from the numerical fit to the contrast curve in the working region. The factor A is used to adjust for the etch selectivity. A=1 would represent an etch selectivity of 1:1. A mod 2π diffractive structure to be operated at 1550 nm requires total sag of 3380 nm. Thus it is possible to fabricate a diffractive structure on 1813 resist with a total height of 1690 nm and then etch it with a selectivity of A=2 to achieve the required structure.

For an orthogonal basis set the exposures do not overlap but for a non orthogonal basis set the exposure time is added up and the actual exposure time for each pattern is given as,

$$\tau_p = t_p - \sum_{i=1}^{p-1}\tau_i$$ 3.10

where tp is the time calculated from the numerical fit and the summation represents the total exposure time from previous exposures.

Thus if we use N rings to form a rotationally symmetric micro-optic element then the phase function realized can be written as

$$\Phi = \sum_{p=1}^{N} \phi_p \qquad 3.11$$

These rings can be fabricated on a single reticle or multiple reticles depending on the aperture size of the micro optic to be fabricated. In our case we used rings with diameter increments of 4 μm, i.e. ring widths of 2 μm. The stepper does a 5X reduction on the substrate hence the increment of the masking patterns is 20 μm on the reticle. To be able to fabricate micro optic elements with 252 μm apertures 63 rings were fabricated on a single reticle starting with the smallest feature, a circle of diameter 20 μm on the reticle. The successive patterns are rings with successively increasing diameters of 20 μm and width of 10 μm. Thus the largest ring had an outer diameter of 1260 μm.

(a)

(b)
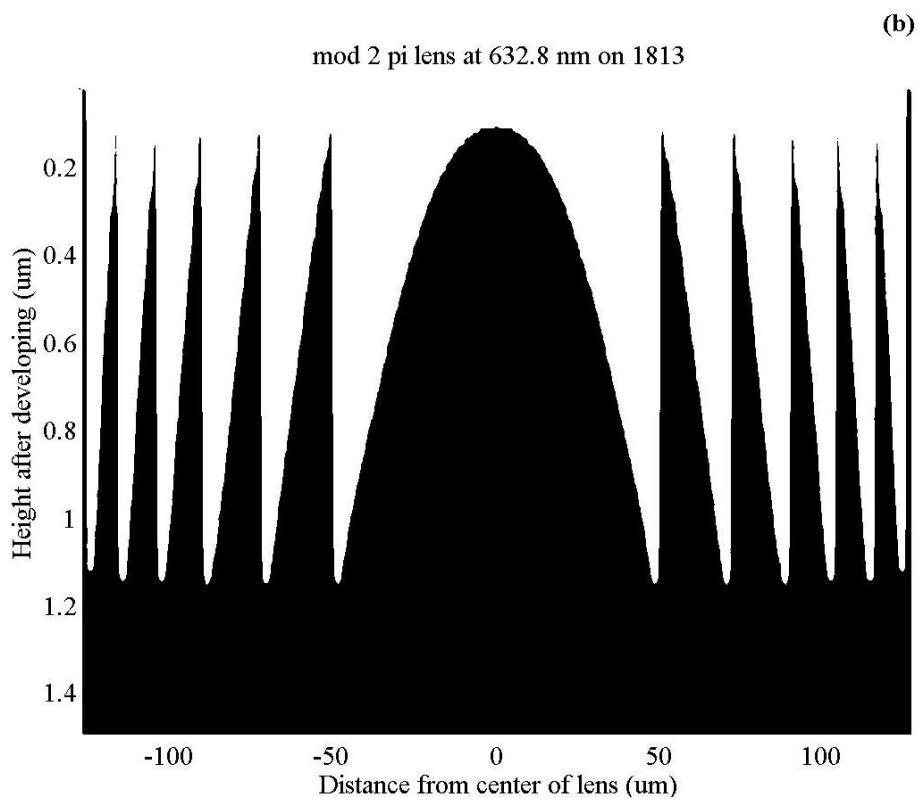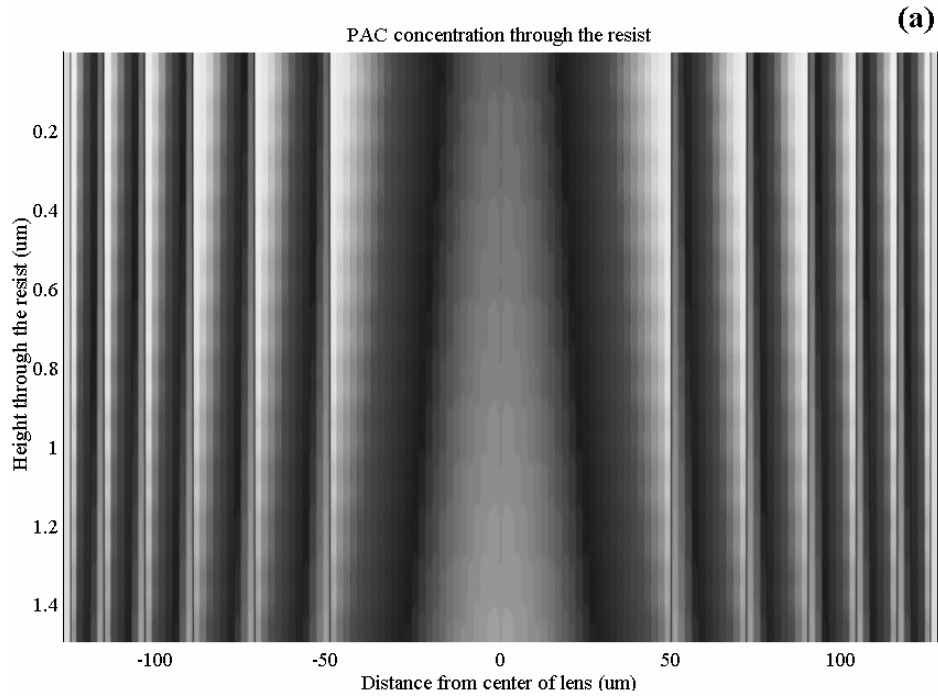
Figure 3-15 mod 2π diffractive lens for operation at 632 nm. (a) PAC concentration after exposure, (b) Resist profile after developing.

The two dimensional PAC distribution for a diffractive mod 2π positive lens fabricated by exposing 63 ring patterns with 2 micron width and exposure time calculated from equation 3.5 for photoresist 1813 is shown in figure 3-8 (top). The resulting profile on the resist after developing is shown in figure 3-8 (bottom).

A finer basis set, i.e. smaller increments in diameter of the rings can be used to get a better representation of the optical function to be fabricated at the cost of fabrication time. As can be seen in figure 3-8, a 2 μm grid is enough since the exposure and developing process provides an almost analog looking profile. Though we expose a single ring at a time the throughput can be easily increased by fabricating multiple similar rings on a reticle thereby allowing us to create multiple elements with the same number of exposures.

3.2.4 *Hybrid Optical Elements*

DOEs such as vortex lenses or spot array generators and other beam shaping elements modify the input beam to render it into the desired output profile. Usually these beam shaping elements are designed to obtain the required pattern in the far field except if the near field intensity distribution is of more interest to the particular application. Thus other optical elements such as focusing lenses are usually inserted in their path so as to obtain the far field distribution at the focal point of the inserted lens. These elements can be multiplexed to provide the combined properties of two optical elements. Hybrid optical elements such as gratings on a positive lens used to correct chromatic dispersion or

introduce dispersion and sub-wavelength structures as anti reflection structures multiplexed with other optical elements are also interesting because of their unique properties. Additive lithography provides a very elegant method of fabricating such hybrid optical elements utilizing single step successive exposures with very high alignment tolerances [46]. The resulting elements can be fabricated as shown in Figure 3-16. The fabricated elements can then be easily etched into the substrate with the required selectivity for operation at the designed wavelength.
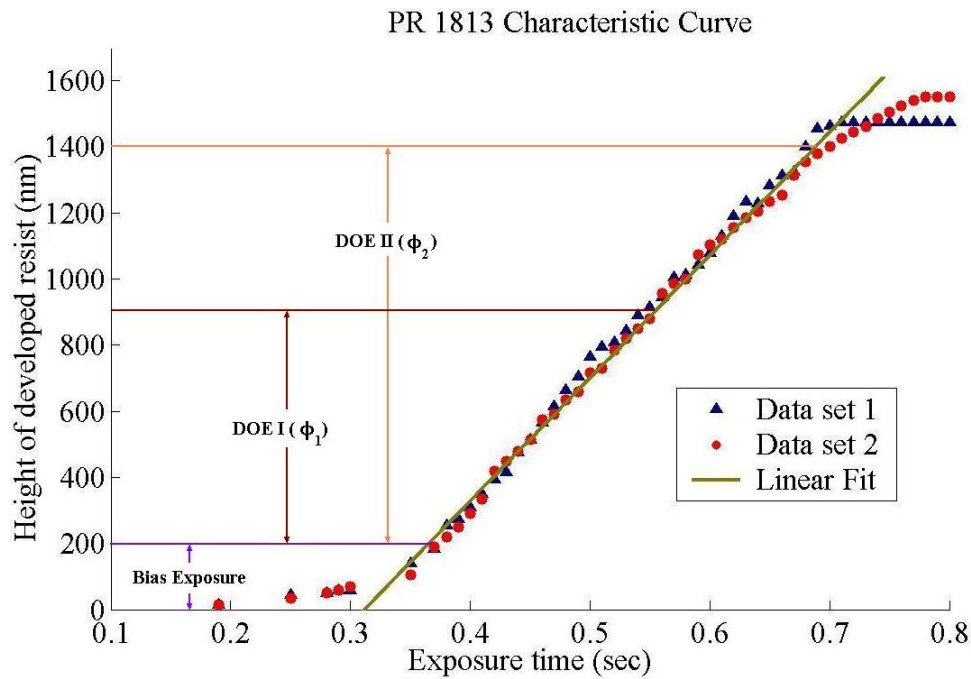
Figure 3-16 Hybrid DOEs fabricated using the contrast curve for S1813

The phase function $\phi 2$ extends over $\phi 1$ and covers a larger portion of the contrast curve than that covered by $\phi 1$. The hybrid element thus formed provides a point by point addition of phase thus modifying the local phase of the input wavefront. This hybrid

element thus provides a modified output wavefront that will form the required intensity distribution in the plane of observation. Multiplexing of two optical elements to form a hybrid element is shown in Figure 3-17. As can be seen the grating extends over a larger region of the contrast curve then that covered by either the lens or he grating by itself.
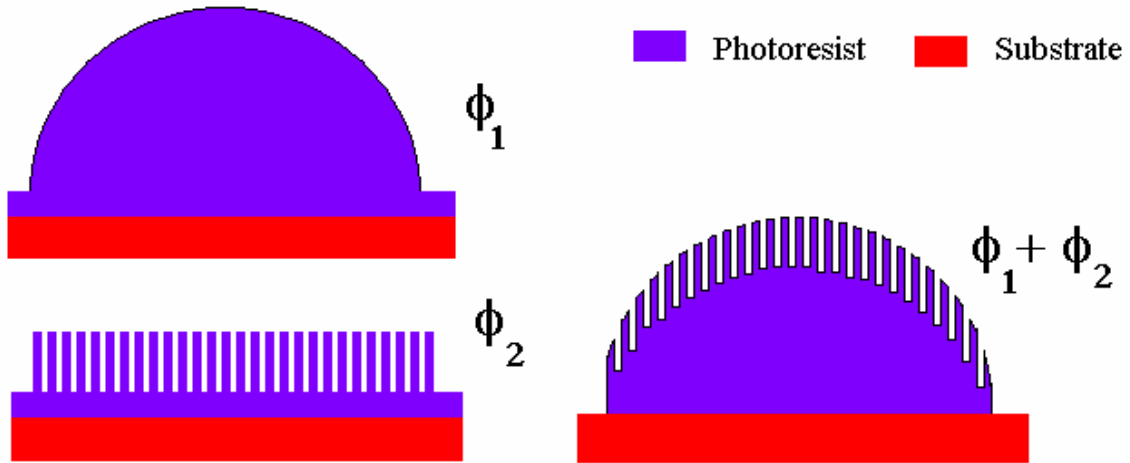
Figure 3-17 . Addition of phase functions to fabricate hybrid optical elements

CHAPTER 4: PRE-SCULPTING AND CONTROLLED REFLOW

FABRICATION OF OPTICAL ELEMENTS

Additive lithography using different masking techniques for fabricating multilevel micro-optic elements was discussed in the previous chapter. As shown through simulations, Figure 3-15, the sixty three level exposure scheme with a 2 μm grid leads to rounding off due to effects of the depth of focus of the exposure system, diffusion of the PAC during PEB and the nature of the developing process. This results in an analog profile on the resist. Though this allows the fabrication of refractive micro-optics, the total time required for exposing one sixty three level lens element increases exponentially as the size of the grid becomes smaller, as shown in Figure 4-1. Another parameter contributing to total exposure time is the stage translation and settling time on the stepper, which is a fixed value per exposure. A large number of levels used results in more stage translation, leading to lower throughput. Thus, fabrication time for a 10x10 array of 250 μm lenses using a 1 μm grid will be 29 min, but for a 10 μm grid it will be 3 min. This does not include the stage translation and settling time.

In an effort to reduce the total process time and thereby increasing the throughput, an alternative technique was developed. Using the sub-domain masking scheme and the photoresist characteristic curve, a multilevel profile is sculpted in the resist. This sculpting is done on a coarse grid, with approximately three to four levels approximating the required final analog profile. The multilevel photoresist structure is then reflowed by melting, to fabricate perfectly analog refractive micro-optics. The coarse grid used in the

pre-sculpting process results in reducing the total exposure time by a factor of ten or more, as compared to using a 2 μm grid. As mentioned earlier, the stage translation and settling take up a large part of the total fabrication time and increase linearly with the number of exposures involved in the fabrication. A coarser grid requires fewer exposures and hence the actual reduction in total fabrication time is a lot higher.
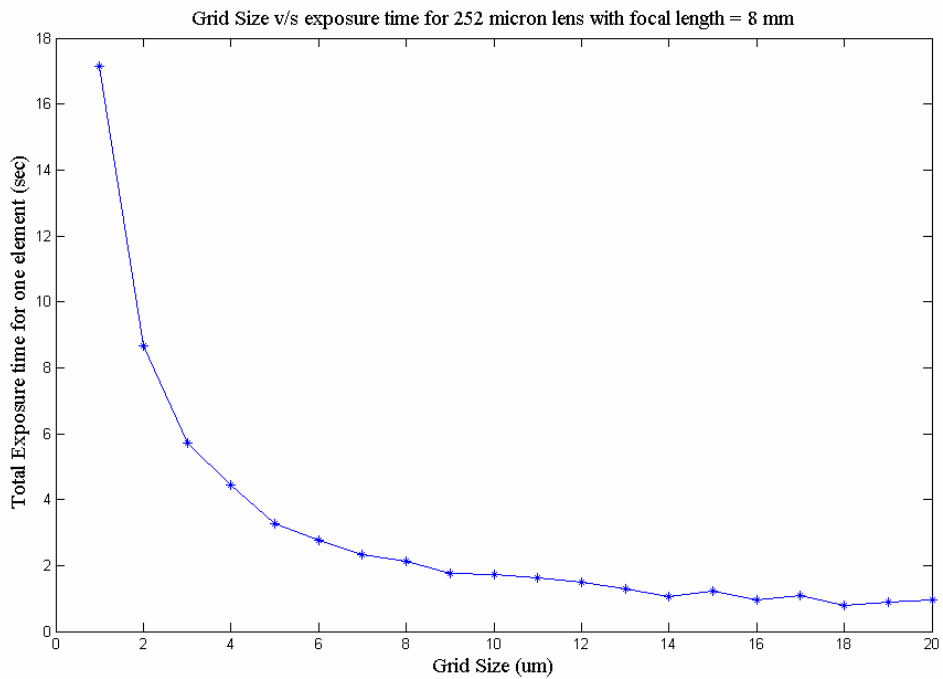
Figure 4-1 Grid Size v/s Total exposure time for a f/32 refractive lens on S1813

The reflow process for forming analog micro-optics is well studied and documented and is widely used in the fabrication of microlens arrays [24-29, 52, 53]. Typically, a solid photoresist pillar formed by standard resist processing is heated beyond its glass transition temperature into the liquid phase. The surface tension and line tension reshapes the initial surface to minimize the surface energy. The final shape represents a local or a

global minimum for that volume of polymer. This imposes significant constraints on the optical parameters that can be obtained using this technique. Unique optical properties are usually obtained by tailoring subsequent process steps, such as transfer etching, to allow better control and conformance to design. As a consequence of the pre-sculpting procedure in our case, the sculpted structure evolves through different stages (corresponding to different local minima). Thus, by controlling the time and temperature unique beam-shaping optical elements can be obtained. As a result, by combining additive methods with pre-existing techniques of analog optics fabrication, we have achieved major improvements in process control and throughput maximization. In this chapter, pre-sculpting of the resist using additive lithographic techniques to extend the flexibility of the reflow fabrication technique is described.

4.1   <u>Photoresist reflow</u>

Photoresist reflow is likely the most efficient method demonstrated for the fabrication of refractive micro lenses with very high numerical apertures. The photoresist reflow process was first demonstrated by creating cylindrical columns in the photoresist and then heating the photoresist beyond its glass transition temperature. Surface tension of the photoresist in its liquid state tends to modify the shape of the initial cylindrical surface to minimize the surface free energy of the structure, resulting in an aspheric shape. Pre-sculpting of the photoresist for approximation of the actual surface of the lens before reflow has also been suggested and implemented using laser beam direct write techniques [25, 26].
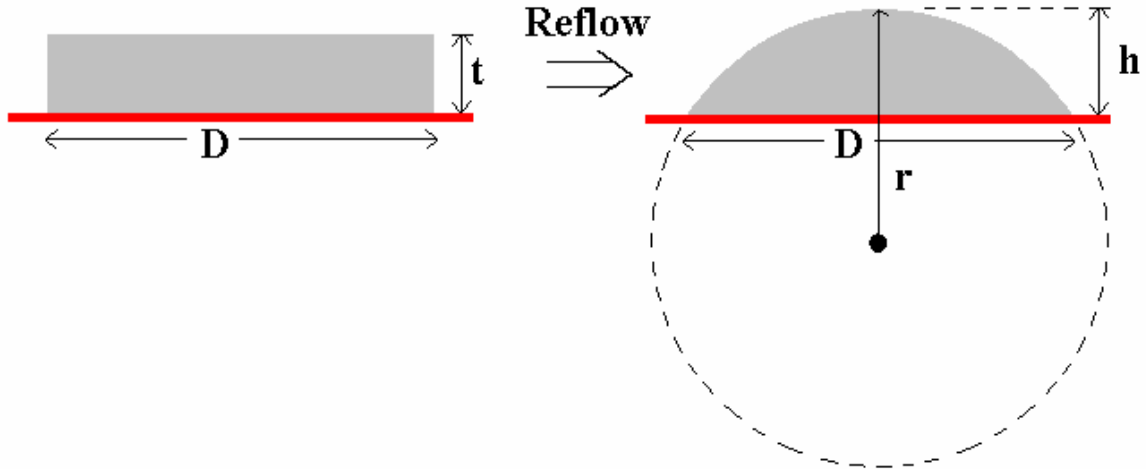
Figure 4-2 Reflow of a resist pillar and resulting approximate spherical cap

The height of the cylinder required before reflow can be determined by considering the final surface to be a spherical cap with height 'h', Figure 4-2. The diameter of the structure and the volume do not change during the reflow. In a real case, however, there would be shrinking of the material due to reduction of solvents during the high temperature reflow process but these effects are neglected. If we assume a cylinder with height 't' and diameter 'D', it will result in a spherical cap of height h > t and radius of curvature at the vertex 'rL' [2].

Because the volume is fixed, we equate the initial volume of the cylinder VC and final volume of the spherical cap VL giving

$$V_C = \frac{\pi D^2 t}{4} = V_L = \frac{\pi}{6} h \left(3 \left(\frac{D}{2} \right)^2 + h^2 \right)$$

4.1

Thus, we have an expression for the initial thickness 't',

$$t = \frac{2h^3}{3D^2} + \frac{h}{2} \qquad\qquad 4.2$$

In reality, the reflow leads to aspheric surfaces and therefore the initial cylinder needs to be thicker than that obtained from equation 4.2. Aspheric surfaces are defined by the sag equation,

$$h(r) = \frac{r^2 / r_L}{1 + \sqrt{1 - (1+k)\frac{r^2}{r_L^2}}} + a_2 r^2 + a_4 r^4 + \dots \qquad\qquad 4.3$$

where k is the conic constant representing different surfaces: k = 0 spherical; k = -1 parabolic; k > 0 oblate ellipsoid; -1 < k < 0 prolate ellipsoid; and k < -1 hyperboloid. The radius of curvature at the vertex of the aspheric surface is then,

$$r_L = (k+1)\frac{h}{2} + \frac{(D/2)^2}{2h} \qquad\qquad 4.4$$

The focal length of the lens is related to the radius of curvature and is given as,

$$f = \frac{r_L}{n(\lambda) - 1} \qquad\qquad 4.5$$

4.2   Limitations of photoresist reflow

The reflow process is simple and efficient for fabricating refractive structures but has several important limitations,

1. Initial resist thickness determines the final sag of the structure and hence the focal length. Thus, to fabricate lenses with different focal lengths the initial thickness of the resist needs to be changed. Therefore it is not possible to fabricate a microlens array with varying focal lengths on the same wafer.

2. The total surface area is smaller for thinner cylinders. In this case, line tension dominates, driving the reshaping process through the edges of the structure. The surface tension of the structure is not enough to drive the change in surface shape, hence leading to non local minimal surfaces as shown in Figure 4-3. Thus, low sag structures cannot be fabricated by simply coating a thinner layer of resist since this will lead to undesired resist profiles.
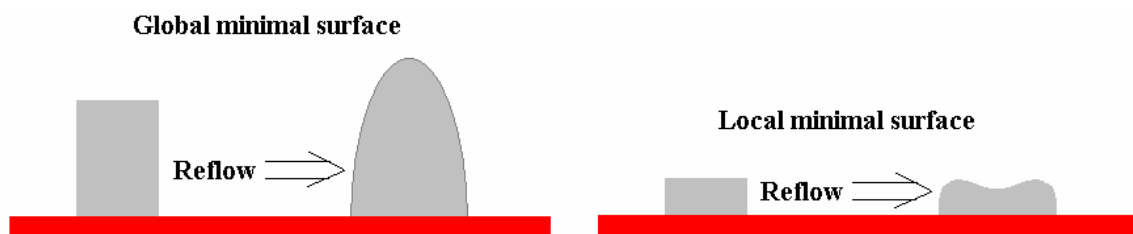
Figure 4-3 Global and Local minimal surface formed as a result of thick and thin cylinders respectively.

3. It is not possible to fabricate other refractive optical elements for beam shaping by using the reflow technique employing simple structures such as cylindrical or rectangular pillars. Thus, the technique is restricted to the fabrication of positive refractive aspheric lenses.

Additive lithographic pre-sculpting can be employed to alleviate these limitations. In addition, process control is greatly enhanced due to this added degree of freedom. This enables the fabrication of complex shapes with simple initial geometries. Micro lens arrays with each lens element having different focal length and refractive beam-shaping elements can be fabricated by pre-sculpting the resist using additive lithography. But before going into pre-sculpting schemes for optics fabrication we will first try to develop a 2-D analytical model to understand the shape of the aspheric surfaces formed using photoresist reflow.

4.3   2-D Analytical Model for reflow

In order to quantitatively define the optical surface, it is necessary to be able to predict the surface profile of the reflowed structures. To understand the effects of pre-sculpting and the motivation for initial geometry modification, we will need to understand the physics of the basic 'reflow' process. An analytical solution to the problem of reflow for simple geometries such as a cylindrical column is presented. The problem of polymer reflow and shape evolution as a function of time, temperature and other process parameters involves very complicated computational fluid dynamics. Thus, a simple

model to determine the final minimal energy surfaces for simple geometries has been developed and the obtained results are presented here.

For a liquid drop on a solid substrate, the shape of the liquid surface is governed by the free energy of the solid-liquid system. The shape at the three phase interface is given by Young's equation [49,],

$$\gamma_{SV} - \gamma_{SL} - \gamma_{LV} \cos\theta_e = 0 \qquad\qquad 4.6$$

where γsv is the surface tension at the solid vapor interface, γlv is the surface tension at the liquid vapor interface, γsl is the surface tension at the solid liquid interface and 'θe' is the macroscopic contact angle, Figure 4-4. The three surface tension terms in equation 4.6 define the liquid wetting on the solid surface.
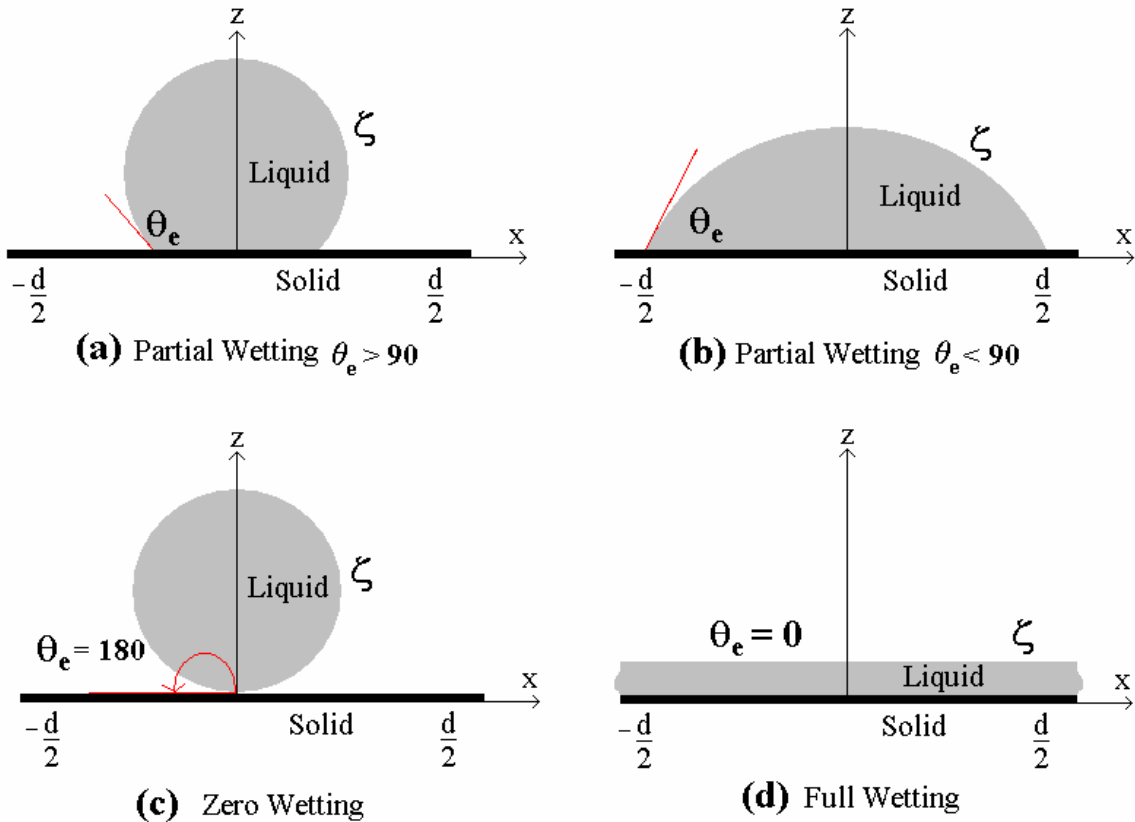
Figure 4-4 Wetting of a Liquid drop on a flat substrate.

The free energy of the liquid has a volume contribution and a surface contribution. The liquid forms a surface that would minimize the surface free energy contribution of the liquid and the volume is assumed fixed. The shape of this minimal energy surface depends on the properties of the liquid and the solid, the surface morphology of the solid and hydrostatic forces. Depending on these parameters, the liquid will form a specific contact angle with the surface. In actuality there could be a range of contact angles bound by minimum wettability (defined by an advancing contact angle) and a maximum wettability (defined by a receding contact angle). The actual contact angle for the specific solid-liquid system has to lie within these bounds. This phenomenon is termed the contact angle hysteresis. This is another reason why the final profile is not always easily

66

predicted when using reflow methods. The resulting profile depends on a number of process parameters.

If γSV is less than γSL, then the contact angle θe is larger than 90o and if γSV is more than γSL then the contact angle θe is less than 90o. Partial wetting of the surface occurs in the range 0o< θe < 180o. For the case where θe=180o, the liquid does not wet the surface at all, resulting in a single point of contact and for θe=0o, the liquid completely wets the surface, Figure 4-4 c and Figure 4-4 d respectively.

Thermodynamic and mechanical equilibrium is established for the liquid drop by minimizing the free energy of the liquid. The free energy has contributions from the internal energy that depends on the volume, the surface energy that depends on the surface area and the line energy that depends on the discontinuities in the surface [50]. The volume of the liquid does not change during reflow and hence, the only contribution to the free energy comes from the surface and the line tensions. This free energy is minimized by minimizing the surface area and the line length of the structure. We neglect the line energy contribution for reflow of tall columns. This can be done by considering that the original surface does not have any sharp discontinuities, except at the liquid solid interface. This is a reasonable assumption because the surface tension contribution is much larger than the line tension in the system. The line tension term dominates during the reflow of thin cylinders and the resulting final shape is a local minimal surface as shown in Figure 4-3. In our analysis we will ignore this effect and discuss the reflow of cylinders where the surface tension term dominates the process.

We will consider a two dimensional problem where the liquid surface shape factor 'ζ' depends only on the x coordinate, i.e. $\zeta \equiv \zeta(x)$. The total free energy defined as 'U' of the liquid drop on the substrate is derived from thermodynamics and Uo is a constant chemical potential.

Thus the free energy of the drop is given as [51]

$$U = U_0 + \int_{x_{min}}^{x_{max}} \left[-S + \frac{\gamma}{2} \left[\frac{d\zeta}{dx} \right]^2 + P(\zeta) + G(\zeta) \right] dx \qquad 4.7$$

Using equation 4.6 the term S is defined as the spreading coefficient and is given as

$$S = \gamma_{SV} - \gamma_{SL} - \gamma_{LV} = -\gamma(1 - \cos\theta_e) \qquad 4.8$$

$\gamma = \gamma LV$ is the liquid vapor surface tension. $P(\zeta)$ is due to Van der Waals forces or double layer forces that generally affect the shape at the solid liquid interface and exist within 100 nm of this interface. This gives rise to a microscopic contact angle close to the solid liquid interface. We neglect this term in our analysis. The term $G(\zeta)$ describes hydrostatic and gravitational effects and is given as [51]

$$G(\zeta) = \rho g (\frac{\zeta^2}{2} + \zeta H) \qquad 4.9$$

where 'ρ' is the density of the liquid and 'g' is the gravitational acceleration. 'H' in this case is the difference in level between the solid plate and the liquid surface.

On minimizing the free energy 'U' with respect to 'ζ' and taking the first integral we get the condition for mechanical and thermodynamic equilibrium as [51]

$$-\frac{\gamma}{2}\left[\frac{d\zeta}{dx}\right]^2 - G(\zeta) + S = 0 \qquad\qquad 4.10$$

Experiments show that the footprint of the structure does not change during the reflow process. Since the volume does not change it is evident that the sag of the lens is larger than the height of the photoresist column we begin with.

The boundary conditions for this problem is then defined as

$$\zeta = h \text{ and } \frac{d\zeta}{dx} = 0 \text{ at } x = 0 \qquad\qquad 4.11$$

$$\zeta = 0 \text{ at } x = \pm D/2 \qquad\qquad 4.12$$

We substitute equation 4.8 and 4.9 into equation 4.10 to get

$$\frac{\gamma}{2}\left(\frac{d\zeta}{dx}\right)^2 - \frac{\rho g \zeta^2}{2} - \rho g \zeta H - \gamma(1 - \cos\theta_e) = 0 \qquad\qquad 4.13$$

On applying the first set of boundary conditions in equation 4.11 to equation 4.13 we have

$$\frac{\rho g h^2}{2} + \rho g h H + \gamma(1 - \cos\theta_e) = 0 \qquad\qquad 4.14$$

On rearranging the terms and adding (H2-H2) we get

69

$$(h + H)^2 - H^2 - \frac{2\gamma}{\rho g}(1 - \cos \theta_e) = 0 \qquad \text{4.15}$$

Solving this equation for (h+H) we have

$$h + H = \sqrt{ H^2 - \frac{2\gamma}{\rho g}(1 - \cos \theta_e) } \qquad \text{4.16}$$

Rearranging the terms in equation 4.13 we have

$$\frac{d\zeta}{dx} = \sqrt{ \frac{\rho g}{\gamma} \left[(\zeta + H)^2 - \left(H^2 - \frac{2\gamma}{\rho g}(1 - \cos \theta_e) \right) \right] } \qquad \text{4.17}$$

Substituting equation 4.16 into 4.17 and setting u=ζ+H we have

$$\frac{du}{\sqrt{u^2 - (h + H)^2}} = \sqrt{ \frac{\rho g}{\gamma} } \, dx \qquad \text{4.18}$$

Let

$$u = (h + H) \cosh(\alpha)$$

$$du = (h + H) \sinh(\alpha) \, d\alpha \qquad \text{4.19}$$

Substituting 4.19 into 4.18 and rearranging we have

70

$$\frac{sinh(\alpha)}{\sqrt{cosh^2(\alpha)-1}} \, d\alpha = \sqrt{\frac{\rho g}{\gamma}} \, dx \qquad\qquad 4.20$$

Recognizing that cosh2(α)-sinh2(α)=1 and integrating we have

$$\alpha = \sqrt{\frac{\rho g}{\gamma}} \, x + C \qquad\qquad 4.21$$

Substituting for α and for u into 4.21 we have

$$cosh^{-1}\left(\frac{\zeta + H}{h + H}\right) = \sqrt{\frac{\rho g}{\gamma}} \, x + C \qquad\qquad 4.22$$

At x = 0, ζ = h and this gives C = 0. At x = ± d/2, ζ = 0 and substituting this into equation 4.22 with C = 0 we have

$$\frac{H}{h + H} = cosh\left(\sqrt{\frac{\rho g}{\gamma}} \, \frac{d}{2}\right) \qquad\qquad 4.23$$

Rearranging equation 4.22 with C=0 we have

$$\zeta = (h + H)\cosh\left(\sqrt{\frac{\rho g}{\gamma}}\, x\right) - H \qquad\qquad 4.24$$

Another constraint in the reflow process is the volume. The initial volume of the cylinder of resist is td where t is the thickness and d is the diameter of the initial cylinder. Thus equating the initial and final volumes we have

$$\int_{-\frac{d}{2}}^{\frac{d}{2}} \zeta \, dx = td \qquad\qquad 4.25$$

Substituting for ζ from equation 4.24 and integrating we have

$$(h + H) = \frac{d}{2}\sqrt{\frac{\rho g}{\gamma}}\, \frac{t + H}{\sinh\left(\frac{d}{2}\sqrt{\frac{\rho g}{\gamma}}\right)} \qquad\qquad 4.26$$

Squaring equation 4.26, substituting for (h+H)2 from equation 4.23 and solving for H we have

$$H = \frac{\beta\, t}{\tanh(\beta) - \beta} \qquad\qquad 4.27$$

where

$$\beta = \sqrt{\frac{\rho g}{\gamma}}\ \frac{D}{2} \qquad\qquad 4.28$$

The shape of the final surface is then given as

$$\zeta(x) = \frac{H}{\cosh[\beta]}\cosh\left[\sqrt{\frac{\rho g}{\gamma}}\ x\right] - H \qquad\qquad 4.29$$

where H is given from equation 4.27 and 4.28 and t is the initial thickness of the cylinder.

The reflow technique can be used to fabricate very high numerical aperture aspheric surfaces. Pillars of photoresist are formed on the substrate by exposing a bright field mask with circular opaque regions. Increasing the temperature of the substrate-photoresist system beyond the glass transition causes the photoresist to behave like a solid-liquid system. The surface tension of the liquid photoresist drives surface shape modification, resulting in the final surface defined by equation 4.29. In the next chapter we will show how our analytical model fits the fabricated surfaces using reflow. It is also possible to use other masking shapes such as rectangles, ellipses, bent cylinders, etc. to fabricate more complicated final surfaces.

Since the contact angle cannot be smaller than the receding contact angle the final surface shape obtained using simple pillars of photoresist is limited. As seen from equation 4.6 this is controlled by the interfacial tension γSL, γSV and γLV. Various methods have been developed to modify these parameters to obtain more interesting final surface

profiles after reflow [52, 53]. Though these techniques provide unique minimal surfaces, precise control of the shape is difficult to achieve.

4.4   Pre-sculpting scheme

Pre-sculpting of the photoresist using additive lithographic techniques before reflow combined with process time and temperature control help alleviate many of the limitations of traditional reflow [45]. It also allows us to fabricate more controlled surfaces while extending the range of surfaces that can be obtained using this technique. Using a set of circular transmitting apertures on a dark field mask and a set of circular opaque patterns on a bright field mask, the resist can be shaped to any desired multilevel initial profile corresponding to the desired final rotationally symmetric analog surface. This enables us to efficiently fabricate other refractive beam shaping elements on the photoresist such as toroidal lenses. The volume and the footprint of the photoresist remain constant during reflow. Pre-sculpting can be thought of as a way to adjust the initial volume or surface shape of the cylinder before reflow by removing controlled volumes of photoresist in different areas of the element. The height can be kept constant to avoid local minimas during reflow. The volume can be adjusted by exposing smaller cylinders to sculpt the large patterned cylinder without changing the total height of the structure. This method of volume sculpting will also allow us to modify the sag of the lenses without having to adjust the initial thickness of the photoresist and enable fabrication of arrays of elements such as lenses on the same wafer with each element having a different focal length. Pre-sculpting to approximate the final required surface and controlling the time and temperature of reflow will allow for fabrication of more

74

controlled surfaces that need not be the global minimal surface. Some of these techniques

for sculpting are represented schematically in Figure 4-5.
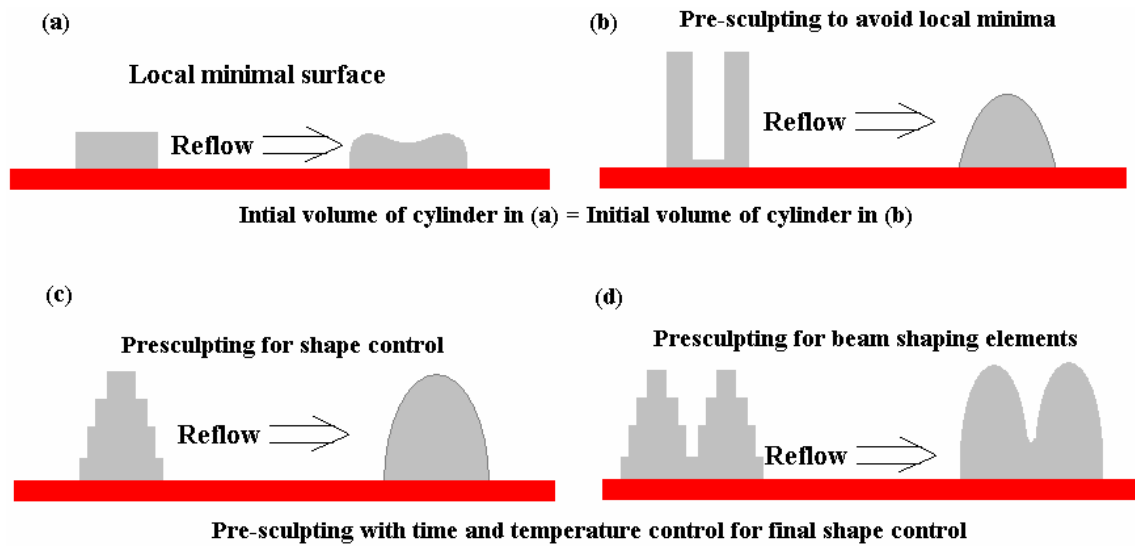
Figure 4-5 Techniques for presculpting to avoid (a) local minimas and to extend
flexibility of reflow fabrication process.

In the next chapter we will discuss the fabrication of refractive optical elements using

these pre-sculpting techniques and analyze the resulting minimal surfaces.

CHAPTER 5: MICRO-OPTICS FABRICATION USING ADDITIVE LITHOGRAPHY

The additive lithographic technique for the fabrication of refractive and diffractive optical elements was discussed in Chapter 3. In this chapter, we will discuss the fabrication of various optical elements using a wafer stepper and aligner. We will demonstrate fabrication using both thin and thick photoresists coated on either glass or silicon substrates, using the additive technique and masking schemes introduced in Chapter 3. he characteristic curves for S1813 and SPR220-7 photoresist introduced in Chapter 3 will be used for determining the exposure times. We will discuss the performance of these fabricated elements in terms of diffraction efficiency and output profiles. Finally we will present the method of pre-sculpting using sub-domain masking schemes for the fabrication of refractive optical elements by employing the photoresist reflow method.

5.1   Entire Domain Masking

A preliminary test of the additive process was performed by fabricating positive diffractive micro-lenses using the entire domain masking technique. As discussed in Chapter 1 and Chapter 3, an 8 (2N) level lens needs N=3 masking patterns and a bias open aperture corresponding to the size of the fabricated element. The mask used on the stepper and the close-up of the first exposure pattern is shown in Figure 5-1. The RMS windows are necessary to ensure that the mask is aligned with the stepper system. They help to remove the translation and rotational errors and align the center of the mask with

the axis of the projection system for repeatability. The first row on the mask shows a circular aperture for bias exposure. The three masking patterns for fabricating the eight level diffractive positive lenses are on the second row. The third row has three patterns corresponding to a different lens design. Multiple patterns on the mask can be individually exposed, using the aperture control features available on the stepper. This allows us to place all the masking patterns needed for the fabrication on the same mask, thus reducing the overall cost of mask fabrication. As can be seen from Figure 5-1, patterns corresponding to other optical elements can be easily added onto this mask if required, and these patterns are then selectively exposed for fabricating the corresponding elements.
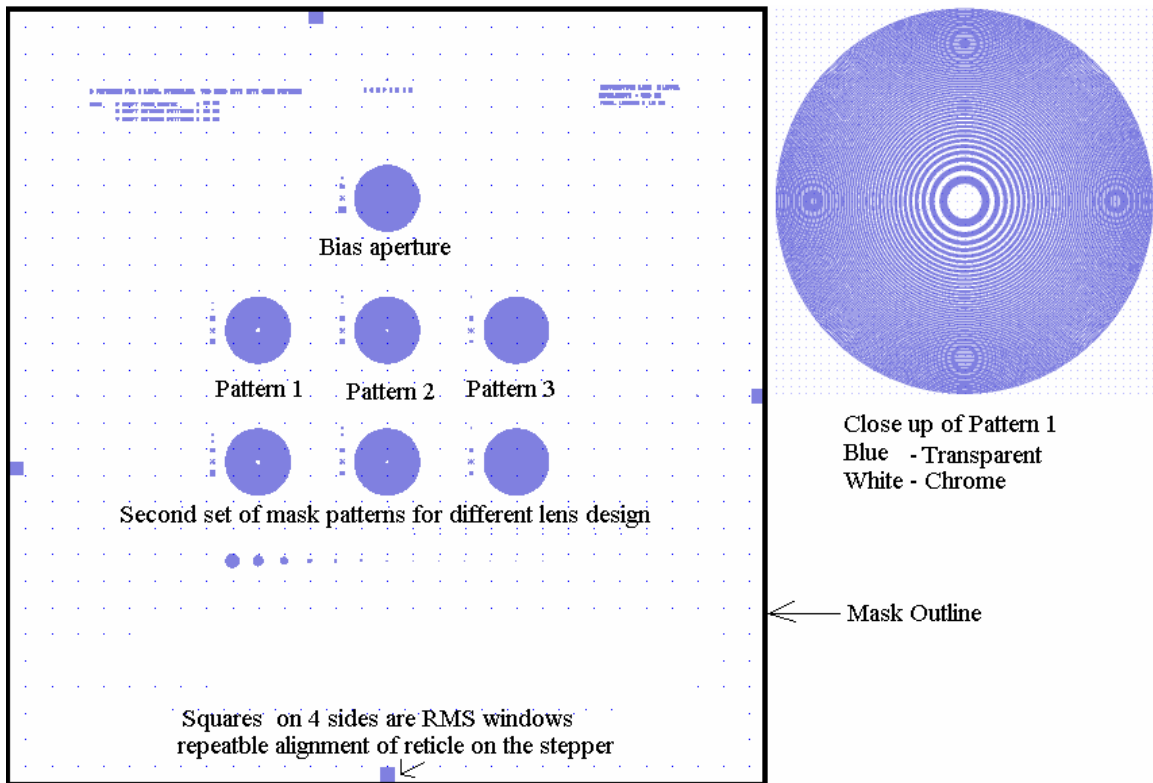
Figure 5-1 Mask pattern for fabricating positive diffractive lens on the stepper

A mod 2π lens with a focal length of 1 mm and a 2 mm aperture to be operated at 632 nm was fabricated on a 1.5 μm thick S1813 layer coated on a fused silica glass substrate using the mask shown in Figure 5-1. The size of the pattern is five times larger on the mask since the stepper performs a 5X reduction.

The fabrication process started with spin coating a uniform 1.5 μm layer of S1813 photoresist on a 4″ diameter, 1mm thick fused silica glass substrate at 3000 rpm. The wafer was then baked in a convective oven at 105oC for 45 min to remove the solvents in the film and then allowed to cool down to room temperature for 30 min before exposure. The contrast curve in Figure 3-7 for S1813 gives us a bias exposure time of 0.37 sec. The three patterns for fabricating the eight level positive diffractive lens were then exposed for 0.18 sec, 0.085 sec and 0.04 sec respectively. The wafer was then developed in a 5:1 mixture of de-ionized water: 351 developer for 60 seconds to obtain a diffractive structure with a total sag of 976 nm on the photoresist. This is the height corresponding to mod 2π on S1813 with refractive index of 1.64 at 632.8nm. The intensity delivered at the substrate on the GCA 6300 wafer stepper with a 350W lamp is 150 mJ/(cm2sec). Hence the energy delivered to the substrate during the exposures can be easily computed.

Figure 5-2 shows the 3-D and 2-D surface profile of the lens on the photoresist measured using the Zygo white light interferometer. The level heights on the photoresist were 140 nm with an accuracy of ±12nm. Any alignment errors present in the exposure process would leave spikes or sharp dips at the edge of the levels. The absence of such peaks and holes at the level edges in Figure 5-2 is an indication that the alignment was very

accurate. The advantage of the additive technique on the stepper lies in the accuracy and simplicity of this alignment. The alignment error without removing the mask or the wafer during the successive exposures was measured to be $\leq \pm 50$ nm on the stepper. This is the tolerance to be expected in the additive process using automatic alignment on a stepper.
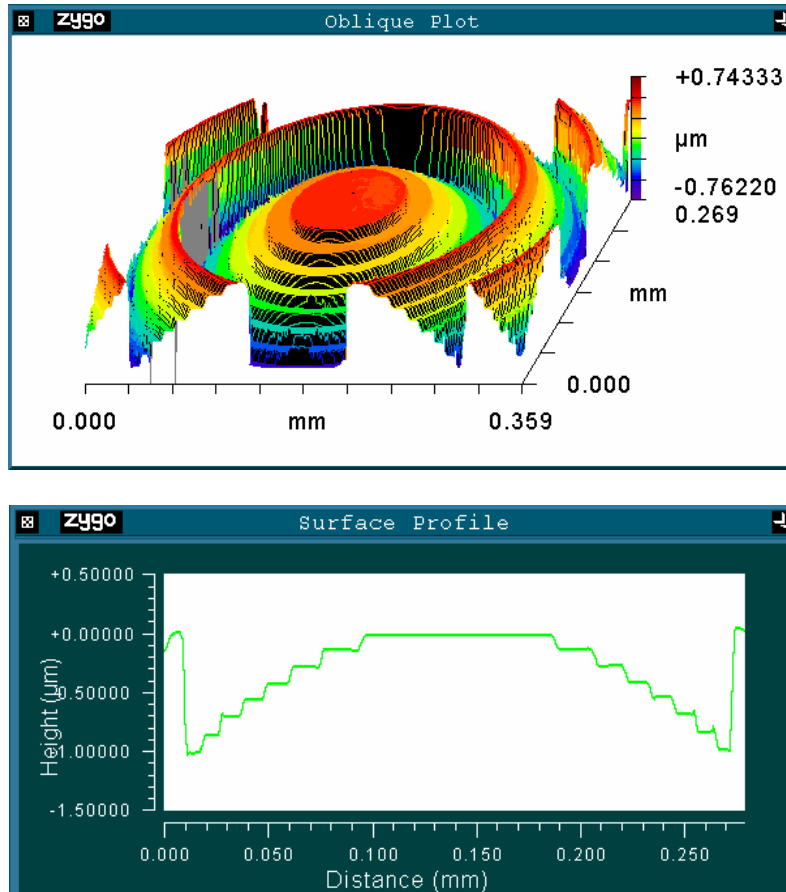
Figure 5-2 3-D and 2-D profiles of the first zone of a mod 2π eight level positive lens on S1813 for operation at 632.8 nm. Height of the structure is 976nm.

The profile should ultimately be transfer etched into the substrate, since environmental effects tend to deteriorate the photoresist. When transfer etching, there are three options. The first option is to create the element on the photoresist based on the refractive index of

the fused silica substrate at the given wavelength (1.64 at 632.8 nm). This method would result in a 1375 nm element in photoresist and utilize a 1:1 etch selectivity for transferring the photoresist pattern into the substrate. The second option would be to create the element based on the photoresist refractive index at the given wavelength, and then use the etching selectivity given by the ratio of (nresist-1) to (nglass-1) where nresist and nglass are the resist and glass refractive indices at the operating wavelength (1.64 and 1.46 for resist and glass respectively at 632.8 nm). This second option makes it possible to test the fabricated optical elements on the resist before transfer etching into the substrate. The third option is to fabricate elements with a suitable initial height on the photoresist. This can then be etched into the substrate with a selectivity given by the ratio of the required height on the substrate at the operating wavelength to the initial height on the resist. This method will be useful in cases where the required height on the substrate is either too shallow to be fabricated with good accuracy or too thick to be fabricated on a thin resist. For e.g. at 250 nm the height of a mod 2π, 8 level diffractive on glass is 492 nm, requiring the level heights to be 70 nm. It was mentioned in Chapter 3 that the additive process has a ±12 nm variation in level heights due to inconsistency in the shutter open time. In this case, this inconsistency leads to a 21% error in the level heights thereby reducing the diffraction efficiency of the fabricated diffractive elements. Hence, it would be better to fabricate a structure with a height of 986 nm or 1478 nm on the photoresist and transfer etch into the substrate with a selectivity of 0.5 or 0.33 respectively. This transfer etching process of the fabricated profiles on the photoresist into the substrate will be discussed in Chapter 6.

The bias exposure removes approximately 300 nm from the top of the resist. The height of the fabricated optical element is 1000 nm and the initial resist layer thickness is 1500 nm. Thus we are left with a 200 nm layer of photoresist under the optical element. These parameters will determine the exact transfer etching time and hence need to be measured before the resist profile is transfer-etched into the substrate. A thick layer of resist left under the optical element is not recommended as this will slow down the transfer etching process dramatically, especially in the case of high selectivity etching and may also affect etch characteristics.
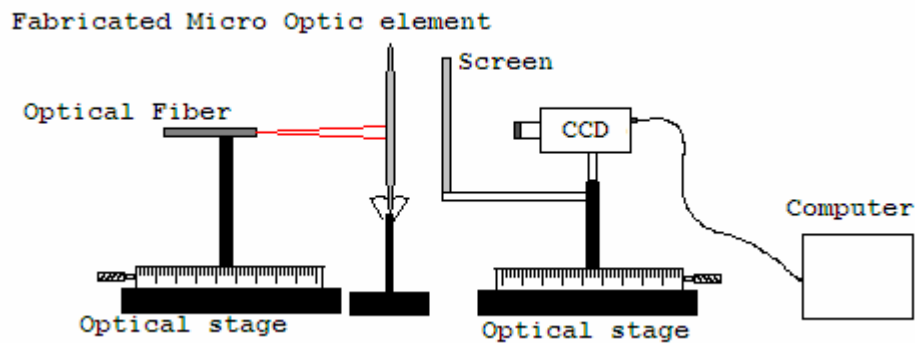
Figure 5-3 Optical Setup for characterization of the fabricated element

The fabricated diffractive lenses were tested using the setup shown in Figure 5-3. The power of the spot with and without the fabricated element was obtained using the setup with a 632.8 nm He-Ne laser. The diffraction efficiency of the microlens on photoresist was thus observed to be 89%. This efficiency also included Fresnel losses at the interfaces. Thus the actual efficiency of the lens is expected to be higher. The theoretical maximum efficiency for an eight-level diffractive optical element is 94%.
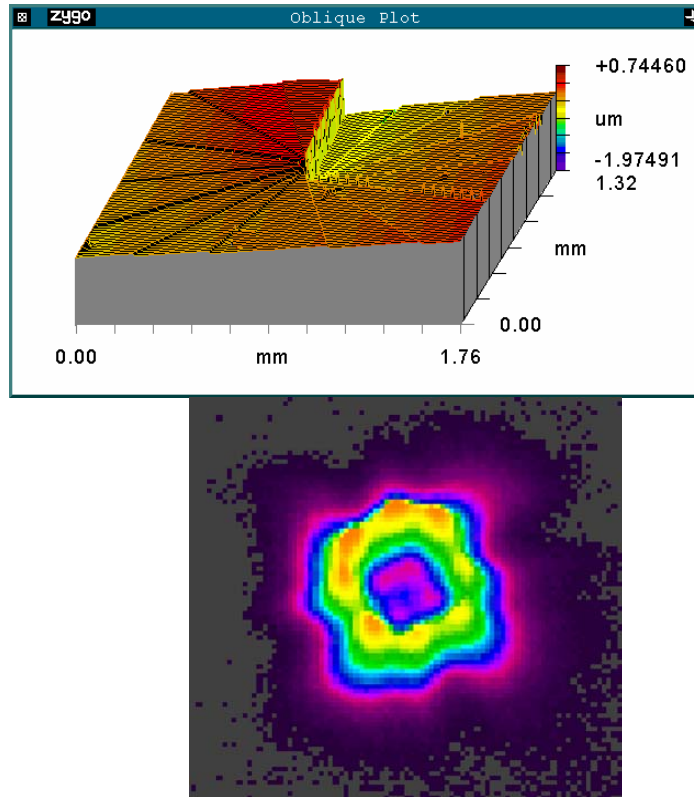
Figure 5-4 Charge m=1, 16 level vortex lens on 1813 for operation at 632.8 nm and output donut profile.

The entire domain masking scheme was employed to fabricate other multilevel diffractive optical elements on S1813. The 3-D profile for a sixteen-level charge-one vortex element is shown in Figure 5-4. The vortex element provides a ring-shaped intensity profile in the far field. This intensity profile can be used to couple higher order modes in a fiber for reducing losses and increasing bandwidth. Biological cell manipulation, materials processing and trace light detection are just a few other potential uses for this "donut" intensity profile. The measured intensity profile in the far field is also shown in the Figure 5-4.
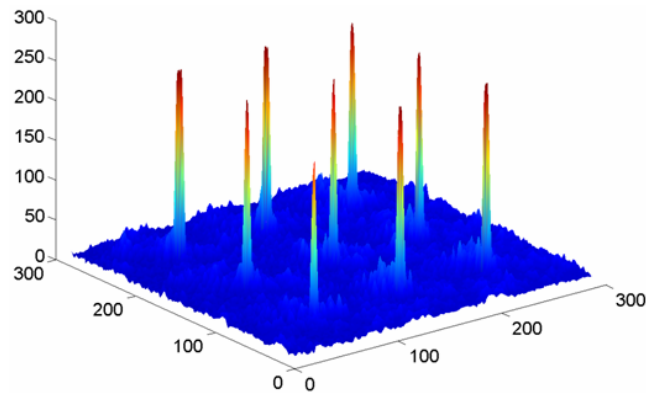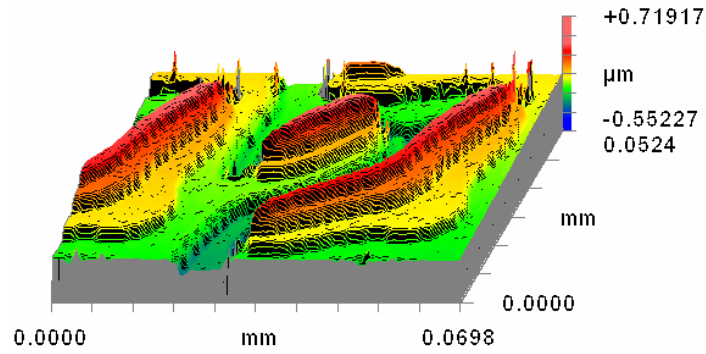
Figure 5-5 Phase profile of a 3x3 fan out grating. Far field profile of a 3x3 fan out grating

Figure 5-5 shows the phase profile for a 3x3 fan out diffractive. The Gerchberg-Saxton projection algorithm discussed in chapter 2 was used to obtain the phase of the optical element. This phase was then quantized to obtain an 8-level phase element which is then broken down to obtain three amplitude masking patterns. These three mask patterns are utilized for generating the 8-level element. The measured far field output profile of this element is also shown in the Figure 5-5.

The 3-D and 2-D profiles for a negative 8-level diffractive lens on S1813 for operation at 632.8 nm, are shown in Figure 5-6. The height of the structure is 1010 nm which corresponds to mod 2π on S1813 at 632.8 nm.
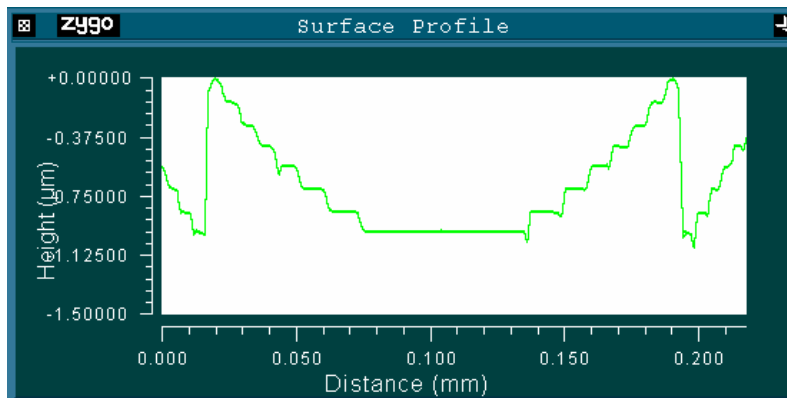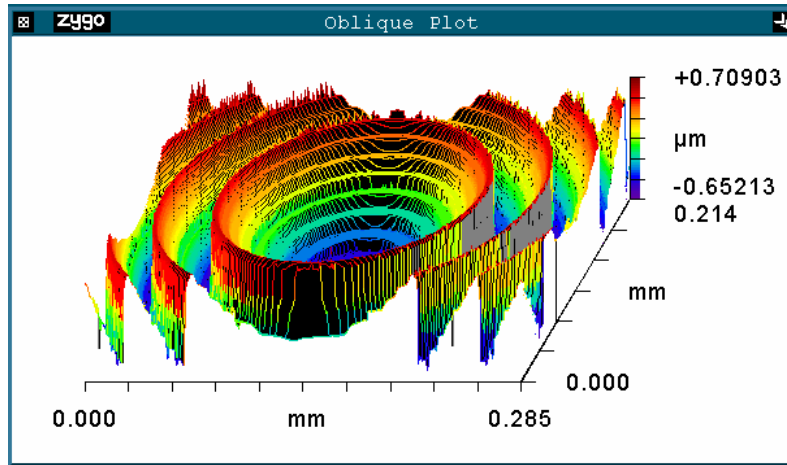
Figure 5-6 3-D and 2-D profile of the first zone of a negative diffractive lens on Photoresist for operation at 632.8 nm. Total Height of structure is 966 nm.

As evident by those previously discussed, a wide range of multilevel optical elements can be fabricated by successive exposures using the entire domain technique. The diffraction efficiency of the structures thus fabricated was measured to be within 5% of the theoretically expected values.

All the above micro-optical elements were fabricated on thin resist S-813. As was shown in Chapter 3, for thick resist SPR 220-7 the working region is non linear. Figure 5-7

Shows the 8 level diffractive lens using the mask shown in Figure 5-1. The level heights are also listed in the figure and it is seen that the heights of these levels are unequal as expected from the response curve for SPR 220-7. This inaccuracy can be corrected for in the transfer etching process using morphing schemes discussed in Chapter 6.
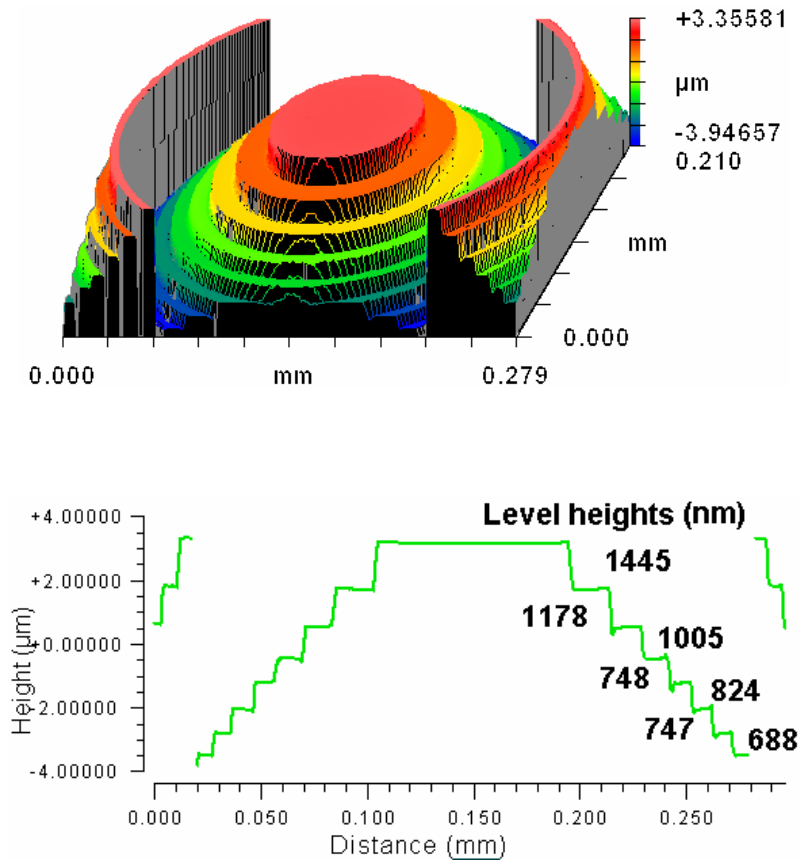
Figure 5-7 -level diffractive lens on SPR 220-7 with entire domain masking showing unequal level heights. The standard deviation of the level heights is 278.85 nm

Pattern to pattern alignment of the additive process on the stepper is automatic and very accurate. This allows for fast and efficient fabrication of multilevel structures with very high tolerances using the cost-effective amplitude masking technology. Since all the

patterns can be typically placed on the same mask, the cost of mask fabrication can be further reduced.

In Chapter 3 we discussed the response curve for S-1813 on the aligner at I-line exposures. Using this curve we performed additive lithography on a Quintel contact aligner. The process starts by first laying down a set of alignment marks on the wafer. The first, second and third mask patterns are either placed on different quadrants of the same mask or on different masks. Each pattern is then aligned to the alignment pattern on the wafer and exposed with the exposure time obtained from the response curve corresponding to the required height. Figure 5-8 shows 3-D and 2-D profiles of an 8-level positive diffractive lens for the central zone and the outer zones.
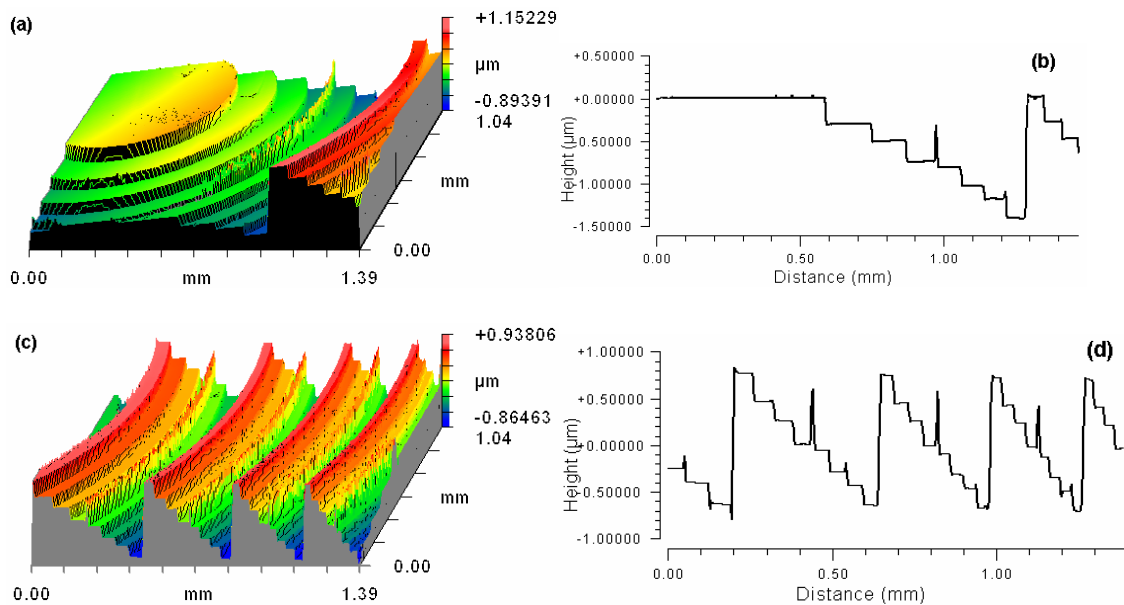
Figure 5-8 Fabrication of 8 level lens using Additive lithography with contact printing. (a)-(b) 3-D profile 2-D profile of 1st zone. (c)-(d) 3-D profile 2-D profile of 2nd–4th zone.

Problems associated with the contact aligner are evident from Figure 5-8. The sharp peaks seen on each zone represent alignment errors due to the manual alignment scheme required on the aligner. The level height errors are caused because of the 0.1 sec minimum exposure time control allowed by the shutter control on the aligner. Thus morphing schemes as discussed in Chapter 6 will be required to correct for the level height errors. Alignment errors on the other hand are defined by the tool, user and alignment scheme used and are usually of the order of 1 μm. The advantage of performing additive lithography on an aligner is that it allows for fabrication of optical elements with apertures larger than 20 x 20 mm allowed on the wafer stepper.

5.2   Sub Domain Masking

The sub-domain basis masking technique was discussed in section 3.2.3. We will demonstrate the fabrication of refractive and diffractive rotationally symmetric elements using both the non-orthogonal and orthogonal basis sets.

Non-orthogonal basis set

A basis set of circular apertures with successively increasing diameters either transparent or opaque form a non-orthogonal basis set. This set can be used for the fabrication of rotationally symmetric optics such as positive and negative refractive lenses. This set is identified as non orthogonal since the patterns overlap in space causing the addition of exposures due to the contributions from other patterns in the set. Positive lenses are

fabricated using opaque circles on a bright field mask with successively increasing diameters. Negative lenses can be fabricated using similar but transparent circles on a dark field mask. Because the exposure time for any member of the non-orthogonal set is affected by exposure times of the other member's of the non orthogonal set, diffractive optical elements cannot be implemented using this mask set.

A positive refractive lens was fabricated using a mask similar to that in Figure 5-12, except with opaque circles on a bright field mask instead of rings. The spherical lens to be fabricated was designed for a focal length of 2.2 mm with an aperture of 250 μm. The maximum lens sag was calculated to be 8.2 μm. This lens was to be fabricated on SPR 220-7 resist which could be coated uniformly to a thickness of 10.5 μm. As can be seen from the characteristic curve for SPR-220 shown in Figure 3-7, the bias exposure removes approximately 2 -3 μm from the top depending on the chosen bias exposure. Hence the maximum sag of the elements fabricated on SPR-220 could be 8.5 μm. The local sag of the lens on the photoresist was obtained by placing the designed lens on a 2 μm grid. The sag values thus obtained were then used to calculate the exposure times 'ti' from the characteristic curve for SPR-220 shown in Figure 3-7. The actual exposure time for the ith element of the non orthogonal basis set is then given as

$$t_{actual,i} = t_i - \sum_{n=1}^{i-1} t_n \qquad\qquad 5.1$$

where n=1 represents the circle with the smallest diameter and n=63 represents the circle with 252 μm diameter.

The fabrication process begins by coating a 10.5 μm thick layer of SPR220-7 on a pre-cleaned 4″-1 mm thick fused silica glass wafer at 1000 rpm. The wafer is then baked in a convective oven at 105oC for 60 min to remove the solvents in the film and then allowed to cool down to room temperature for 30 min. The wafer is then exposed with a 250 μm open circular aperture for 0.7 sec to bias the resist. Sixty-three patterns consisting of opaque circles starting with a diameter of 4 μm and successively increasing by 4 μm are exposed with the exposure times $t_{actual,i}$ calculated from equation 3.6 and equation 5.1 . The chemical reaction, leading to the increase in dissolution rate of the exposed regions for SPR 220 requires water as a catalyst after the exposure. Thus the wafer is allowed to sit for 45 min after the exposure, allowing the water from the ambient atmosphere to be absorbed for the reaction to proceed. The wafer is then subjected to a PEB at 115oC for 90 sec on a hot plate. The wafer is then allowed to cool down to room temperature for a minimum of 30 min before developing to avoid cracks due to the thermal shock. The resist is then developed in MFCD-26 developer for 3 min to obtain the final refractive lens profile shown in
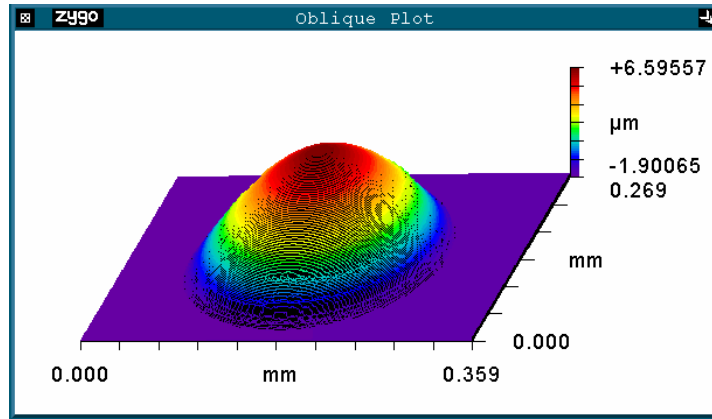
Figure 5-9 3D profile of positive refractive lens with f = 600 μm and D = 250 μm fabricated using non orthogonal basis set. Sag of the lens is 8.3 μm.
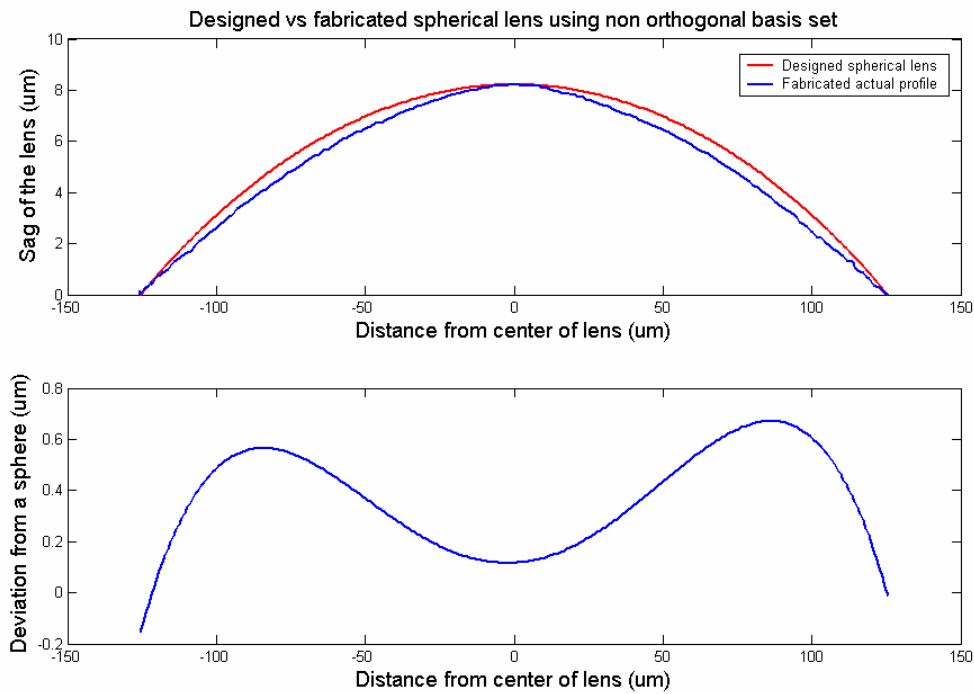
Figure 5-10 Non orthogonal basis set, 63 level spherical lens design vs fabricated lens shape (top) and deviation of fabricated lens from a sphere (bottom).
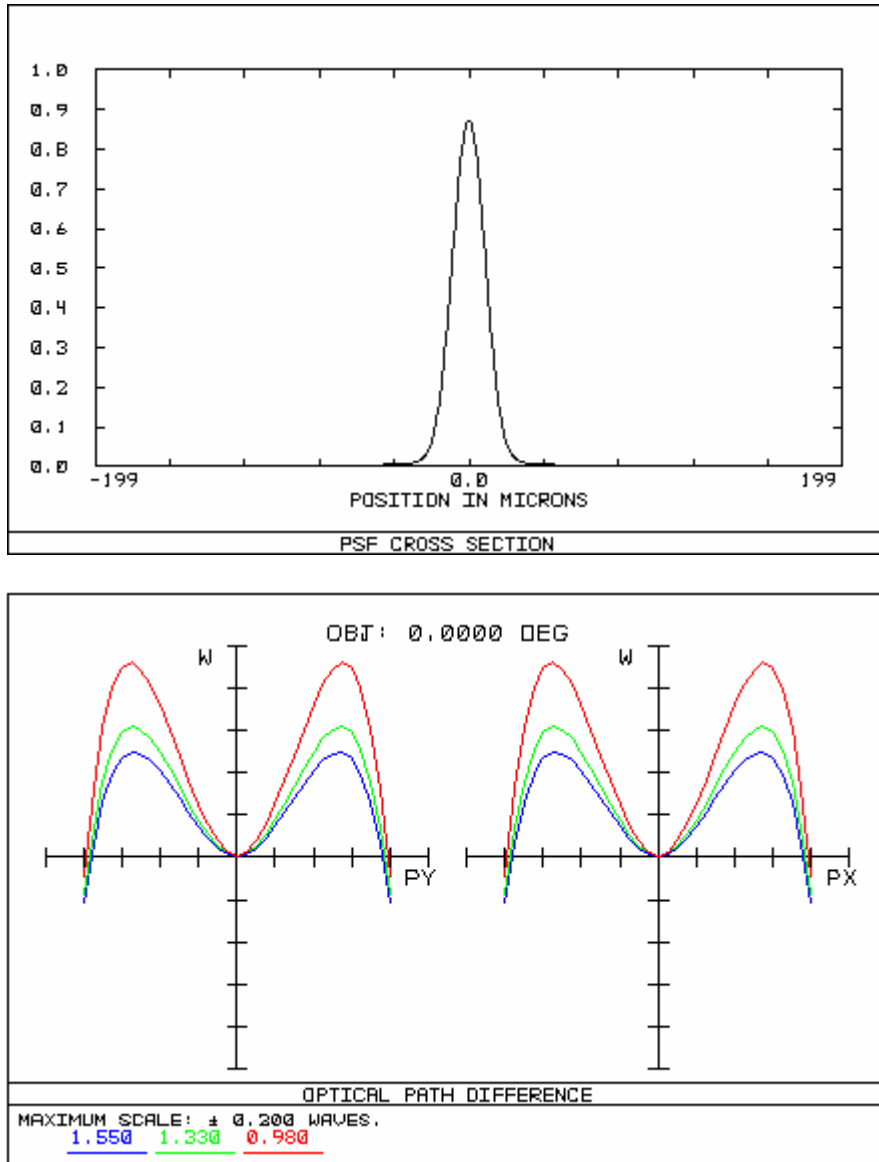
Figure 5-11 ZEMAX analysis of fabricated lens, Top: Point Spread function;
Bottom: OPD plot for 980nm, 1330nm and 1550nm wavelengths.

Figure 5-10 shows the comparison between the designed spherical lens shape and the actual fabricated profile. The deviation from the sphere is also plotted in the figure. It is evident that resolving the 2 μm grid increments through thick resists leads to rounding off of the edges because of the depth of focus of the system, the PEB and the developing process. This leads to a perfectly analog profile. The deviation from the designed profile

is partly due to the fact that the actual exposures calculated need a 4th decimal precision whereas the smallest exposure that can be consistently performed on the stepper is only 10 msec. If we keep the total developing time constant and slow down the developing process by using weaker developing solutions the required exposure for the same depth will be higher thus leading to better profile control. There are other issues involved in adjusting these parameters and they need further process development.

The fabricated lens profile was fitted to the sag equation for an odd aspheric surface and the coefficients were obtained from this fitting in MatLab. These were then supplied to Zemax and the fabricated lens was analyzed for aberration and spot size. Figure 5-11 shows the point spread function and the aberrations in the lens for 980 nm, 1330 nm and 1550 nm. The aberration was found to be approximately 0.18, 0.12 and 0.1 waves, respectively. Lenses are considered to be diffraction limited if the aberration is roughly one quarter wave or less. Thus we see that the fabricated lenses are diffraction limited. The effective focal length of the fabricated lens was found to be 2.1 mm with a spot size of 7.5 μm.

The fabricated lenses can then be etched into the substrate with a 1:1 selectivity as will be discussed in the next chapter. If the fabricated lenses have aberrations, the etching selectivity can be varied during the etching process to adjust the profile transferred onto the substrate for reducing the aberrations. It is also possible to design lenses for low F#'s by etching the lenses with a high selectivity process. For selectivity different than 1:1, the

selectivity of the etch process needs to be considered during the design of the lens and the local sag obtained accordingly.

Orthogonal basis set

The orthogonal basis set for a rotationally symmetric optical element is formed by a pattern of rings, with 4 μm diameter increments on the wafer scale, in our case, Figure 5-12. The smallest of these is just a circle with a diameter of 20 μm on the mask reduced by the projection system in the stepper by five times, to 4 μm. Successive patterns are rings with a width of 10 μm on the mask scale with inner diameters equal to the outer diameters of the previous ring. These rings get reduced to a width of 2 μm on the wafer scale and do not overlap if they are overlaid. The additive exposures do not add up in this case, thus forming an orthogonal basis set. The outer diameter of the largest ring is 1260 μm on the reticle thus leading to a ring with outer diameter of 252 μm on the wafer scale after the 5X reduction. Thus, there were sixty-three rings all fabricated on the same mask, Figure 5-12. The maximum aperture of any rotationally symmetric element fabricated using this mask is therefore 252 μm. An aperture can be opened around each ring, allowing us to independently expose each ring. Since the rings do not overlap, the exposures are independent of each other.
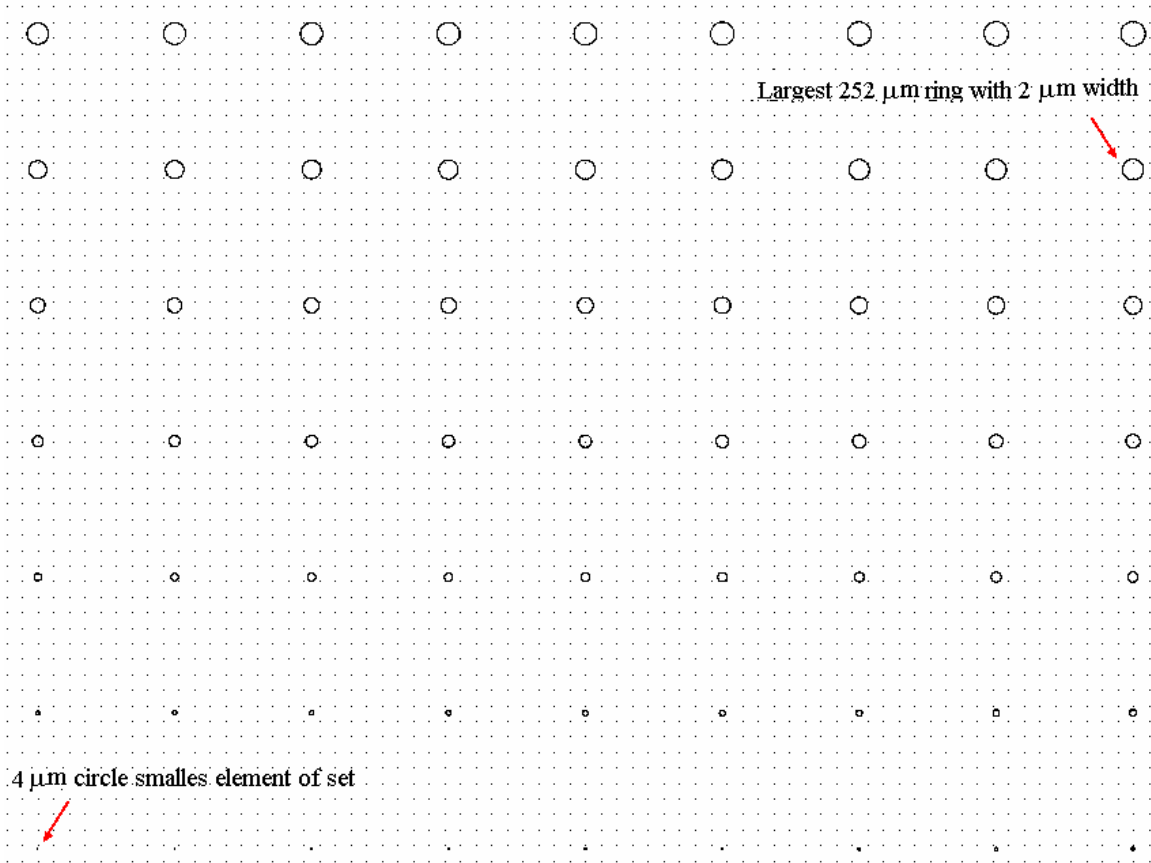
Figure 5-12 Mask with ring patterns represents the sub domain orthogonal basis set for rotationally symmetric elements. Smallest element is a ring with center diameter zero and largest is a ring with diameter 252 µm, width of elements is 2 µm.

The micro optic phase profile to be fabricated is placed on a 2 µm grid and the local sag at the specific location is calculated. From the numerical fit to the contrast curve for S1813 resist, Figure 3-7, the exposure time corresponding to this height is obtained.
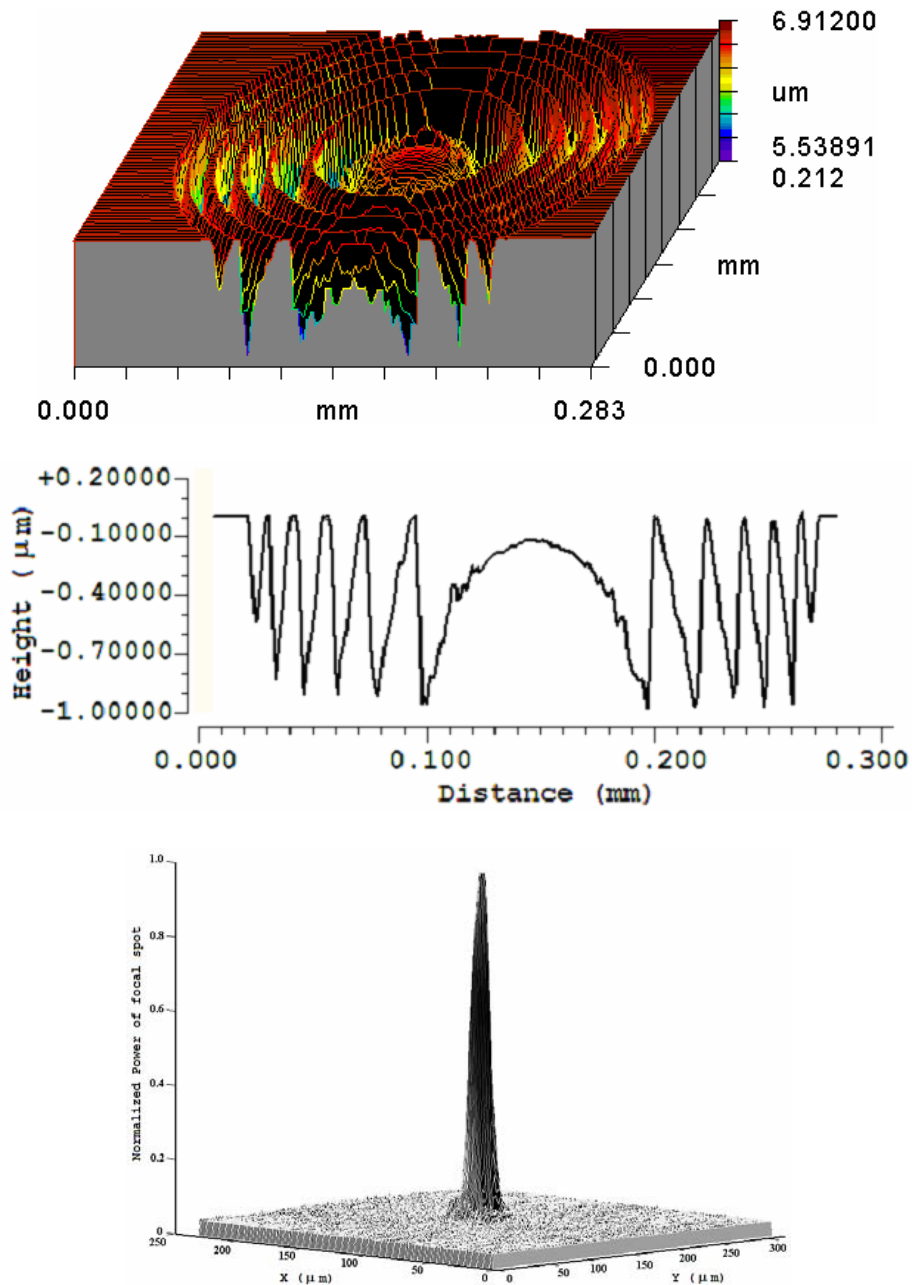
Figure 5-13 Top: 3D and 2D positive Mod 2π lens for 632 nm, f = 2mm, D = 252 μm. Bottom: Measured spot at the focal point of the lens.

The processing steps for S1813 resist are discussed earlier in section 5.1. On developing the exposed photoresist, we are left with the required phase profile on the substrate. The sag of the diffractive structure for mod 2π and mod 4π is 980 nm and 1960 nm,

respectively, for operation at 632.8nm on S1813, which has an index of 1.64 at this wavelength.

An F/8 lens was designed for a focal length of 2 mm with a circular aperture of 252 µm. Figure 5-13 shows the 3-D and 2-D profiles for the mod 2π positive diffractive lens fabricated using the orthogonal basis set for operation at 632 nm. The sag of the optical element was measured to be 975 nm. Using the setup in Figure 5-3, the fabricated lens was tested and the measured focal spot profile is shown in Figure 5-13. The efficiency of the lens was measured to be 88%. The spot size was measured to be 14.5 µm.

[a]   [b]

[c]   [d]
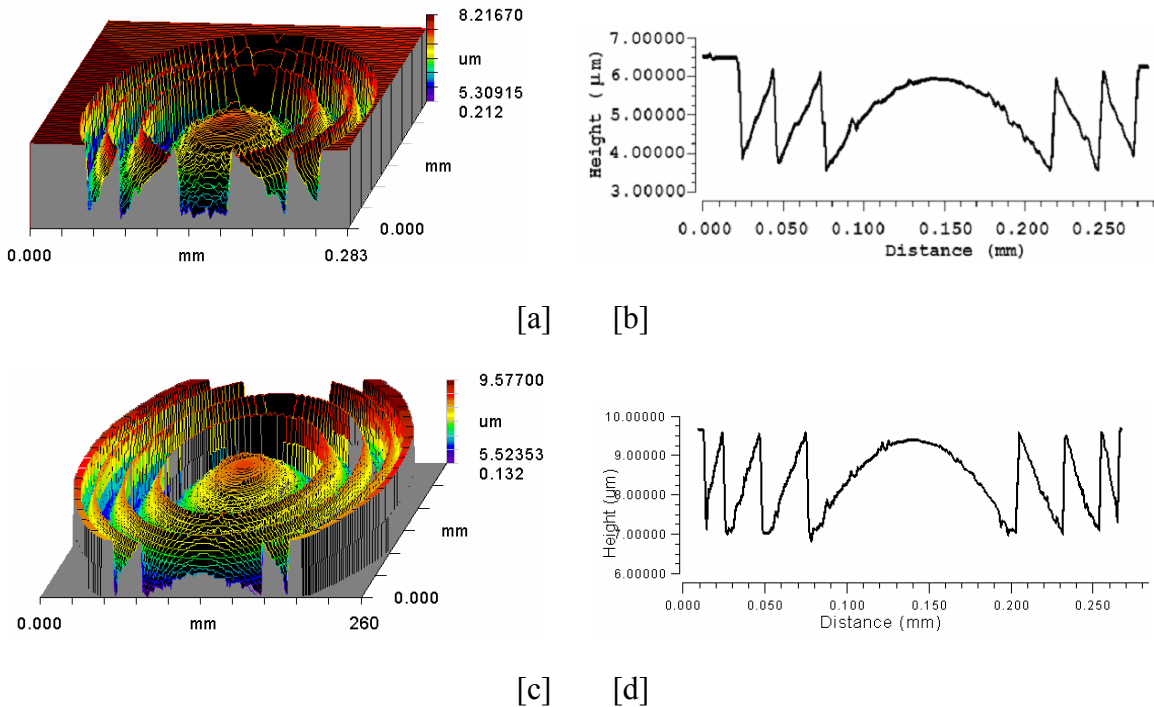
Figure 5-14 3-D and 2-D profiles for F/8 positive lens Top: Mod 4π for λ = 632.8 nm. Bottom: Mod 2π lens for λ = 1550 nm.

To demonstrate the flexibility of this technique, mod 4π F/8 lenses for operation at 632.8 nm and a mod 2π F/8 lenses for operation at 1550 nm were also fabricated. The 3-D and 2-D profiles of the fabricated lenses are shown in Figure 5-14. The diffraction efficiency of the mod 4π lens at 632.8 nm was measured to be 87% with a spot size of 17 μm. The total sag of the mod 4π diffractive lens for operation at 632.8 nm was measured to be 2 μm. Similarly the total sag for the mod 2π diffractive lens for operation at 1550 nm was measured to be 2.6 μm.
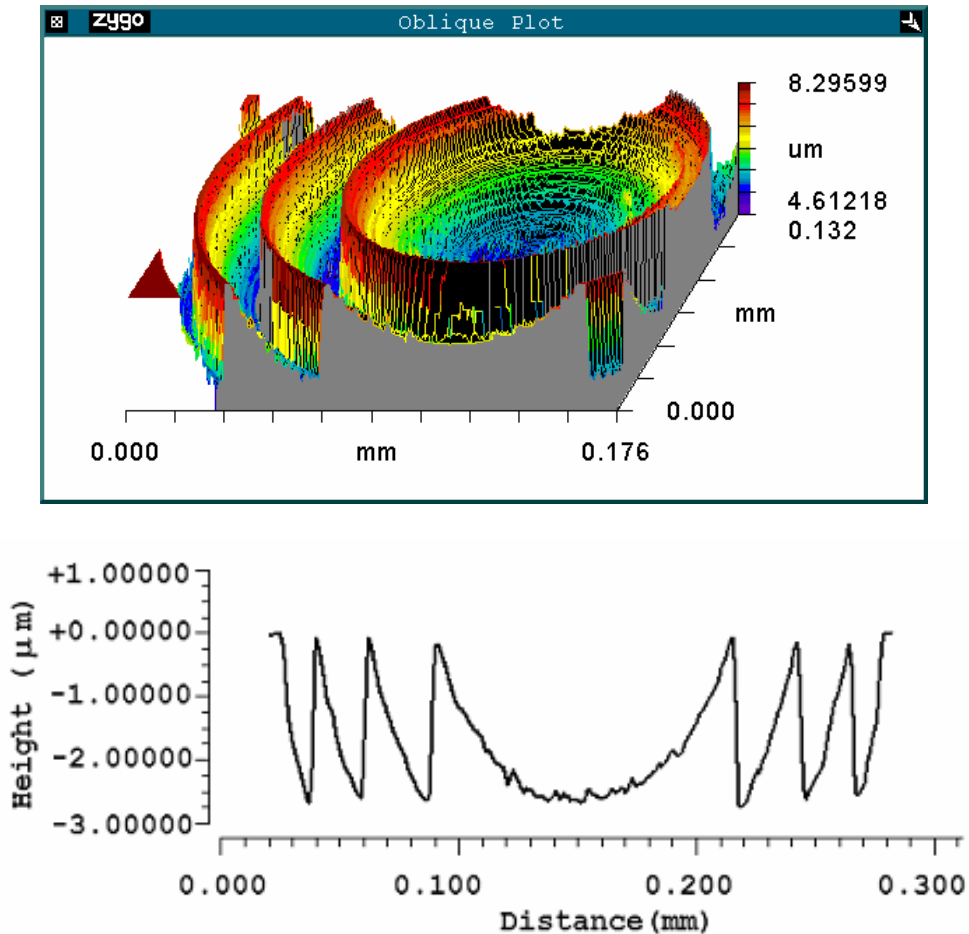
Figure 5-15 Mod2 π negative lens with aperture 252 μm for 1550nm.
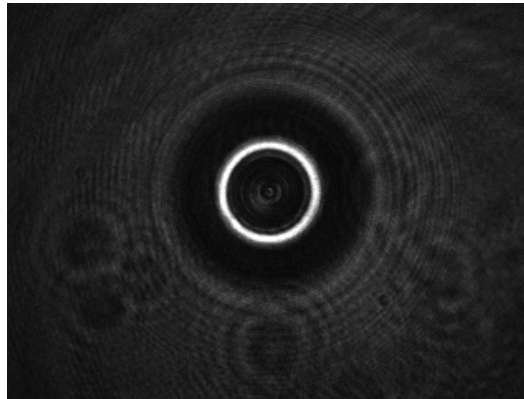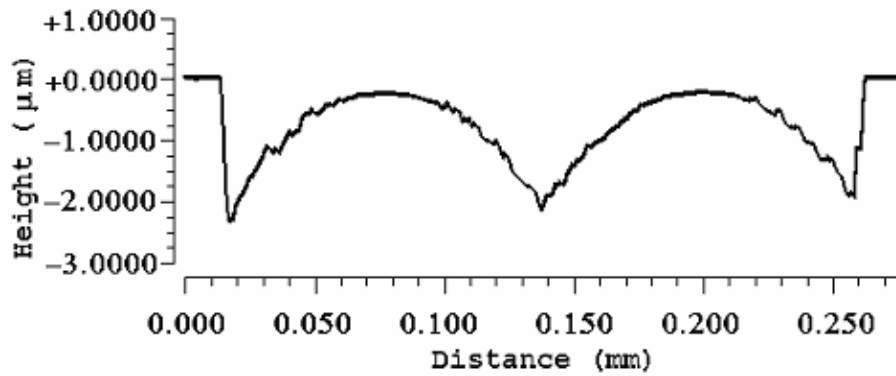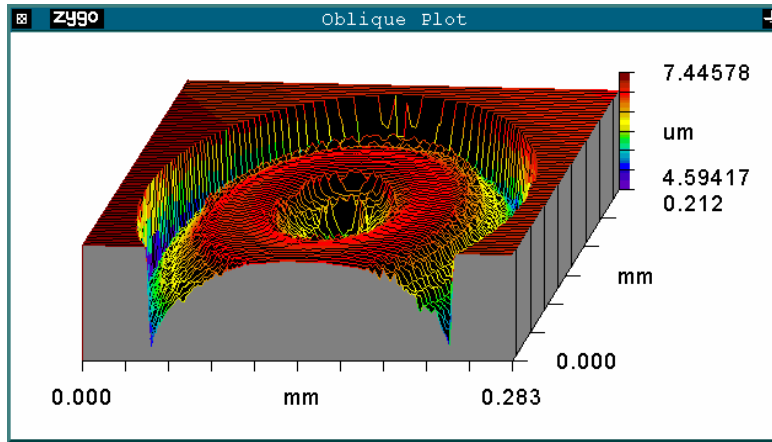
Figure 5-16 Top: 3-D and 2-D profiles of a toroidal lens with Aperture size = 252 μm
Bottom: measured intensity at the focal point of the toroidal lens.

The sub domain set was used for fabricating other optical elements such as negative and toroidal lenses. Figure 5-15 shows the 3-D and 2-D profiles for the fabricated negative mod 2π lens at 632.8 nm. Figure 5-16 shows the 3-D and 2-D profiles of a refractive

toroidal lens fabricated using the same orthogonal basis set as well as the observed

intensity distribution at the focal point of this lens.

5.3 Photoresist Reflow and Pre-sculpting using Additive Lithography

The fabrication of some simple aspheric lenses was done by forming cylinders in

SPR220-7 photoresist by using a bright field mask with circular opaque patterns with

varying diameters. Lenses with aperture sizes ranging from 20 µm to 252 µm were

fabricated. The photoresist used was positive photoresist, SPR-220-7 spun on to a

thickness of 9 µm on a fused silica substrate. Figure 5-17 shows an SEM image of a

cylinder with a 50 µm base diameter. The photoresist was reflowed in a convective oven

at 170 oC for 30 minutes. The sag of the final aspheric structure after reflow is 14 µm.
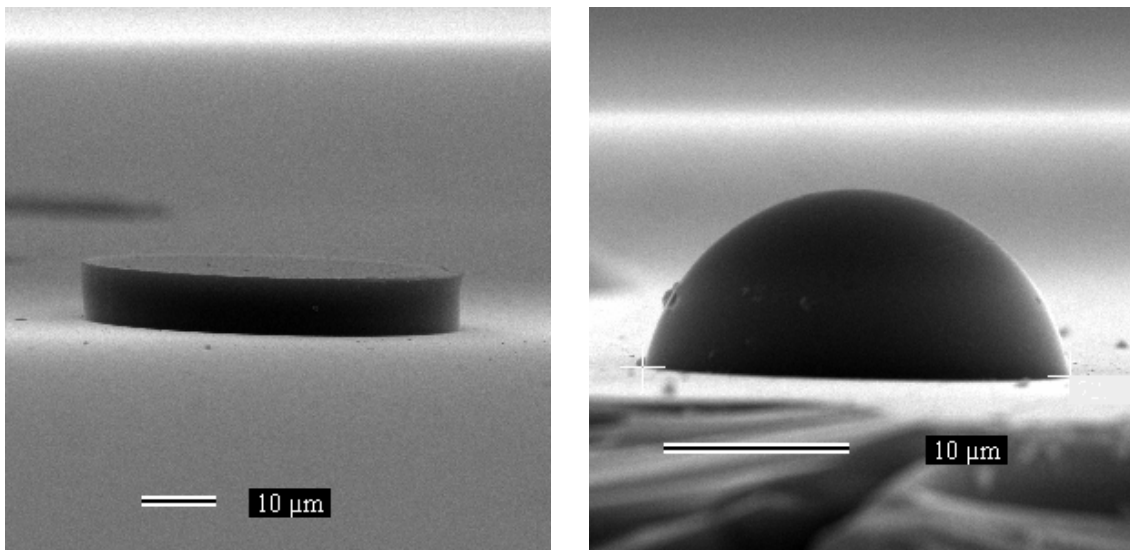
Figure 5-17 SEM images Left: 50 µm cylinder before reflow. Right : 20 µm lens formed
after reflow of 20 µm photoresist cylinder.

By approximating the surface to be part of a sphere, the calculated focal length is 16.5 μm and the F# is 0.826. These can be easily etched into the substrate with the required selectivity using reactive ion etching techniques discussed in the next chapter. The etching process can be morphed to adjust the aspheric coefficients of the fabricated lenses so as to correct for aberrations involved with the initial profile.
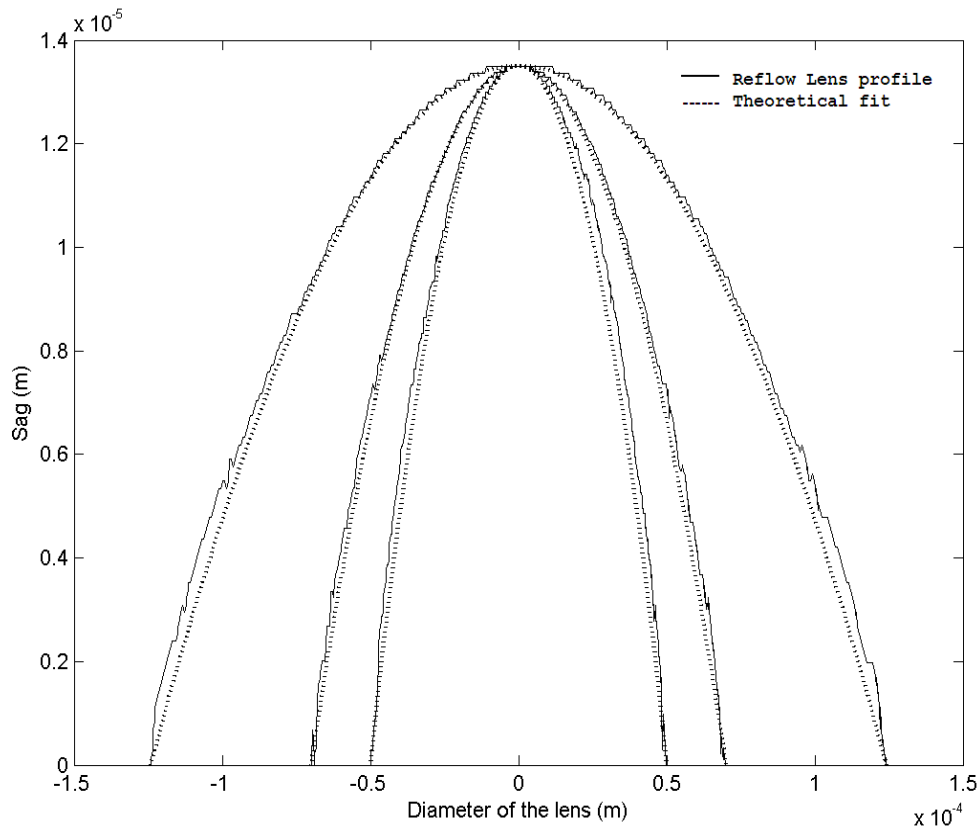
Figure 5-18 Plot showing the profile of the lenses formed by photoresist reflow and the expected profile for three different lens diameters.

Figure 5-18 shows the 2-D profile for three lenses with diameters of 100 μm, 140 μm and 248 μm. The dotted line is the expected surface profile according to equation 4-29. It is seen that our 2-D analytical model fits well to the actual fabricated profiles.

The reflow technique has a number of limitations and these were mentioned in Chapter 4. Pre-sculpting of the photoresist using additive lithography and a non orthogonal basis set were discussed as a solution to avoid these limitations. The first limitation of the photoresist reflow process is the need for thinner resist cylinders when fabricating low numerical aperture lenses. Thinner resist layers have a tendency to reach a local minimal state providing undesired resist profiles.

It is seen from Figure 5-18 and from experiments that during the reflow of cylinders with varying diameters from 20-252 μm and an initial height of 9 μm the final sag of the aspheric lens surfaces was between 14-15 μm irrespective of the base diameter. This can be verified from equation 4.2, which is obtained by approximating the aspheric surface to be a spherical cap. It will also be seen that the final thickness obtained from this equation will be higher than we see in the experiments. This is largely because the shape of the surface bounding the volume is not a sphere. It can be seen from the fitting performed in Figure 5-18 that the more accurate expression, from Equation 4-29, indeed gives us the correct final sag and shape of the surface.

By sculpting using opaque circles on a bright field mask to form the cylinders and transparent circles on a dark field mask, we can reduce the volume of the cylinder without reducing the height of the cylinder. The process is additive since we expose all the patterns needed for the sculpting in one step. This allows us to avoid local minimas while making it possible to fabricate lenses with the same aperture, but varying F#, on the same wafer without having to modify the initial thickness of the photoresist.
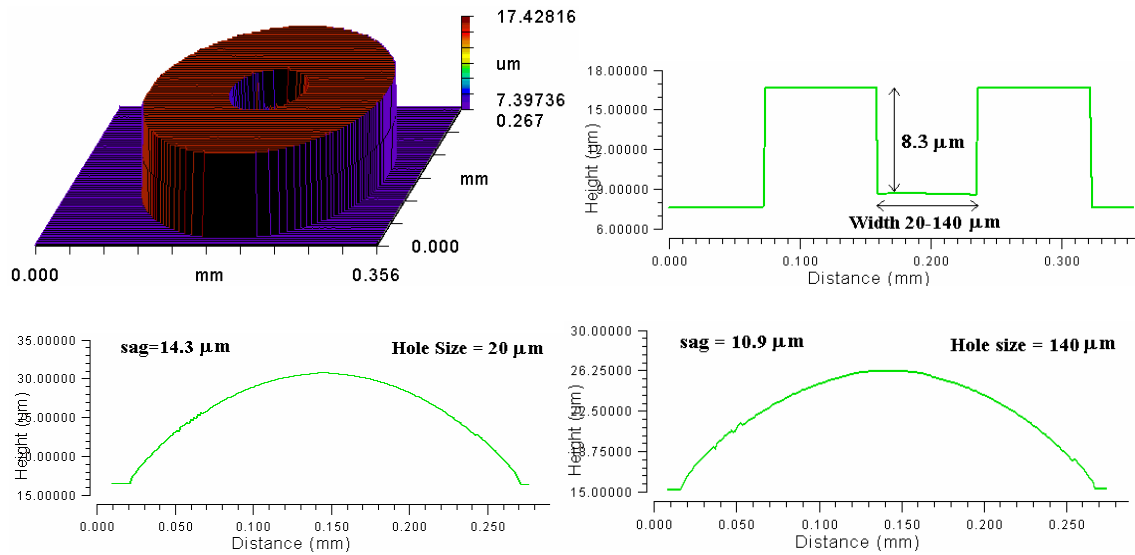
Figure 5-19 Centre sculpting of cylinder with 20-140 µm wide circlesfor controlling sag
Top: 3-D and 2-D profiles of sculpted cylinders before reflow. Bottom : Final profiles
after reflow for 20 µm and 140 µm sculpting.

We created 252 µm cylinders in photoresist with circular holes at the center ranging from
20 µm to 140 µm. The exposures were performed successively to obtain the final sculpted
shape. It was observed that the solid liquid interface established during the lithographic
step was maintained during the reflow. Thus, care was taken not to expose the center hole
with a clear through dose but with a dose slightly lower, so that some resist is left at the
bottom of the holes. The structure formed as a result of this sculpting is shown in
Figure 5-19. The depth of these holes was approximately 8.6µm. The diameter of the
central hole was varied to sculpt out different volumes of the resist. Structures thus
formed were then reflowed in a convective oven at 170 oC for 30 minutes.
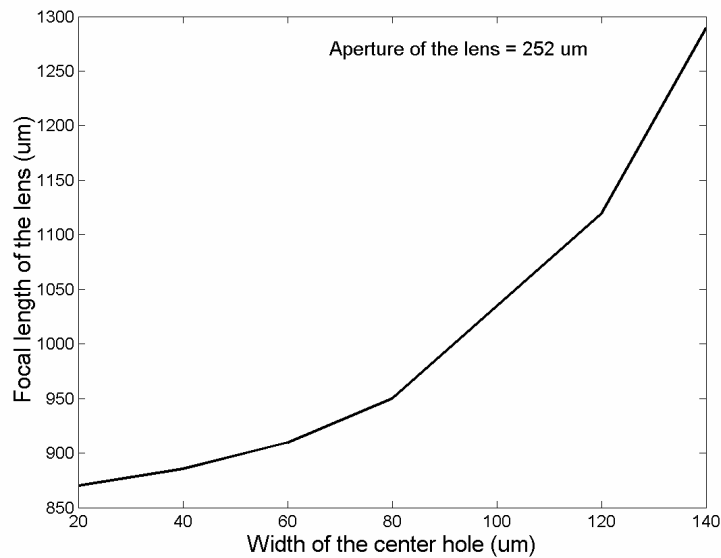
Figure 5-20 Variation of Focal length of the lens with respect to the sculpted hole width from the 252 μm cylinder as shown in Figure 5-19

It is clear that pre-sculpting using additive techniques provides an easy solution to fabricating lenses with varying focal length on a the same wafer in a single coat process. The initial thickness of the resist need not be varied and thus microlens array can be fabricated with differing design parameters for applications including diffusers and focusing elements for non planar detector arrays.

Another limitation of classical reflow is that it is limited to the fabrication of aspheric lenses. Pre sculpting of the photoresist followed by reflow was pointed out as a possible solution in Chapter 4 to overcome this limitation and allow us to fabricate refractive beam shaping elements. The exposure is performed by using a set of circular transmitting apertures on a dark field mask and a set of circular opaque patterns on a bright field mask. This masking set represents the non-orthogonal basis set.

103

Columns of photoresist with a diameter of 252 μm were formed by exposing circular opaque regions on a bright field mask. The height of the two symmetric levels on the inside and outside is 2.8 μm and 5.5 μm respectively. The third level in the center of the structure has a height of 8 μm and widths of 20 μm, 40 μm and 60 μm in Figure 5-21 a, c and e, respectively. The photoresist was reflowed in a convective oven at 140oC for 20 minutes.
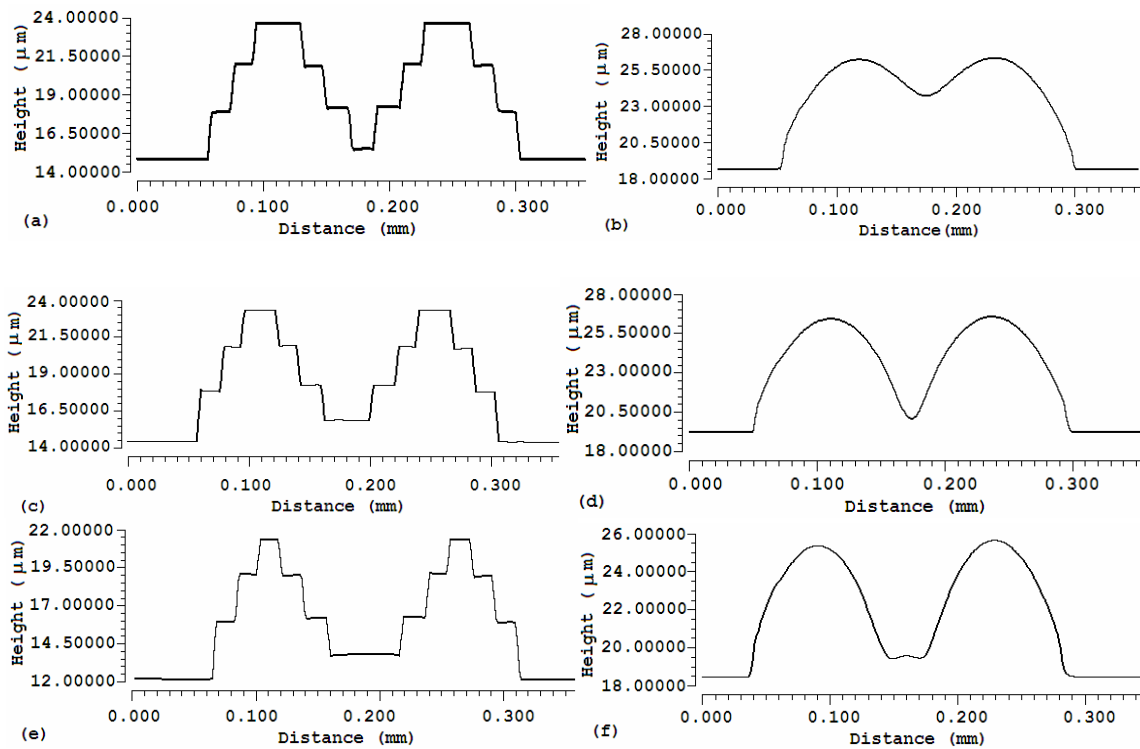
Figure 5-21 Beam shaping elements by photoresist reflow Left : profiles before reflow Right profiles after reflow.

Figure 5-21 a-f shows the sculpted photoresist profile and the profile of the photoresist after reflow. The micro optic thus formed can be used for transforming a beam with a

Gaussian profile to provide a flat top or annular beam profile in the focal plane. By pre sculpting the photoresist according to the characteristics of the beam we can define the reflowed surface profile to perform the optical transformation required. The technique utilizes seven exposures and a reflow as compared to sixty three exposures as used in section 5.2.2 while providing better control and perfectly smooth analog refractive optics with very high numerical apertures.

As mentioned in the previous example, only the outer cylinder is exposed with a clear through exposure, to define the optical surface. All other exposures are performed so that a thin layer of resist is left undeveloped after developing the wafer. These shapes are not minimal shapes and are controlled by the time and temperature of the reflow process. At higher temperatures the structures will achieve the global minimal shapes faster hence allowing less control over the shape restructuring. Therefore performing the reflow at lower temperatures for longer periods of time will allow for better profile control.

5.4   Hybrid optical Elements

Fabrication of multilevel structures using different masking schemes was discussed in the previous sections. It is possible to easily multiplex multiple optical elements using the same techniques. The fabrication process is again a single step exposure process where the masking patterns for the first element are exposed followed by exposure of the masking patterns for the second element. The wafer can then be developed to obtain hybrid optical elements. The alignment of the two optical elements is automatically performed on a stepper with 50-100 nm accuracy. This eliminates any passive alignment

and packaging requirements in the final assembling of these elements while providing equal or better diffraction efficiencies. The 2D and 3D profiles of a 9-spot fan out element multiplexed on a diffractive lens and a vortex lens multiplexed on a diffractive lens are shown in .
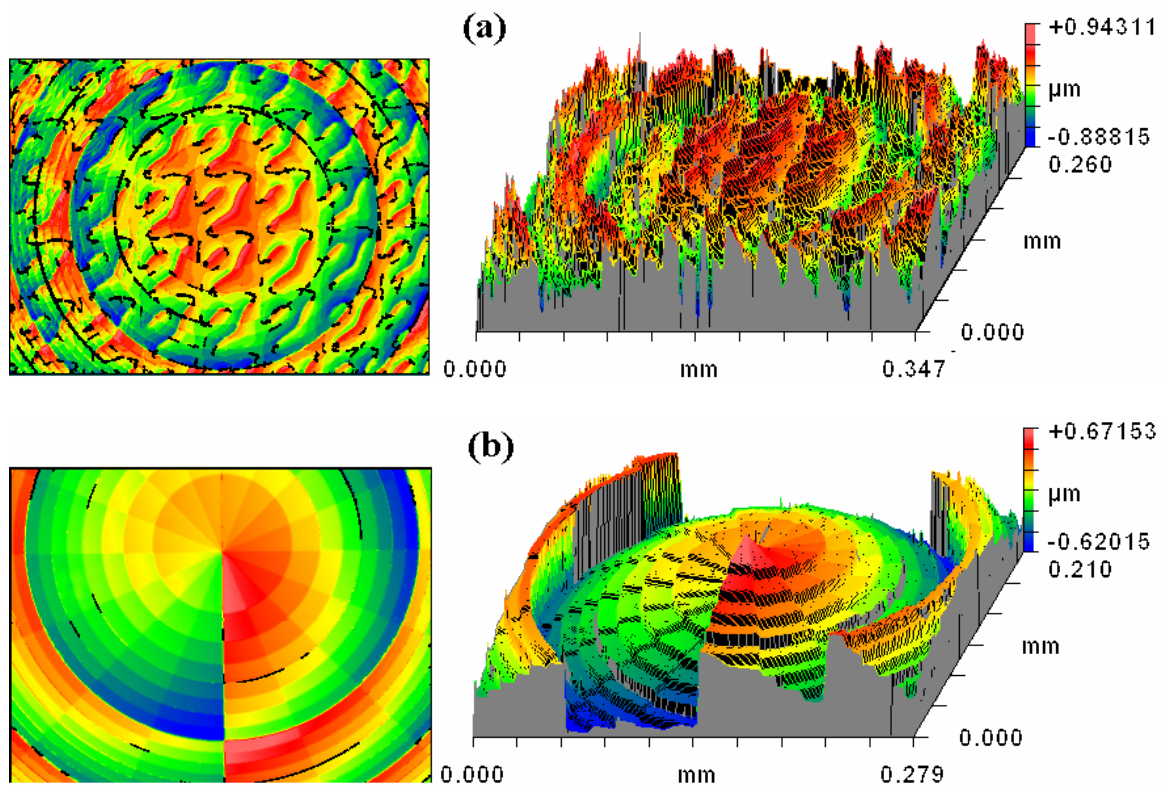
Figure 5-22 Multiplexed optical elements (a) Top view and 3D profile of a 9-spot 8-level fan out DOE on a positive diffractive lens. (b) Top view and 3D profile of a charge one 16-level vortex element on a 8-level positive diffractive lens

Figure 5-23 shows the top view of a grating and Figure 5-24 a hole array multiplexed onto a positive diffractive lens. The gratings provide dispersion and can be used in micro spectrometers while a 2D array of holes can be designed to act as a subwavelength antireflection structure. The period of the multiplexed grating and hole array is 2.2 μm.
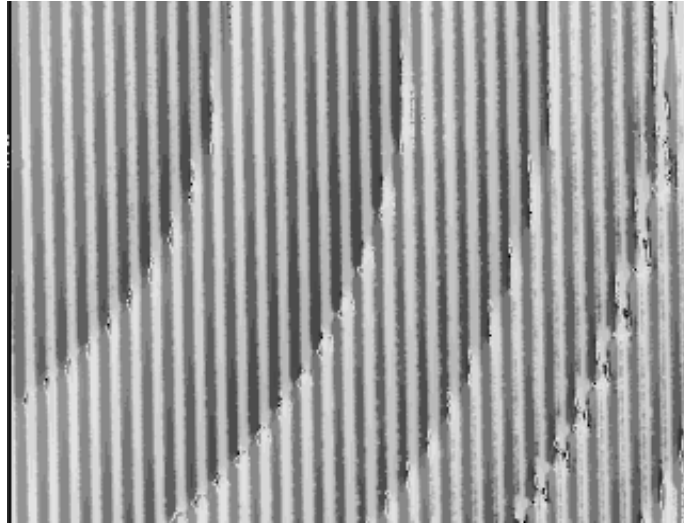
Figure 5-23 2.2 µm grating multiplexed on a positive diffractive lens
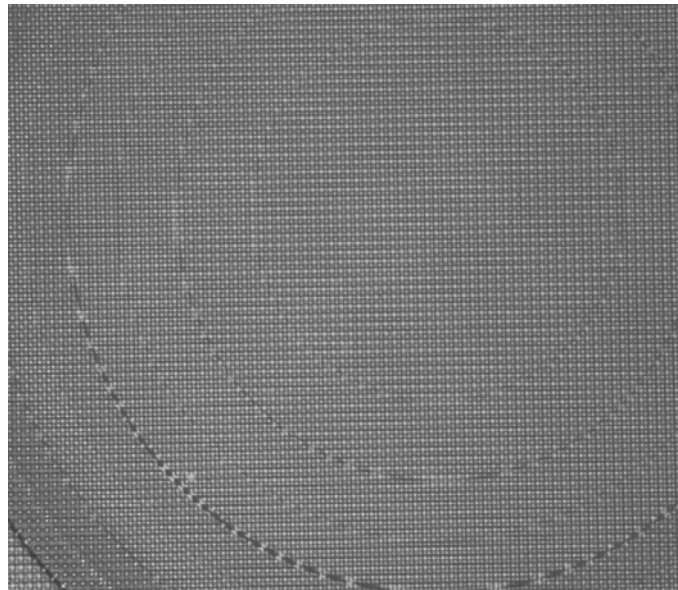
Figure 5-24 2.2 µm hole array multiplexed on a positive diffractive lens

We have demonstrated the fabrication of various refractive and diffractive optical elements. These include positive, negative and toroidal lenses, vortex elements and fan out gratings fabricated using either additive lithography or photoresist reflow or both. We

have also demonstrated through testing the fabricated components that the additive technique does indeed provide optical elements with very high efficiencies. It was shown that the fabrication involves successive exposures to provide the final profile in a single developing step, thus increasing throughput, tolerance and the utilization of masking schemes. This allows enormous flexibility in the design and fabrication. These elements were implemented on both thick and thin photoresists. Since most photoresists are sensitive to the ambient conditions such as temperature and deteriorate when exposed to various contaminants in the environment, the fabricated structures should be transferred into the substrate so that the devices can be operated in any environment. This is performed by utilizing dry etching technology which is widely used in the industry. We will discuss the transfer etching of the fabricated components and study the etch rate of the substrate and photoresist with respect to various parameters such as gas flow, power etc., in the next chapter.

CHAPTER 6: TRANSFER ETCHING

In the previous chapters we have discussed the fabrication of optical elements on photoresist using additive lithography. Photoresist is not a stable material as it tends to deteriorate over time, being soft is very easily destroyed by handling and does not have the ability to handle extreme operating conditions such as temperature, power etc. required in many applications. Thus the patterns formed on the photoresist need to be etched into a suitable substrate which could be Glass, Silicon Gallium Arsenide or some other material chosen depending on the application.

6.1   Wet V/s Dry Etching

Traditionally there are two types of etching, wet etching and dry etching and each of these can be further classified depending on the etching mechanisms and the chemistries chosen [42]. Both these techniques have been extensively studied in the IC industry and as with lithography we need to study these etching processes and tailor them for fabrication of micro optical elements. The problem in the electronics industry predominantly involves transferring binary patterns formed on a mask onto the underlying substrate. Though this forms part of the problem in optics, e.g. fabrication of binary phase/amplitude gratings, waveguides etc. the main problem is usually the transfer etching of 3-D surface relief optical elements. The difference between these two applications is the type of masking that can be employed during the etching. Etching of binary patterns can employ hard masking layers e.g. metals etc. and can provide very

high selectivity with very little mask erosion during the etch process. It also provides more flexibility in adjusting the process parameters to obtain very high anisotropy. Fabrication of surface relief elements is performed by sculpting photoresists using various techniques discussed in the earlier chapters. This sculpted photoresist surface then becomes the masking layer during the transfer etching process. Photoresists have a lower sputtering threshold and also react with many of the etch gases used in the transfer etching process. This has a disadvantage since it provides much lower selectivity than seen with hard masks and decreased flexibility in process characterization. The advantage obtained from this nature of the photoresist is that the initial surface relief profiles can be modified during the etching process into the substrate by adjusting selectivity and/or anisotropy to reduce/eliminate initial fabrication errors during the sculpting.
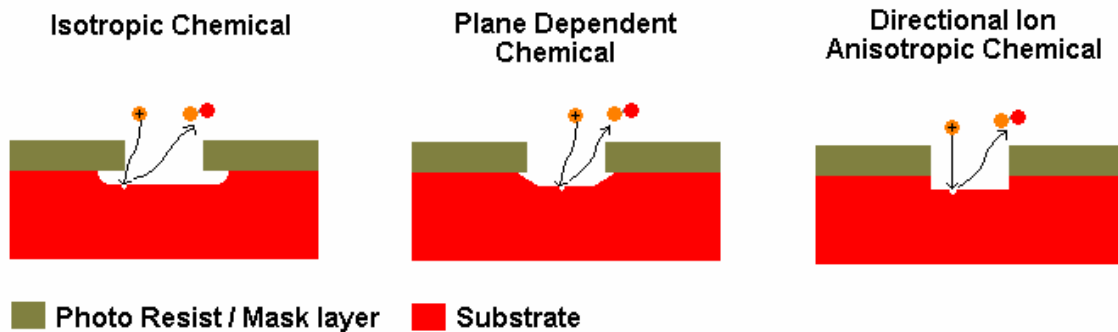
Figure 6-1 Chemical (wet/dry) v/s ion assisted dry etching

Wet etching is unsuitable for transferring 3-D surface profiles into the substrate and due to its inherent isotropic nature presents a problem even in the fabrication of binary structures, see Figure 6-1. Dry etching techniques eliminate this problem as they can provide highly anisotropic profiles. Dry etching usually provides lower selectivity and

etch rates than wet etching, but provides larger control over many etch parameters such as selectivity, etch rate and anisotropy through process control. The flexibility in controlling selectivity allows us to adjust for variations and/or limitations in the lithographic process and allows for fabrication of elements operating over a wide range of wavelengths.

Dry etching can be defined as the process where material from the solid surface is etched in the gas or vapor phase, physically by ion bombardment, chemically through a chemical reaction or the combination of the two. Physical etching occurs through momentum transfer from a neutral ion species to the substrate resulting in removal of material from the surface. Chemical etching occurs when radicals, ions or neutrals of the etchant adsorb onto the surface of the wafer and react with the substrate material to provide volatile byproducts, Figure 6-1. The etching mechanism could be spontaneous or induced by external means. Some etching processes use both physical and chemical mechanisms where the physical component initiates the chemical reaction.

In this chapter we will look at dry etching techniques for transferring 3-D optical elements into the fused silica glass substrate which is a preferred substrate in many applications over a wide range of wavelengths due to its low loss characteristics.

6.2   Introduction to a simple Plasma Etcher

Dry etching techniques use either plasma driven chemical reactions or energetic ion beams to remove material through physical sputtering or sputter assisted chemical etching [54-56]. Plasma etching was developed as a cheaper and less toxic alternative to wet solvent photoresist stripping in the late 1960's. The advantages of highly anisotropic etching were soon realized since line-width control was an important factor and it became a tool of preference. The high energy electric and magnetic fields in the plasma reactor induce rapid dissociation of the feed gases into neutrals, ions and radicals. The surface in contact with the plasma is exposed to fluxes of these neutrals, ions, radicals, electrons and photons and etching results through reactions between the substrate and the neutrals, ions and radicals produced in the plasma. A variety of other reactions affect the etching rate and selectivity and these are alternatively dependent on process parameters such as gas feed type and ratio, pressure, temperature and power.
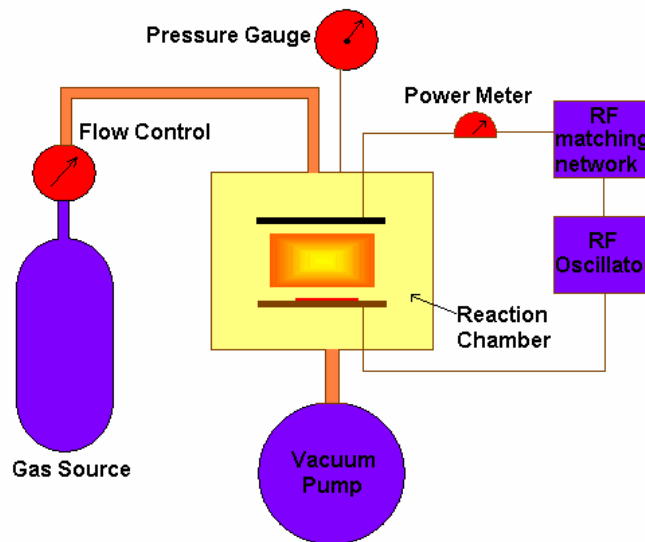
Figure 6-2 Schematic of a Plasma Etching tool

The most standard plasma reactor consists of opposed parallel plate electrodes in a chamber maintained at a pressure around 1 to 1000 mTorr. Inert or reactive gas species are fed into the chamber through mass flow controllers and when a dc or ac field is applied across the parallel electrodes an ionized gas species with equal positive and negative charges called plasma is generated. The electrons are light and mobile and energy transfer during collision with gas molecules is inefficient. Thus the electron temperature rises steadily in the plasma while the gas temperature in the plasma is near ambient with the ion temperature just slightly higher. Elevated temperature of the electrons helps electron molecule collisions to excite high temperature type reactions leading to free radicals and ions in a low temperature neutral gas. The faster moving electrons hit the walls of the chamber before the ions due to their higher mobility and this leads to a net negative charge of the chamber walls with respect to the plasma. The net negative charge build up on exposed surfaces pushes all the other electrons away from these surfaces, thus exposing the positive charges near the walls. This region is called the sheath. Since there are no excitations or de-excitations in this region the sheath is a dark region. The field created between the plasma and the substrate or the walls is what is called the DC Bias, and the ions in the plasma are accelerated onto the walls and the substrate. In the steady state the rate of arrival of ions and electrons is then balanced due to this effect.

The electric fields are weak inside the plasma and are strongest in the sheath region. This field is what controls the directionality of the ions and leads to the anisotropic etching in the RIE system. As mentioned earlier a DC or AC field can sustain the plasma, but with

DC fields dielectrics in the chamber will tend to collect charge leading to distortion of the electric fields. This can affect the etch process and can also present other problems with plasma stability and hence AC fields are generally used to generate a plasma. Another problem with DC plasmas is that secondary electron collisions are required to sustain the plasma and hence the chamber pressure needs to be higher. This can affect anisotropy due to larger angular spread of the ions reaching the substrate. Since electrons pick up enough energy during oscillation in a RF field to cause ionization the chamber pressure can be lower and hence provide better anisotropy.

One of the electrodes in the parallel plate configuration is capacitively coupled to the RF source and since no charge can be transferred across a capacitor this electrode maintains a negative DC bias VDC. The center of the plasma is nearly neutral but the glow region which is the edge of the sheath inside the plasma loses electrons to the surfaces and hence is charged positive and has a positive potential called plasma potential VP. Figure 6-3 shows the time averaged potential distribution and the various potentials associated with such a capacitively coupled planar RF discharge system.
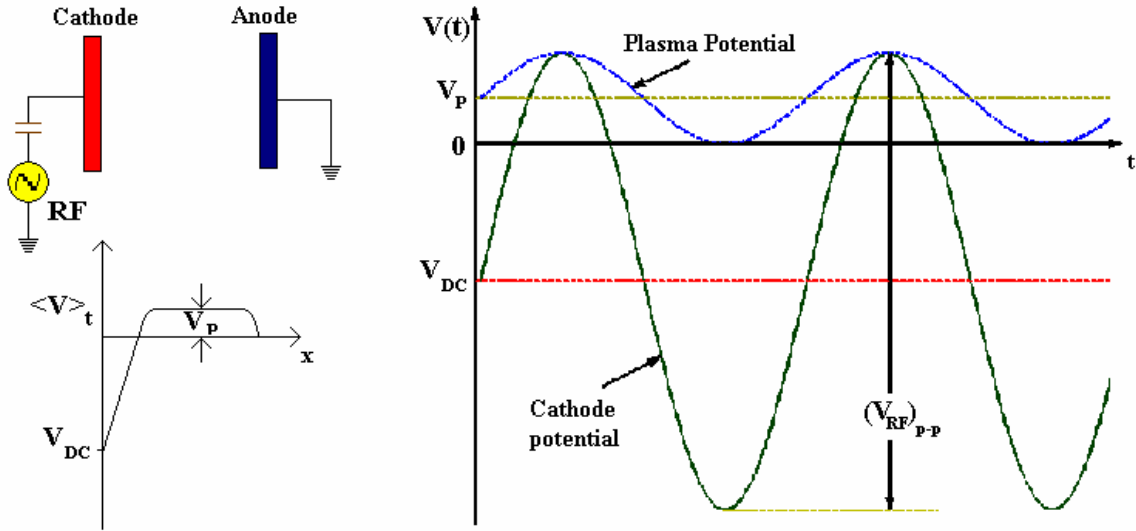
Figure 6-3 Electrode configuration and time averaged potential distribution (left);
Potential distribution in glow discharge reactors

The self bias VDC on an insulating electrode due to the flux of electrons from the plasma

is given as [42]

$$V_{DC} = \frac{kT_e}{2e} \ln \frac{T_e m_i}{T_i m_e}$$ 6.1

where Te, Ti, me and mi are the electron and ion temperatures and masses respectively, k

is the boltzmanns constant and e is the electron charge. The electron temperatures are

approximately 2x104 K while the ion temperature is around 500K. Most of this self bias

is dropped across the sheath in a plasma reactor, since as mentioned earlier the interior of

the plasma is almost neutral and the fields are set up in the region where the plasma

interacts with any surface due to loss of electrons to the surface.

The time averaged plasma potential Vp, the self bias and the applied RF voltage (VRF)pp are approximately related by

$$2V_P \approx \frac{(V_{RF})_{p-p}}{2} - V_{DC}$$
6.2

The self bias on the electrode depends on the magnitude of the RF signal applied to the electrodes. This self bias creates a field close to the substrate so that the ions reaching the substrate arrive at near normal incidence. The spread of the ion incidence angles affect the anisotropy and are in turn controlled by the mean free path of the ions. Thus at lower pressures we get more anisotropy since ion collisions are reduced leading to more directional ions. The maximum energy of the ions striking a substrate placed on the electrode is then proportional to

$$E_{max,C} = e(|V_{DC}| + V_P)$$
6.3

whereas the maximum energy of ions striking a substrate on the grounded electrode is

$$E_{max,A} = eV_P$$
6.4

Systems where the substrate is placed on the grounded electrode are called plasma etchers and systems where the substrate is placed on the cathode are referred to as reactive ion etchers.

The anisotropy of the process is controlled by the self bias which in turn is controlled by the applied RF field and the pressure in the chamber. The RF field is also responsible for generation and sustaining of the plasma. High RF power increases the self bias and hence higher ion energies thus reducing the selectivity and increasing the possibility of device damage. To reduce ion energies the RF power has to be reduced leading to reduced dissociation and hence very low etch rates due to unavailability of radicals and ions for the reaction. Thus RIE reactors are usually used at higher pressures to increase the number of ions and radicals available for etching. This lead to the development of Inductively Coupled Plasma (ICP) systems and Electron Cyclotron Resonance (ECR) systems wherein very high quantities of low energy ions and radicals can be produced at low pressures.

An ICP system has the advantage of using two different RF power controls, one for controlling the dissociation of the neutral species and sustaining the plasma and another to apply a bias on the substrate for the etching. The inductively coupled power can be very high ($\approx$1.5-3 KW), leading to highly dense plasmas while keeping the ion energies low. The ion bombardment for etching the substrate can be independently controlled using the bottom electrode allowing for better etch control and higher anisotropy. The power is transferred to the plasma inductively through a transformer. Thus power transfer efficiency is very high.

In a plasma etching process there are two processes assisting the etching namely ion assisted sputtering and reactive species etching. Ion assisted sputtering is a slow and very

non selective process but chemical etching is more selective and much faster. In reactive ion etching both these processes are present and which of these dominate the etching depends on various parameters such as process pressure, RF power and type of gas. In some cases such as etching of glass, the ion bombardment assists in the chemical etching activity by lowering the activation energy and if the ion energy is very low the chemical etching drops rapidly. In fluorine based silicon etching chemical reactions are spontaneous and hence isotropic and hence ion sputtering and polymerization based side wall passivation is utilized to obtain anisotropy. Etching selectivity, rate and substrate quality after etching depends on process pressure, RF power, gas flow rate and temperature. We will discuss the effect of each of these parameters on our etching process in the next few sections.

6.2.1 *Gas Pressure*

The manner in which etching depends on plasma pressure is complex as many effects occur simultaneously. As the gas pressure is raised the mean free path of the plasma components is reduced producing more radicals and ions. This can increase the etch rate of the substrate or the free radicals can recombine with each other forming higher molecular weight species. These higher weight species are polymers that also perform the function of passivation that allows deep anisotropic etching of many substrates. This polymer formation slows down the etching process mainly on the sidewalls and the sputtering component of the etching removes the polymer constantly. The sputtering is much lower on the sidewalls because of the directionality of the ions and thus the rate at

which the passivation layer is removed from the surfaces is usually much higher than that on the sidewalls. There is competition between formation and removal of the polymer from the substrate and if the rate of removal is very low as compared to formation then the etching process will come to a stop. The addition of oxygen helps inhibit the formation of polymer as it oxidizes the polymer layer to form a volatile byproduct. Reducing the pressure also increases the ion energy and thus helps sputter away the polymer. Thus we can go from a low selectivity very clean etch process progressively to a high selectivity process and then to a point where the etching stops due to polymer buildup by increasing the pressure. Deep reactive ion etching of Silicon takes advantage of this passivation process and brief steps of etching are followed by passivation steps leading to highly anisotropic high aspect ratio structures.

6.2.2   *RF power*

The RF power determines the density of the plasma and the ion energy bombarding the surface due to the DC bias between the sheath and the substrate. Increasing the RF power will lead to higher plasma densities, more free radicals and higher DC bias especially at lower pressure. If the free radicals are reactive species the etching rate of the substrate increases. Increasing the RF power also increases the sputtering component and very high RF powers can lead to damaged surfaces. High energy ion bombardment also heats up the substrates and this can destabilize the photoresist if its temperature is close to or beyond its glass transition temperature. Thus the advantages and disadvantages of higher RF power go hand in hand and there is no independent control of the two. This was the

reason Inductively Coupled Plasma (ICP) systems were developed. Here a top electrode is coupled to an RF generator through a matching network and this generates and controls the plasma density and the concentration of free radicals. The bottom electrode has its own RF generator and this is used to control the ion bombardment to the substrate. Thus there are two knobs to tune the etching characteristics. This allows for very highly dense plasmas with a large number of radicals thus providing very high etch rates and very good control over the anisotropy. An ICP system generally operates at lower pressures than an RIE, in the range of 1-100 mTorr. As seen in the earlier section this helps increase anisotropy by reducing random collisions.

Though we can make a qualitative comparison between etchers the chamber design and RF matching network design may vary from machine to machine and hence it is not possible to make a one to one comparison of the etch rate with RF power for different etchers.

6.2.3   *Gas flow*

As mentioned earlier there are very few radicals in the plasma as compared to the neutral species. There is equilibrium in the chamber between the supply into and the removal of gases from the chamber. Below a critical flow rate there is an inadequate supply of reactant to etch the material and thus a small increase in flow rate beyond this critical point can rapidly increase the wafer etch rate. Similarly it is possible that very high flow rates might actually be detrimental as they can assist in polymer formation on the

substrate especially with etching of silicon or silicon dioxide in CF_4, CHF_3, C_4F_8 gases that form hydro-carbon or fluoro-carbon polymer chains. This effect though is not very significant with other gases such as Cl_2 or BCl_3 used in the etching of III-V compounds and Silicon. The most important factor affecting the selectivity and etch rate is usually the ratio of the gases fed into the system. This is because as mentioned earlier very few of the molecules actually form the radicals that take part in the reaction while the rest are pumped away constantly as they are fed into the system. Increasing the flow rates beyond a certain point may have minimal or no effect on the etching. As an example, addition of oxygen helps quench the polymer forming carbon in the fluorocarbon gas such as CF_4 thus providing more fluorine radicals for the reaction. This increases the etch rate of the Silicon substrate. Beyond a specific ratio of O_2 and CF_4 in the system the addition of O_2 reduces the etch rate since excessive quantities of O_2 tends to dilute the fluorine radical concentration available for the reaction. Similarly addition of hydrogen reduces the fluorine radical content in the plasma thus leaving polymer forming radicals behind. The formation of polymer enhances the selectivity of the process in the case of SiO_2 etching and can completely stop the etching in the case of Silicon etching.

6.2.4 *Temperature*

The rate of the etching may depend on the temperature because the chemical reaction involved is subject to an activation energy and also because the surface coverage of chemisorbed species is temperature dependent. But the photoresist can degrade at higher temperatures and needs to be protected by cooling the substrate. Degrading of resist or

etching of the resist at temperatures close to the glass transition can lead to rough etched surfaces unsuitable for optics.

On the other hand etching of certain substrates have to be done at elevated temperatures, since one of the by products of the chemical etching process may be nonvolatile at lower temperatures. This would provide very rough surfaces after etching and the byproducts may also form an etch stop, e.g. while etching Indium Phosphide, Phosphorous forms volatile by products and may get etched off but Indium tends to stay on the surface and this affects the etching dramatically. The temperature also needs to be maintained so that there is a balance in the process of removal of the byproducts formed on the surface during etching so that excessive collection of one of them does not occur. Sometimes ion bombardment is also used to assist in this process.

Ion bombardment also induces a rise in temperature usually within the first few minutes and it is necessary to maintain a stable temperature on the substrate so that the etching can be constant and free of defects. The photoresist needs to be stabilized before the etching process by a robust hard baking procedure or flood exposing to the UV light. This tends to cross link the photoresist and remove all the solvents leaving a sturdier photoresist layer. The wafer is also cooled during etching by flowing helium on the backside of the wafer.

6.2.5 *Loading effects*

As mentioned earlier there is a limited supply of etching species in the plasma. Thus the size of the etched area directly corresponds to the etching rate in the system. For a very small substrate the etching rate may be higher because more of the etching species is available to take part in the chemical reaction while on larger substrates the depletion of etching species from the plasma may reduce the etching rate. This is called the loading effect. Loading effect may also depend on the pressure, species present and their resident time in the plasma.

In the next section we will discuss the etching of fused silica glass in an ICP system and Figure 6-4 shows the schematic for the Unaxis Shuttlelock ICP tool used in our etch experiments.
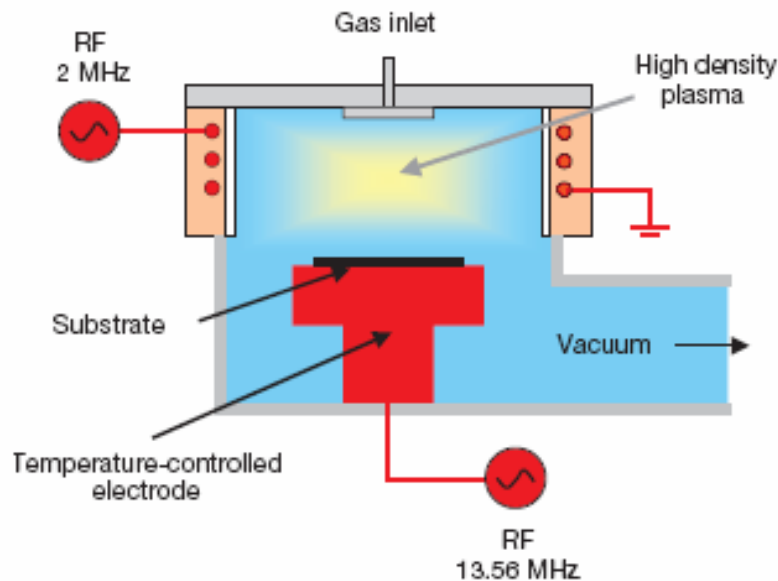
Figure 6-4 Schematic of the Unaxis Shuttlelock Inductively Coupled Plasma tool.

The power is inductively coupled into the plasma through RF source at 2MHz. A maximum power of 2KW can be coupled into the plasma using the source provided on this tool. A substrate bias is applied using a capacitively coupled RF source at 13.56 MHz. The system has a load lock chamber for loading the substrates. This ensures that the etch chamber is not exposed to atmosphere thus eliminating contamination and reducing system pump down time. The lower electrode has a separate RF source and controls the substrate bias independent of the top electrode which controls the plasma characteristics.

We will discuss the etching characteristics of fused silica glass using this tool and look at the etch process and surface quality of the fabricated optical elements in the following sections. We will look at parameters of interest such as etch rates for the glass and photoresist and selectivity and present recipes for varying the selectivity by tuning process parameters.

6.3   Etching of Fused silica Glass

Silicon dioxide etching is routinely performed in the IC industry. Thermal or Chemical Vapor Deposited (CVD) silicon dioxide films are used as the mask for diffusion or etching. In the optics industry fused silica glass composed of amorphous silicon dioxide is used routinely because of its excellent transmission properties over a wide spectrum. The choice of chemistry used in the etching is decided based on whether the reaction is endothermic or exothermic, rate of the reaction, nature of the etching species and the

nature of the by products. Other environmental and cost factors are also involved in the choice of the gases used.

SiO_2 can be etched in plasmas that produce fluorine atoms or alternatively feed mixtures that generate unsaturate-rich fluorocarbon species [57-59]. Fluorine atoms etch Silicon faster than SiO_2 but on III-V substrates they etch SiO_2 selectively. The reaction of SiO_2 with fluorine is given as

$$SiO_2 + 2F_2 \longrightarrow SiF_4 + O_2 \qquad\qquad 6.5$$

With the energy needed in the reaction ΔHo = -704 KJ/mol which implies an exothermic reaction. SiO2 can also be etched by chlorine gas and the reaction is given as

$$SiO_2 + 2Cl_2 \longrightarrow SiCl_4 + O_2 \qquad\qquad 6.6$$
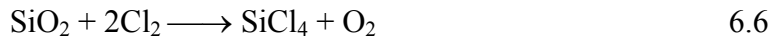
With the energy needed in the reaction ΔHo = 253.9 KJ/mol which implies an endothermic reaction. An endothermic reaction is harder to achieve while an exothermic reaction is spontaneous and the byproducts of the SiO_2, fluorine etch are volatile. On the other hand chlorine does not etch SiO_2 spontaneously since the reaction is endothermic and hence SiO_2 is a good masking layer in the etching of III-V compounds where chlorine is the preferred etching species.

Table 6-1 Etching Chemistry and Mechanisms in Oxide etching

Gas	Additives	Mechanism
NF_3	Ar	Chemical hence Isotropic
CF_4	O_2	Slow etching. Very little passivation and hence chemical component leads to isotropy while ion bombardment gives anisotropy.
CHF_3 C_3F_6 C_4F_8 C_5F_8 CH_2F_2	O_2	Ion assisted chemical hence anisotropic, Higher selectivity to photoresist. Higher etching rates
	H_2	Anisotropic. Polymer forming process leads to higher selectivity than O_2 addition. Higher etching rates

Though fluorine etching is most spontaneous providing volatile etch products there are no etch polymers as a result of the reaction. Fluorine also etches the photoresist nearly at the same rate and this makes selective etching with respect to photoresist very hard. Thus anisotropic and selective etching are hard to achieve in a fluorine based etch chemistry. Thus other polymer forming gas chemistries are utilized in the etching of SiO_2 and are listed in Table 6-1.

NF_3/Ar etching chemistry, where the etching mechanism is purely chemical leads to isotropic etching profiles. Etching with gases such as CF_4, CHF_3, C_3F_6, C_4F_8 etc. lead to unsaturated-rich fluorocarbon plasmas that can provide anisotropic etching due to sidewall passivation as a result of polymer deposition. These C_xF_y fluorocarbons

dissociate into CF, CF_2, CF_3, CF_4 and F radicals in the plasma due to electron neutral and electron radical collisions. Recombination reactions also occur in the plasma along with the dissociation events.

The parent gas e.g. C_xF_y can be dissociated and recombined into atoms and radicals by the following electron impact processes:

$$e + C_4F_8 \rightarrow 2C_2F_4 \qquad\qquad 6.7$$

$$e + C_2F_4 \rightarrow 2CF_2$$

$$e + CF_2 \rightarrow CF + F$$

$$e + CHF_3 \rightarrow CF_3 + H$$

$$e + CHF_3 \rightarrow CF_2 + HF$$

$$e + CHF_3 \rightarrow CHF + F$$

$$e + CHF \rightarrow CH + F$$

$$CH + H \rightarrow CH_2$$

$$e + CF_4 \rightarrow CF_3+ + F + 2e$$

$$e + CF_4 \rightarrow CF_3 + F + 2e$$

$$e + CF_4 \rightarrow CF_3{}^* + F + 2e \rightarrow CF_2 + 2F + e$$

$$e + CF_4 \rightarrow CF_3 + F$$

$$e + CF_4 \rightarrow CF_3 + F \rightarrow CF_2 + F + F$$

$$CF_2 + F \rightarrow CF_3$$
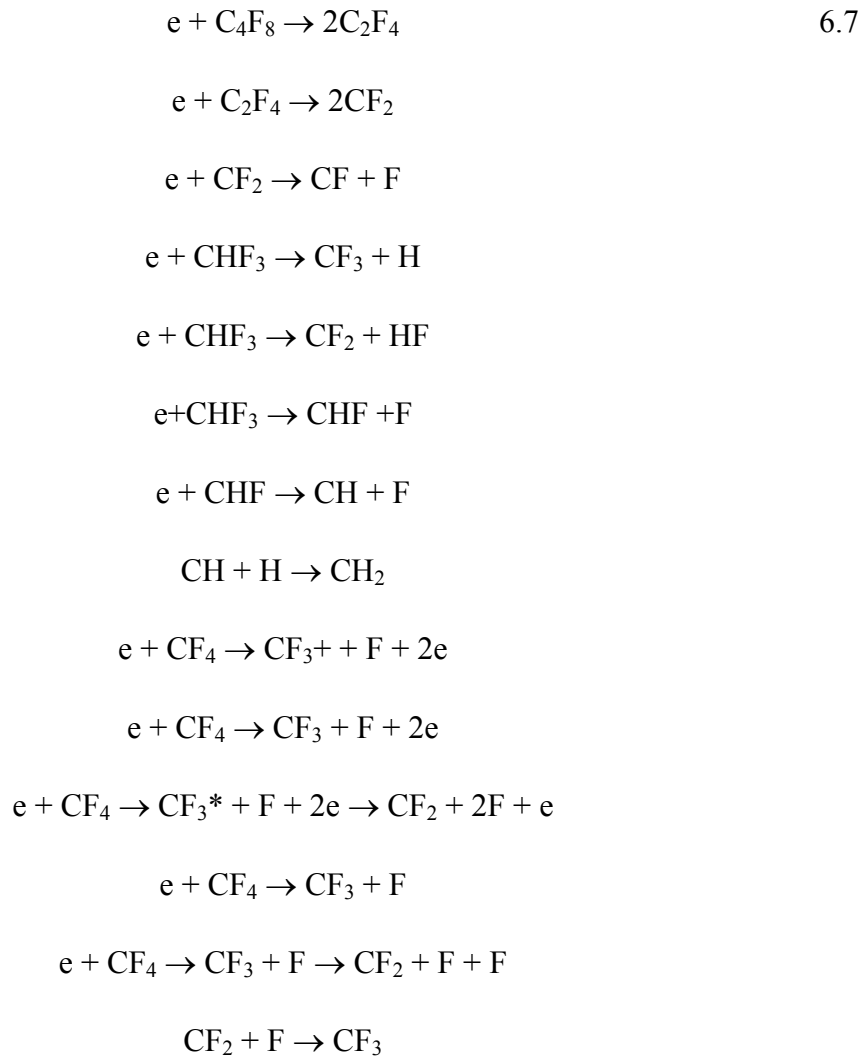
The fluorine atoms are transferred to the substrate from a thin layer of fluorocarbon deposited on the substrate when these species impinge on the oxide surface. As fresh CF_x radicals are added from the gas phase, material in this carbonaceous layer is continuously gasified by ion induced reaction with the SiO_2 substrate and sputtering. Ion damage produces dangling bonds and radical groups at the silicon dioxide interface, where Si bonds are eventually converted into Si_xF_y groups by using the F delivered from the thin fluorocarbon layer. Si_xF_y is volatile and is released into the plasma and pumped away. The exposed defects left behind due this process is then covered with new polymer. The thickness of this layer of polymer depends on the chemistry used, additives in the process and the rate of creation of dangling bonds due to the ion bombardment which depends on the RIE power in the ICP system and the polymer forming radicals formed as a result of dissociation and recombination reactions controlled by the ICP power. The ions impinging on the substrate are directional and hence the exposed surfaces where the ion bombardment is maximum is etched much faster than the sidewalls where the number of ions arriving at the surface are much lesser, thus leaving a layer of polymer that defends this surface against etching, Figure 6-5. This is called sidewall passivation and is the basis for anisotropic etching.
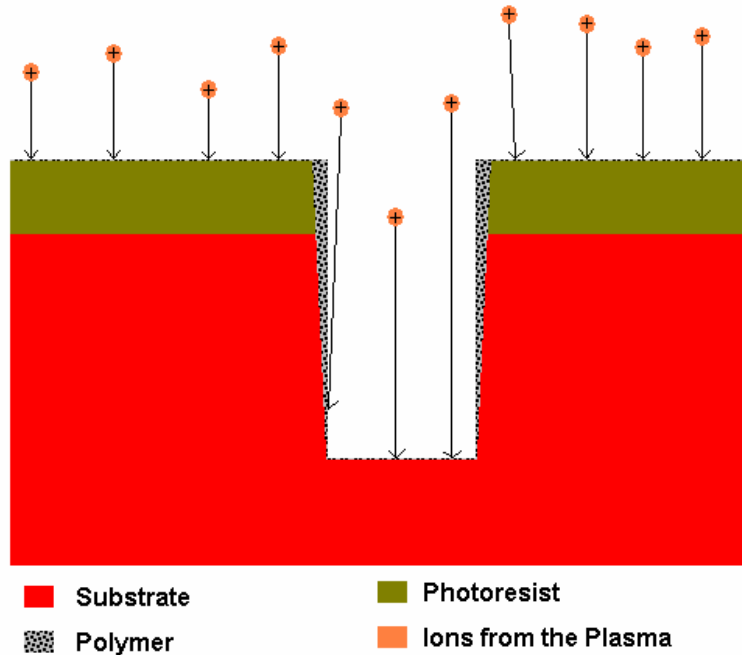
Figure 6-5 Polymer sidewall passivation and ion directionality during ICP etching

It is evident that there is a competition between the rates of polymer deposition and its subsequent removal due to the reaction and sputtering, and this depends on parameters such as gas additives in the plasma, power and pressure. If the rate of deposition is much higher than the rate of removal, a thick layer of polymer is formed. Formation of this passivation layer on the side wall at a very high rate without its removal can actually change sidewall profiles beyond acceptable limits and if removal rate from the exposed surfaces is much lower than the deposition rate it can completely stop the etch process. Thus by adjusting the parameters of the plasma process we can change the rate of polymer formation to aid etching with different selectivity between the mask and substrate.

In any plasma the energy required to form molecules by breaking a bond is much lower than the energy required for ionization and hence there are more radicals than ions in the plasma. Various fluorocarbons given in Table 5-1 have different dissociation energies in the plasma. Their dissociation mechanisms will help us understand the advantages of the various etching gases available. The typical dissociation mechanisms for C_4F_8, C_5F_8, C_4F_6 are given below,

$$[C_4F_8] \qquad\qquad C_4F_8 \rightarrow 2.3\ eV \Rightarrow 2C_2F_4 \rightarrow 6\ eV \Rightarrow 4CF_2 \qquad\qquad 6.8$$

$$[C_5F_8] \qquad\qquad C_5F_8 \rightarrow 7.2\ eV \Rightarrow C_3F_5 + C_2F_3$$

$$C_3F_5 \rightarrow 5 \sim 6.2\ eV \Rightarrow 3CF + 2F$$

$$C_2F_3 \rightarrow 5 \sim 6.2\ eV \Rightarrow CF_2 + CF$$

$$[C_4F_6] \qquad C_4F_6 \rightarrow 3\ eV \Rightarrow CF_2 + C_3F_4 \rightarrow 3\ eV \Rightarrow 2CF_2 + 2CF$$
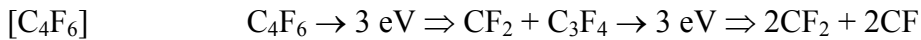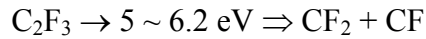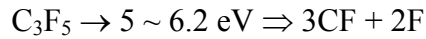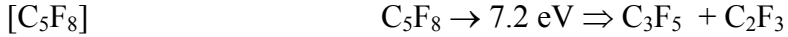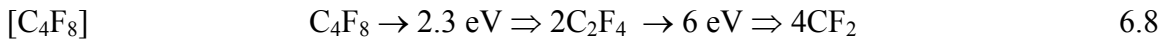
Additives such as oxygen increase the etchant concentrations and suppress polymer formation. In the etching of SiO_2 the formation of Si_xF_y species during the etching is followed by the release of O_2 which reacts with the carbonaceous film deposition on the surface thereby releasing volatile byproducts into the plasma reducing the polymer formation further. In the etching of Silicon, O_2 is not available as a byproduct of the reaction thus aiding in the formation of a polymer layer of the surface that inhibits etching. Positive DNQ photoresists have C-H groups and the presence of oxygen also assists in etching the photoresist by the same mechanism. Increase of fluorine radicals due to increased dissociation in the presence of oxygen also increases the photoresist etch

rate and leads to lower selectivity. Thus by controlling the feed of Oxygen in the plasma the selectivity of the SiO_2-photoresist etching can be controlled.

Addition of hydrogen to the plasma has the opposite effect as that of oxygen. Hydrogen tends to deplete the F radicals thus increasing the concentration of the polymer film formers in the plasma. CH_2 radical can form polymer more easily than CF_2; again a reason why hydrogen addition helps in polymer buildup. This then leads to higher selectivity in the etching of SiO_2 with photoresist masking. Addition of too much hydrogen might lead to formation of very thick layers of polymer that can completely halt the etching mechanism. Another effect this polymer formation can have is excessive sidewall passivation that may be detrimental in the etching of microoptical components, as will be shown through examples later in this section. The formation of polymer is also a major concern because it is very hard to remove from the surface after the etching and usually a long oxygen ashing step is necessary to clean the surface. The polymer is also coated on the chamber walls during the etch process and very long etches can lead to a very dirty chamber. This change in the chamber configuration affected over the etch cycle can affect etch process parameters such as etch rate and selectivity due to changes in the DC bias and dissociation. Thus as the F/C ratio decreases the CF_x radical content increases. This can be controlled by addition of O_2 or H_2 into the plasma.

The following types of reactions occur on the SiO$_2$ surface [60]

$$SiO_2 + 4CF \rightarrow SiF_4 + 2CO\uparrow + 2C \qquad\qquad 6.9$$

$$SiO_2 + 2CF_2 \rightarrow SiF_4 + 2CO\uparrow$$

$$3SiO_2 + 4CF_3 \rightarrow 3SiF_4 + 4O_2 + 4CO\uparrow$$

$$2SiO_2 + 6CF \rightarrow Si2F_6 + 4CO\uparrow + 2C$$

$$2SiO_2 + 3CF_2 \rightarrow Si2F_6 + CO_2 + 2CO\uparrow$$

$$2SiO_2 + 2CF_3 \rightarrow Si_2F_6 + 2CO\uparrow + O_2$$
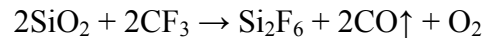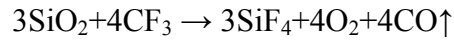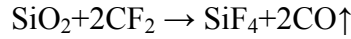
The by products of the etching are Si$_x$F$_y$ species as seen in the reactions. These are just some of the reactions occurring on the substrate and the byproducts from those reactions. These by products are volatile and are pumped out of the system as they are thrown into the plasma.

The parameters we will be looking at are the etch rate defined as

$$Etch\,Rate = \frac{Height\ of\ material\ etched}{Etching\ time} \qquad\qquad 6.10$$

and selectivity which is defined as

$$Selectivity = \frac{Etch\ rate\ of\ fused\ silica}{Etch\ rate\ of\ photoresist} \qquad\qquad 6.11$$

We used multilevel and binary patterns fabricated on S-1813 coated on fused silica substrates to study the etching characteristics using CHF_3 and O_2. Figure 6-6 shows the selectivity and Figure 6-7 shows the etch rate of photoresist and fused silica as a function of the percentage of O_2 in the gas feed mixture. As discussed before, it is seen that increasing the O_2 leads to lower selectivity but higher etch rates for photoresist and lower etch rate for the fused silica. The reason for the decrease in the etch rate of SiO_2 with increase in O_2 is the depletion of etchant concentration from the surface of the wafer due to reaction with oxygen, but this change is very small as compared to increase in etch rate of the photoresist. Further decreasing the RIE power increases the selectivity as seen in Figure 6-8.
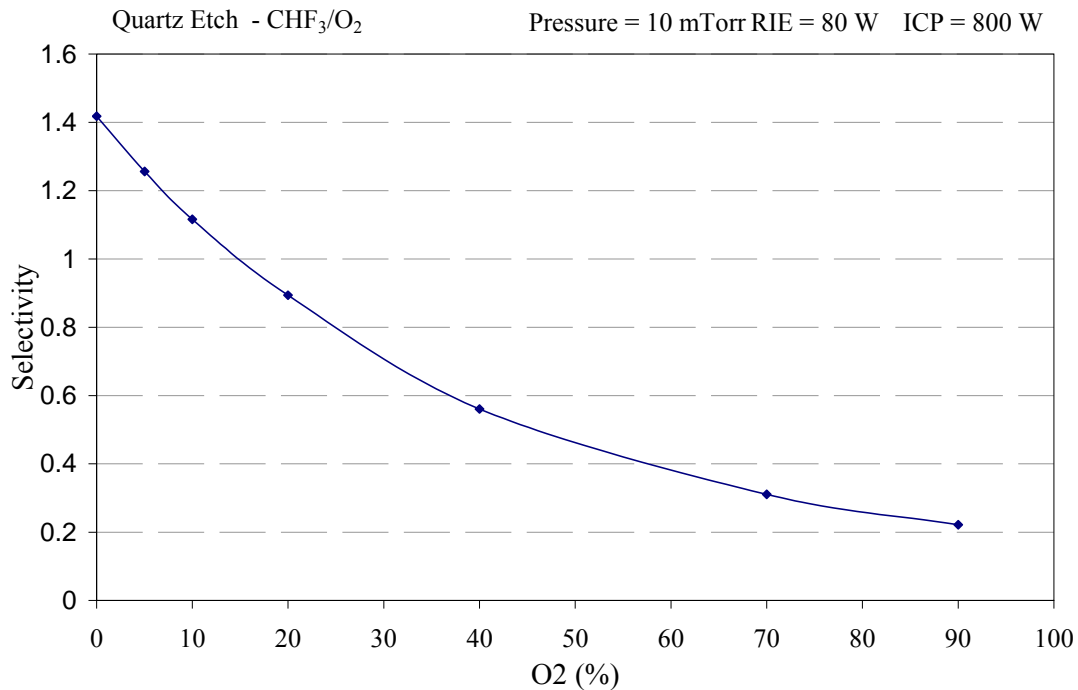
Figure 6-6 Selectivity as a function of % O_2 in a CHF_3 plasma
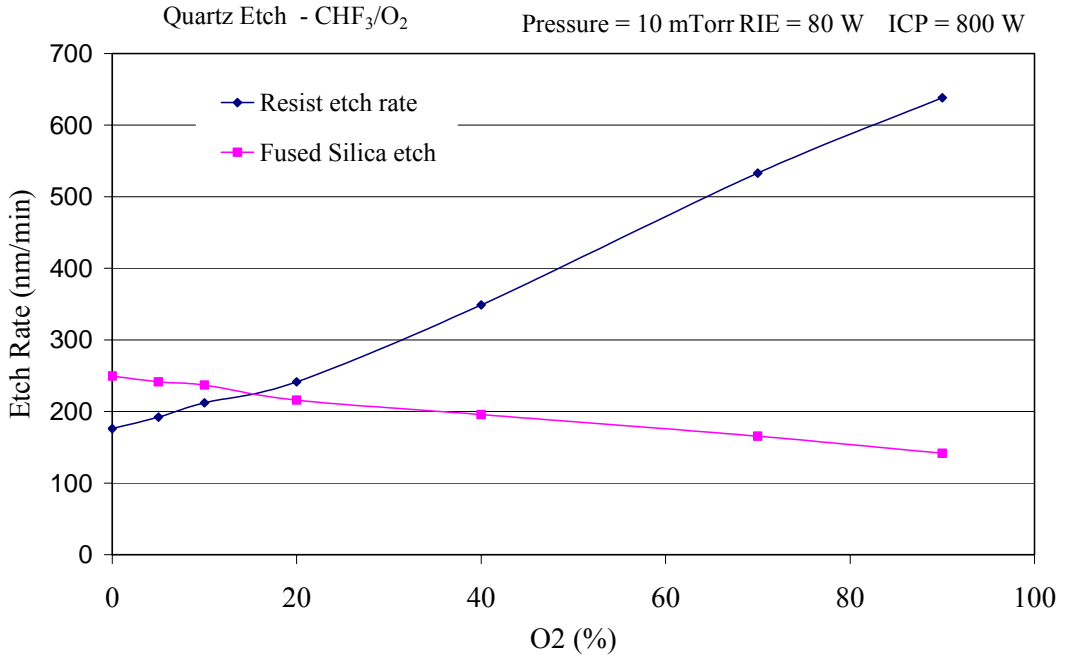
Figure 6-7 Etch rate v/s O_2 % for CHF_3/O_2 plasma
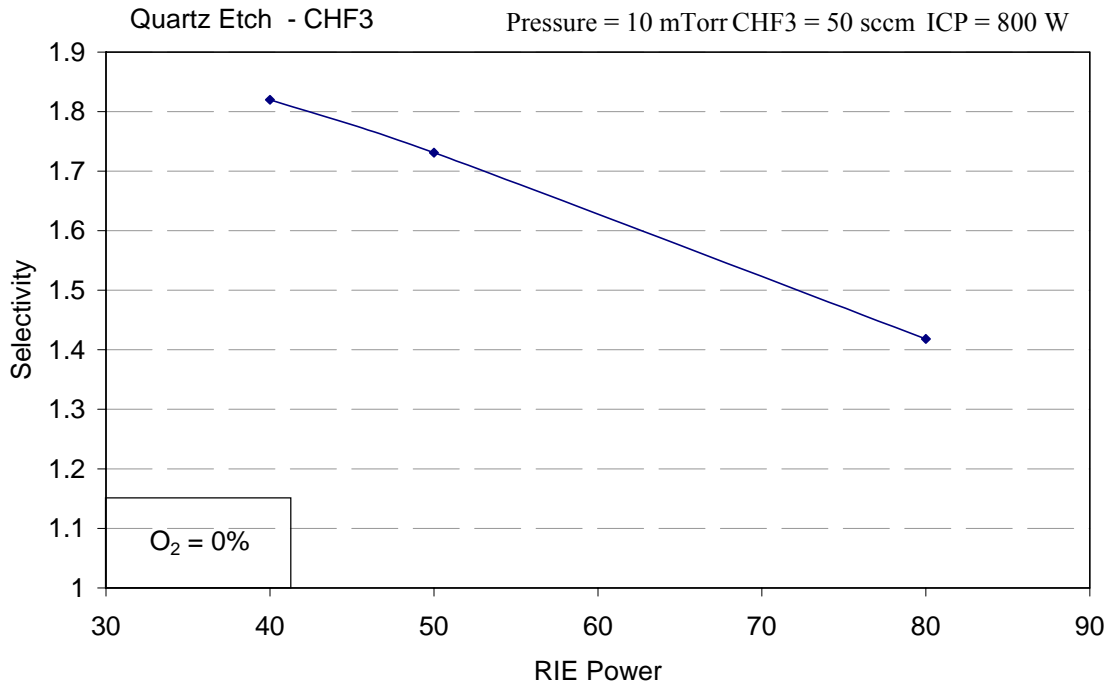
Figure 6-8 Selectivity v/s RIE power in a CHF_3 plasma

We have demonstrated a range of selectivity's from 0.2 to 1.8 using the CHF_3/O_2 chemistry and RF and ICP power control. Lower selectivity is useful for the fabrication of optical components for DUV or X-ray regime while the high selectivity etching can be used for optical elements used at the visible or infrared wavelengths. As seen in the earlier chapter the level height error in the additive lithography process is about 12 nm. This error does not change much when we try to fabricate elements with very small level heights, since it arises due to shutter control on the stepper. Components fabricated on photoresist for the DUV or X-ray regime will require very small level heights; if using a 1:1 selectivity etching to transfer onto the substrate. Instead it is advantageous to fabricate elements with higher sag on the photoresist and perform a low selectivity etch to obtain the optical element for operation at the required wavelength on the substrate. On the other hand it was seen earlier that the required sag may be higher for optical elements to be operated in the infrared regime. The non linear working region of the resist provides unequal level heights and hence it would be better to fabricate elements with lower sag on the photoresist and then transfer etch them using a higher selectivity into the substrate to obtain the required sag on the substrate.

The highest selectivity obtained from the CHF_3 process may therefore not be enough for many applications. We tried to use the C_4F_8/H_2 chemistry to obtain higher selectivity. These experiments were performed on a Versaline tool at Unaxis. The most important modification on the tool was the introduction of heated surfaces to reduce polymer buildup on the chamber sidewalls allowing for longer etches without need for frequent chamber cleaning. It showed excessive sidewall passivation and polymer migration on

the wafer surface leading to surfaces covered with islands of polymer. The SEM images in Figure 6-9 shows these problems associated with the highly polymerizing C_4F_8/H_2 process.

To avoid these problems $C_4F_8/CHF_3/Ar$ chemistry was utilized on the shuttlelock. The thought was to introduce hydrogen through a polymer instead of directly and using Ar to improve dissociation and sputtering to control the polymer removal. In doing so the selectivity control is seen to be through the RIE power. Absence of chemical reactions leading to polymer removal and sputtering being the major contributor to this polymer removal leads to this dependence on the RIE power. Figure 6-10 shows the selectivity in the etching between the fused silica substrate and the S1813 photoresist using this process.

Figure 6-10 shows the etch rate v/s the RIE in this process. Using RIE power above 70W causes excessive sputtering of the resist leading to surface roughness. At lower RIE powers the etch rate goes down drastically but the sputtering due to argon is reduced and better surface profiles are obtained. SEM images of the sidewalls obtained while etching analog elements fabricated using the phase masking technique, using this multi gas process with a 2.7:1 selectivity is shown in Figure 6-12.
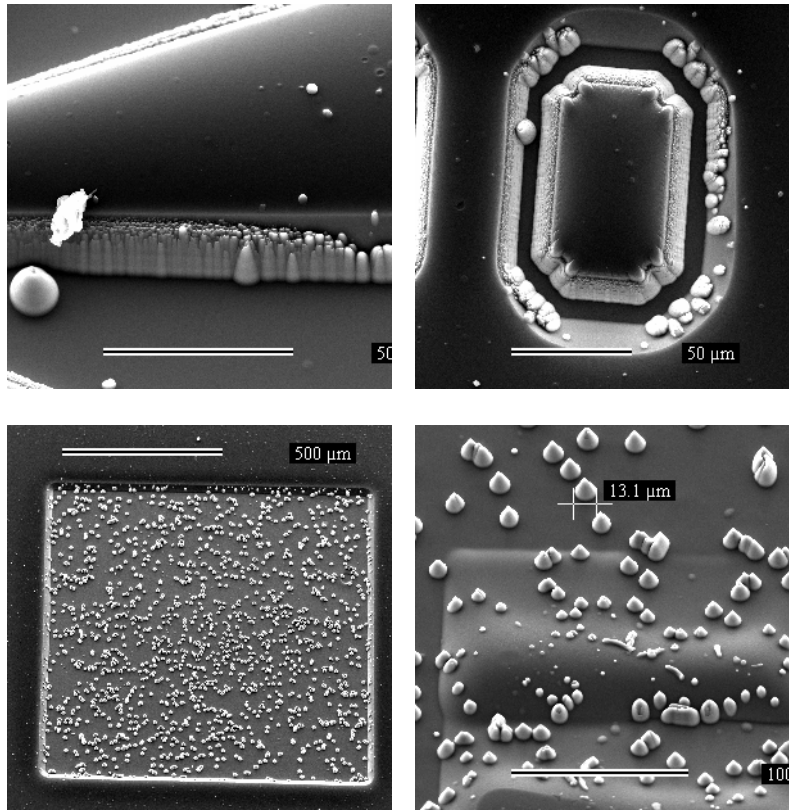
Figure 6-9 SEM images of polymer residue in a C_4F_8/H_2 etch process
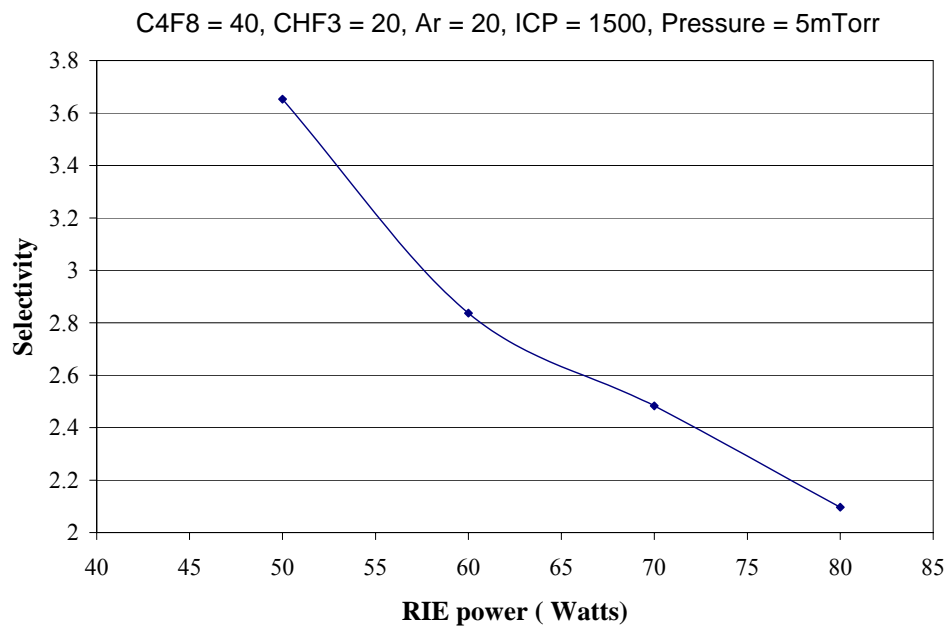
Figure 6-10 Selectivity v/s RIE power for $C_4F_8/CHF_3/Ar$ plasma
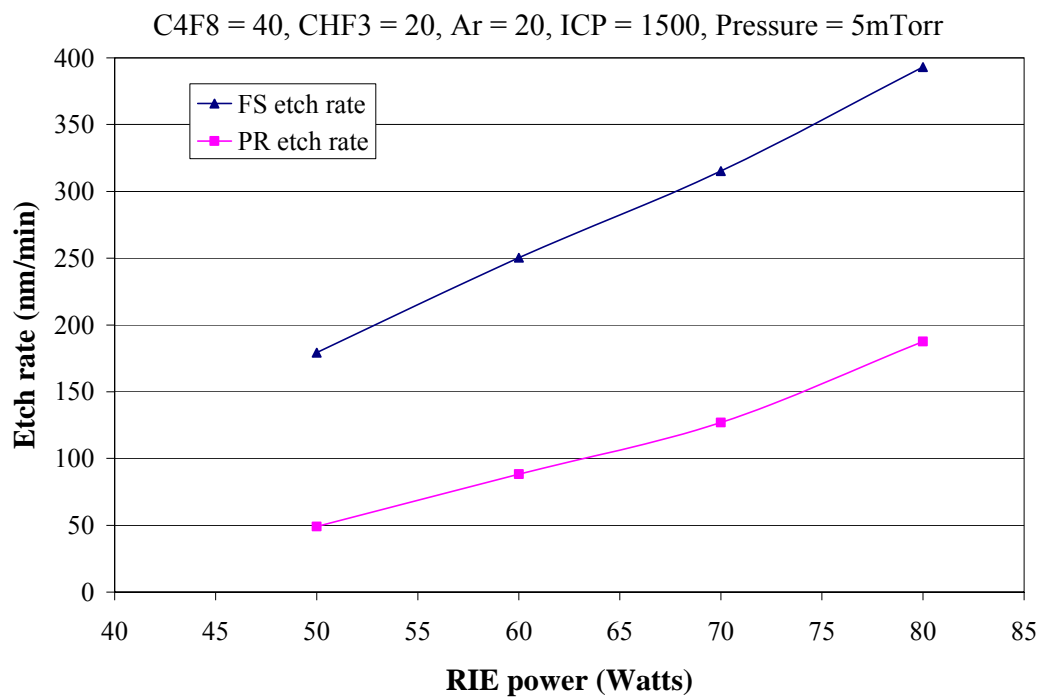
Figure 6-11 Etch rate of Photoresist and SiO_2 v/s RIE power for C_4F_8/CHF_3/Ar plasma.
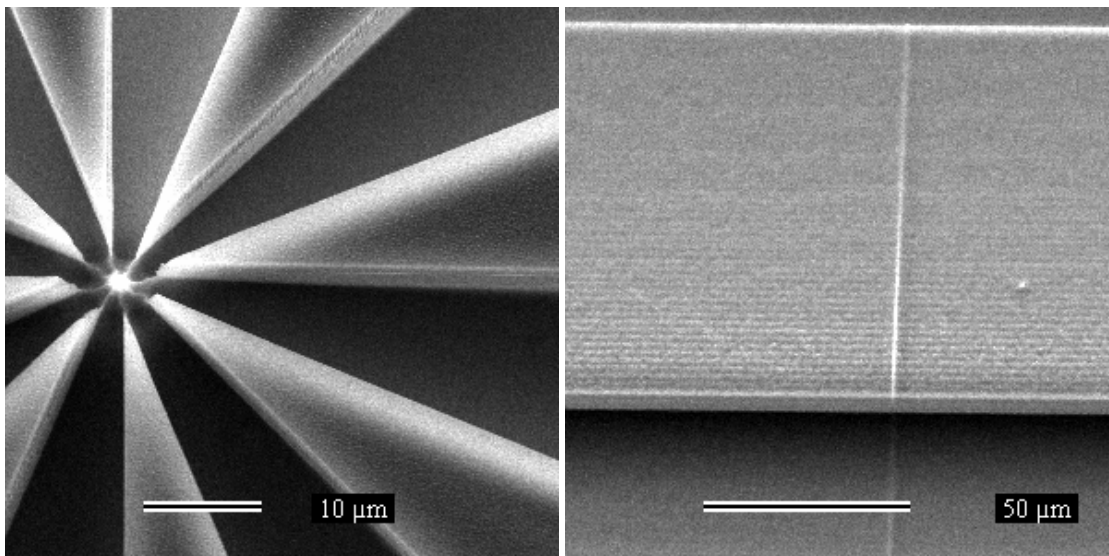
Figure 6-12 SEM of 2.7:1 selectivity with C_4F_8/CHF_3/Ar plasma

Additive positive lenses and multiplexed elements were etched using the low selectivity and high selectivity processes developed using CHF_3/O_2 and with $C_4F_8/CHF_3/Ar$ respectively. The positive diffractive lens with maximum sag of 976 nm fabricated using the entire domain lithographic process, shown in Figure 5-2, was etched for operation at 632 nm. The required sag of the final optic on the fused silica glass substrate is 1380 nm and this was achieved by etching with a CHF_3/O_2-1.4:1 selectivity process from the curve in Figure 6-6. The final 3-D and 2-D profile of the diffractive lens on the substrate is shown in Figure 6-13.
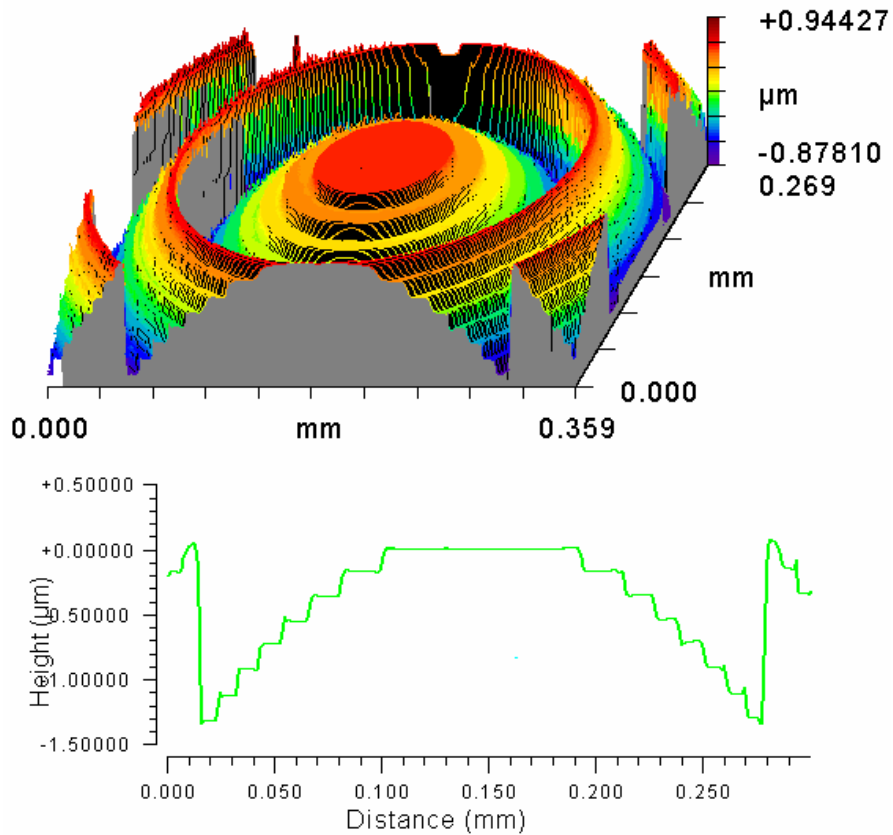
Figure 6-13 3D and 2D profiles of diffractive positive lens etched into the substrate with a 1.4:1 selectivity CHF_3/O_2 process

A similar positive diffractive lens as shown in Figure 5-2 was also etched for operation at 1550 nm on fused silica glass. The required sag for this structure comes out to be 3.5 μm, thus requiring a selectivity of 3.6:1. For this etch selectivity we employed the $C_4F_8/CHF_3/Ar$ chemistry and the final profile of the lens etched into the substrate is shown in Figure 6-14.
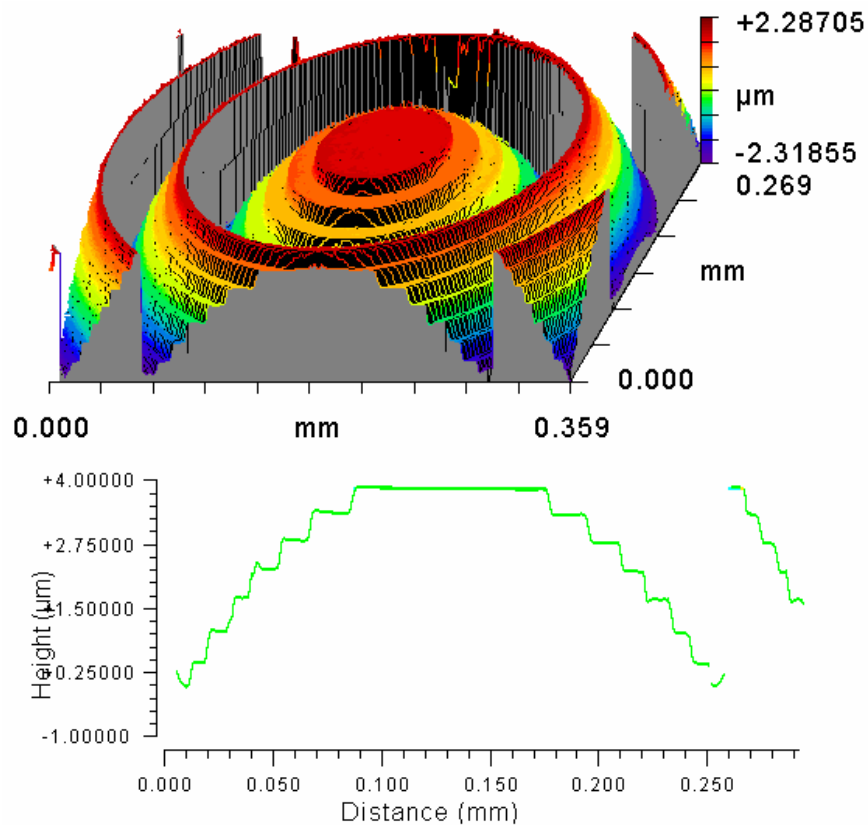
Figure 6-14 3D and 2D profiles of diffractive positive lens etched into the substrate with a 3.6:1 selectivity $C_4F_8/CHF_3/Ar$ process

In Chapter 5 we discussed the fabrication of hybrid optical elements. These elements have large features originating from the positive diffractive lens design and very small features belonging to the multiplexed 2.2 μm period grating and the 2.2 μm hole array.

These hybrid elements on photoresist shown in Figure 5-23 and Figure 5-24 were etched with a selectivity of 1.4:1 in a CHF$_3$/O$_2$ chemistry.
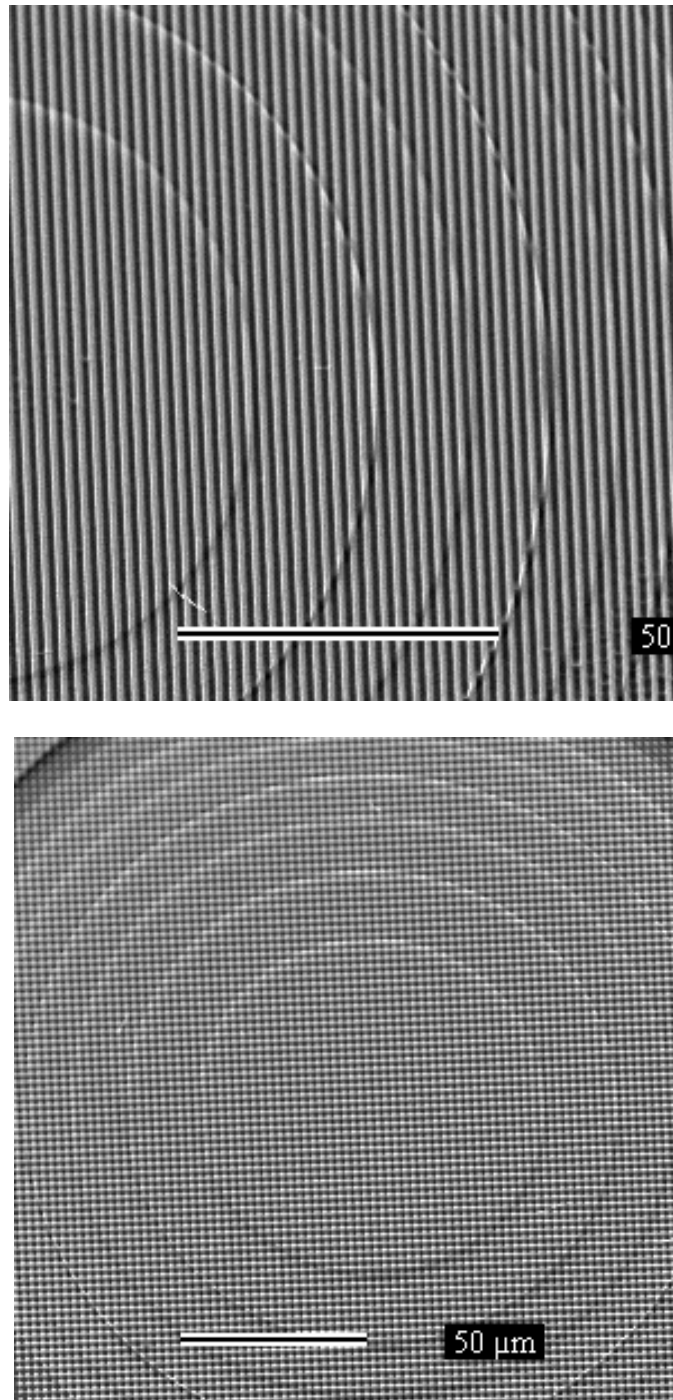
Figure 6-15 2.2 μm grating and 2.2 μm hole array multiplexed on a positive diffractive lens and etched in the glass substrate using a CHF$_3$/O$_2$ chemistry and 1.4:1 selectivity.

6.4   Morphing

In Chapter 5 it was shown that using a resist with a non linear working region results in unequal level heights. It was also shown that additive lithography on the aligner causes similar level height errors even for thin resist. This is undesirable since the multilevel profile is quantized in phase to represent the original analog profile. Variation of level heights will lead to low diffraction efficiencies for the fabricated optical elements. These inaccuracies of the fabricated elements on the photoresist can be corrected during the etching process by using morphing schemes.

As seen in the previous sections the etch selectivity can be easily varied by controlling the process parameters. The etching process starts by transferring the lowest levels in the photoresist into the substrate and slowly proceeding to the higher levels. The height of the level on the substrate is defined by the process as shown in the previous section. In the morphing scheme, the selectivity and time required for transferring each level into the substrate is obtained from the high and low selectivity curves and etch rate curves respectively. The etch process for each level is then fixed for the specific time corresponding to the particular level being etched. The complete process for etching an 8-level element with unequal level heights is then made of 7 steps with each step representing a different process and different time for the specific level being etched during that time. The initial profile of the 8 level lens fabricated on SPR 220-7 shown in Figure 5-7 was then etched to obtain equal level heights of 700 nm using this morphing scheme. The selectivity and time required for each of these levels was obtained from the curves shown in Figure 6-6-Figure 6-8 , Figure 6-10 and Figure 6-11. The final 3-D and

142

2-D profiles of the 8-level diffractive lens on the fused silica substrate obtained as a result of this morphed etching scheme is shown in Figure 6-16. The initial standard deviation of the level heights on photoresist was 278.85 nm and the standard deviation of the final level heights on the substrate was reduced to 39.52 nm after the morphed etching.
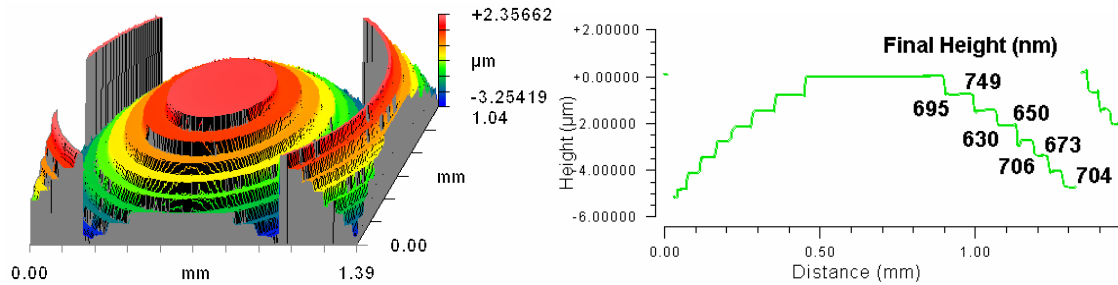
Figure 6-16 Morphed etching of the initial profile on SPR 220-7 shown in Figure 5-7 to obtain 700 nm level heights on the substrate.

Morphed etching can also be implemented in a continuous process modification mode where one of more of the process parameters are varied in along a smooth curve instead of the discrete steps used to etch the multilevel element. This would allow us to correct for surface profiles of analog optical elements so as to reduce aberrations; such as with high NA optical elements fabricated using the reflow process.

CHAPTER 7: CONCLUSIONS

In this work we have presented an innovative technique for the fabrication of multilevel and analog micro optical elements. The technique is based on sculpting the photoresist using cost effective binary masks and controlled partial exposures. Various masking schemes were also introduced to make the process more flexible so as to allow fabrication of a range of optical elements. The exposures are performed successively through multiple masks obtained from the 2N level break up of an optical element and a single developing step results in the required profiles on the resist. Using entire domain masking schemes we have demonstrated the fabrication of various DOEs such as positive and negative lenses, vortex elements, fan out elements. Multiplexing of these structures for increased functionality was also demonstrated. The alignment between these masking patterns on the stepper is very accurate and the error is less than ±50 nm. It was shown that the fabricated structures had a 90% or greater efficiency. The sub-domain masking scheme was introduced for fabricating a variety of optical elements belonging to a specific symmetry using the same mask set. Various optical elements such as high NA lenses, diffractive positive and negative lenses and toroidal lenses were fabricated using this masking scheme. It was shown that the efficiency of the fabricated elements was greater than 87%. Through these examples we demonstrated that the additive lithographic technique is a highly efficient and cost effective process for sculpting complex optical surface profiles onto the photoresist.

These masking schemes were then used to introduce flexibility and control to the photoresist reflow process for fabricating refractive structures. We demonstrated that it is possible through volume sculpting to vary the F# of these lenses over a wide range without the need to modify the initial thickness of the photoresist coated onto the substrate. This can allow for easy fabrication of lenses with different designs on the same wafer using simple binary masking patterns and additive sculpting. Fabrication of other interesting refractive beam shaping elements by controlling the time and the temperature of the process was also demonstrated.

The fabricated structures were then etched into the glass substrate. Selectivity and etch rate curves using different gas feed mixtures and process parameters were developed. We were able to vary the selectivity between the photoresist and the glass substrate from 0.2 to 3.5. It was shown that a linear contrast curve gives equal level heights but requires thinner photoresists. The fabricated patterns have to be stretched through a high selectivity process for operation at infrared wavelengths. Similarly to avoid level height errors for fabricating components for operation at ultraviolet and deep ultraviolet it is necessary to fabricate higher sag structures and etch them with a lower selectivity. We have etched elements for operation at two different wavelengths and have also demonstrated the etching of multiplexed elements.

Thus the additive process was demonstrated as an inexpensive high throughput process for fabricating highly efficient micro optical elements. Though the additive technique is better performed on a stepper it can be easily performed on an aligner. On an aligner,

optical elements with aperture sizes larger than 20x20 mm can be easily fabricated at the expense of decreased tolerance and increased fabrication time because of the manual pattern to pattern alignment process.

Additive lithography is a very promising technique for fabricating highly complex micro fluidic channels and mems devices. It can also be used for fabricating novel optical and mechanical structures using multicontrast photoresist or polymers. By utilizing other etch chemistries we can further increase the etch selectivity, useful in the fabrication of very high NA optical elements. Studying thick photoresist processing parameters may help us increase the linearity of the resist and help us to improve process flexibility.

APPENDIX A: LITHOGRAPHIC MODELING

The basic elements involved in a projection imaging system were discussed in chapter 3. Here we will discuss the modeling of the lithographic exposure system and developing process to obtain the final profile on the photoresist from a given set of masking patterns. There are four parts in this modeling; calculation of the aerial image, computing the bulk image intensity, computing the corresponding Photo Active Compound (PAC) distribution from the bulk intensity, and computing the final photoresist profile after developing of the photoresist in the solvent. We will look at each one of these in detail in the next few sections. For modeling a stepper system with NA ≤ 0.5 scalar techniques are sufficient. At NA ≥ 0.6 the polarization effects cannot be neglected and full electro magnetic wave simulations using Maxwell's equations have to be performed. The stepper in our laboratory is a GCA 6300 G-line system with a NA=0.35 and hence we will stick to scalar computations.

Aerial image

The schematic of a typical projection system with a Koehler illumination is shown in the Figure A- 1. The source illuminates the mask uniformly and the energy transmitted through the mask forms a distribution in the pupil plane where the source image is formed [61,62]. The distribution formed due to the mask is the mask spectrum formed due to the Fourier transforming properties of the lens. The lower spatial frequencies are close to the axis while the higher frequencies are close to the edge of the pupil. Higher frequencies than this are cut off by the pupil. If the object transmittance is represented as

t(x,y) then the distribution of the mask spectrum in the pupil plane corresponding to t(x,y) can be written as T(f,g).
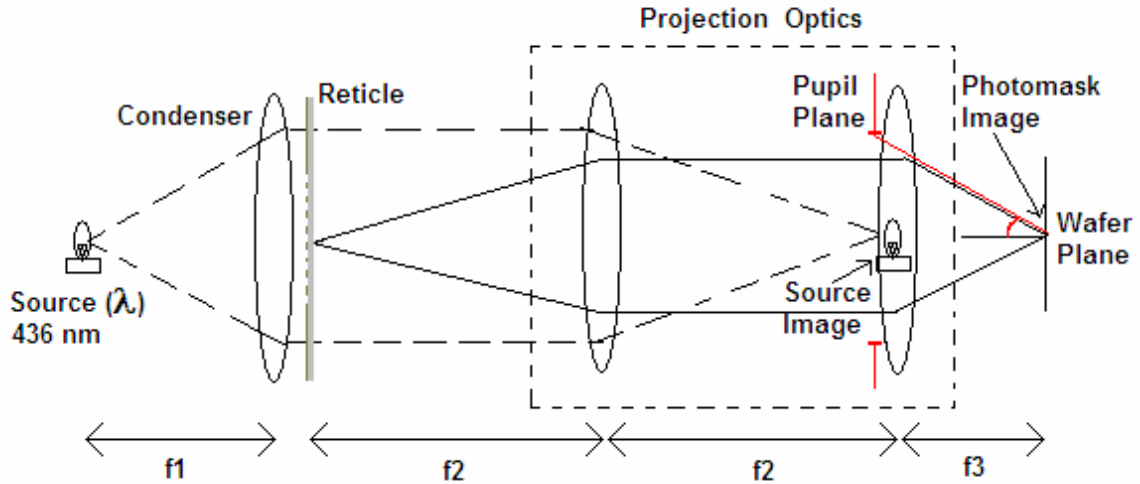
Figure A- 1 Equivalent representation of an optical projection system

The pupil function can be written as P(f,g) and performs the function of filtering the higher spatial frequencies from the mask spectrum. Each spectral component can be thought of as a ray traveling at a specific angle in the system. The maximum angle at which the ray can travel without getting cut off is 'θ' and the numerical aperture of the system is then NA=sin θ. The image plane intensity from the spectral component T(f,g) is then given by $T(f,g)P(f,g)e^{-i2\pi(fx1+gy1)}$ where (x1,y1) are the image plane coordinates. We will perform all our simulations to a 1X system i.e. (x, y) ≡ (x1, y1). The total image plane distribution is formed by the contribution of all the spatial frequencies of the mask spectrum that lie within the pupil.

Thus we have

$$E(x,y) = \int_{-\infty}^{\infty} P(f,g)\,T(f,g)\,e^{-2\pi(fx+gy)}\;df\;dg \qquad\qquad\text{A.1}$$

This means that the image is formed by the interference of all the spatial frequencies and that each spatial frequency T(f,g) is modified by the projection system response at the same frequency P(f,g). For a circularly symmetric optical system the pupil function can be written as

$$P(f,g) = 1 \qquad \sqrt{(f^2+g^2)} \le \frac{|NA|}{\lambda}$$
$$\qquad\quad 0 \qquad otherwise \qquad\qquad\text{A.2}$$

The intensity at the image plane is then given as

$$I(x,y) = |E(x,y)|^2 = \left| \int_{-\infty}^{\infty} P(f,g)\,T(f,g)\,e^{-2\pi(fx+gy)}\;df\;dg \right|^2 \qquad\qquad\text{A.3}$$

This intensity distribution at the wafer plane is obtained for a monochromatic coherent point source. In general the stepper source is partially coherent with a coherence factor defined by 'σ' (0.6 for GCA 6300). A partially coherent source illuminates the mask with light traveling in various directions but incoherent with each other so that they do not interfere and hence do not lead to non uniform intensity impinging on the mask. Thus

150

image plane intensity due to each source point is individually computed and the sum of the intensity due to all these sources is the actual image plane intensity given by,

$$I(x,y) = \frac{\sum_s a_s I_s(x,y)}{\sum_s a_s} \qquad \text{A.4}$$

It was shown earlier that the image of the source is formed in the pupil plane. We can associate with each source point a coordinate (fs, gs) corresponding to its location in the pupil plane. For coherent imaging (fs,gs)=(0,0). For a general point source with (fs,gs)≠(0,0) we make the approximation that the optical system is shift invariant such that the spectrum of the reticle due to the source point 's' is given as T(f-fs, g-gs). This is similar to multiplying the input mask transmittance t(x,y) by a phase ei2π(fs x+gs y)

The partial coherence of the source is given as

$$\sigma = \frac{NA_s}{NA} \qquad \text{A.5}$$

NAs is the numerical aperture of the source. The source frequencies are bound by the numerical aperture of the source and thus the frequencies of the source are limited to

$$\sqrt{f_s^2 + g_s^2} \le \frac{|NA_s|}{\lambda} \qquad \text{A.6}$$

151

The computation of the aerial image is then done for each source (fs,gs) and the intensity due to each source is added up to provide the intensity distribution in the aerial image due to the partially coherent imaging. In imaging systems partially coherent imaging leads to higher resolution than coherent imaging.

Bulk image computation

The above computation provides us the aerial image and we need to compute the intensity distribution in the photoresist. From this we can calculate the concentration of the PAC after exposure.

There are multiple events occurring as the light propagates through the photoresist. There is absorption which leads to change in index of the medium, scattering and reflection at the wafer surface and the formation of standing waves within the photoresist due to the incident and back reflected light. Apart from this the image is sharp only within the DOF and the image diffracts within the photoresist. All these lead to the fluctuations from the ideal profile in the photoresist and therefore need to be studied. Studying this propagation through the photoresist is quite complicated and many approximations are made to compute the bulk intensity profile inside the photoresist.

The aerial image calculator provides the intensity in the plane of best focus. The stepper system can pick up the wafer surface and adjust so that the image is at best focus on the surface of the photoresist. But there could be errors due to temperature, barometric

pressure, wafer surface quality, photoresist uniformity etc. Even otherwise there could be inherent defocus since the photoresist is thick and the image will be out of focus beyond the DOF of the stepper system. Usually the best focus plane is chosen so that it lies at the middle of the photoresist. Thus the surface of the wafer is at a defocus and this needs to be taken into account when calculating the intensity in the photoresist.

The phase error describing a defocus of D is then written as

$$\phi(x,y) = k_z D = D\sqrt{k^2 - k_x^2 - k_y^2}$$
A.7

kz is the z component of imaging wave vector. Under a paraxial conditions this expression can be further simplified to

$$\phi(x,y) = kD - \frac{k}{2}(i_x^2 + i_y^2)D = kD - \frac{k}{2}\lambda^2(f^2 + g^2)D$$
A.8

This phase shift due to the defocus is then included in the pupil plane by simply multiplying the factor 'W' given below to the mask spectrum in the pupil plane.

$$W_D(f,g) = exp(j\phi(x,y)) = exp(j\pi\lambda D(f^2 + g^2))$$
A.9

In the case of the photoresist we can calculate this defocus error for various planes inside the photoresist an effective D can be defined as,

$$D_{eff}(z) = D - \frac{z}{n_r}$$
A.10

This is the first order model and here the intensity at each point in the z direction is calculated as

$$I(x,z) = I(x, D_{eff}(z))I_s(z)$$
A.11

where I(x,Deff(z)) is calculated by taking into effect the defocus factor W for each z point. Is(z) is the standing wave intensity and is calculated assuming a plane wave of light is normally incident on the photoresist coated substrate.

When a thin dielectric film is placed between two media and exposed to monochromatic light standing waves are produced in the film. This is shown in Figure A- 2 where a film of thickness D with complex index of refraction n2 is coated on a substrate with index n3 and the index of air or the surrounding medium is n1. An electromagnetic plane wave is normally incident on this film.
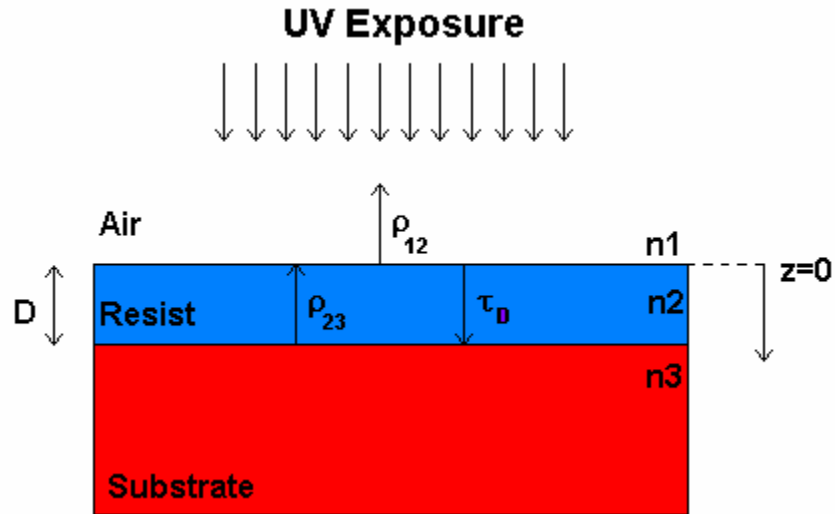
Figure A- 2 Dynamics of the substrate photoresist system during exposure

The standing wave amplitude in the film is then given as

$$E_s(x,y,z) = E_i(x,y)\frac{\tau_{12}(exp(-i2\pi n_2 z/\lambda)+\rho_{23}\tau_D^{\,2}\,exp(i2\pi n_2 z/\lambda))}{1+\rho_{12}\rho_{23}\tau_D^{\,2}} \qquad \text{A.12}$$

$E_i(x,y)$ is the incident wave at z=0

$\rho_{ij}=(n_i-n_j)/(n_i+n_j)$ the reflection coefficient

$\tau_{ij}=2n_i/(n_i+n_j)$ the transmission coefficient

$\tau_D=exp(-ik_2 D)$ the internal transmittance of the film

$k_j=2\pi n_j/\lambda$

$n_j=n_j-i\kappa_j$ the complex index of refraction

The absorption coefficient is related to the imaginary part of the index by

$$\alpha = \frac{4\pi\kappa}{\lambda} \qquad\qquad \text{A.13}$$

This gives us the standing wave intensity and from the earlier equation we can obtain the intensity profile inside the photoresist. We need to still find out the PAC distribution inside the photoresist from this information and that will then be used to find out what the developed photoresist profile will look like.

We will look at the macroscopic absorption in photoresists and study effect of exposure intensity on the PAC. We will apply this mainly positive photoresists and the principle is the same for negative photoresists. A typical diazonaphthoquinone (DNQ) photoresist typically consists of a base resin R which gives the photoresist its structural properties, a photoactive compound M, exposure products P generated by reaction of M when exposed to ultra violet light, and a solvent S. Though most of the solvents are driven out in the soft bake process after coating, typically 5-10% may still be present. The absorption coefficient is then given in terms of Dills A and B parameters as

$$\alpha = Am + B \qquad\qquad \text{A.14}$$

where m=M/M0, where M0 is the initial PAC concentration. A and B are also called the bleachable and nonbleachable absorption coefficients. Thus when the photoresist is completely exposed α=B and when the photoresist is unexposed α=A+B and m=1.

An analysis of the microscopic absorption of a photon in a DNQ photoresist sytem leads us to the time dependence of m during exposure and is given as

$$\frac{dm}{dt} = -C\,I\,m \qquad\qquad\qquad \text{A.15}$$

where C is the third Dill parameter and is also called the standard exposure rate constant and I is the intensity at any point within the photoresist.

We obtained the bulk intensity inside the photoresist and now from the above equation we can calculate the PAC concentration given by 'm' by using the above equation. The exposed photoresist may be subjected to post exposure bake (PEB) either for removing the standing wave effect or for thick photoresists where the reaction needs to be assisted by the presence of water and the PEB.

Photoresist Developing

In the previous sections the PAC distribution inside the photoresist was computed. This was largely determined by the Dill parameters of the photoresist being used. The actual pattern on the photoresist shows up on developing when the exposed material is selectively etched away as in positive photoresists or the unexposed photoresist is selectively etched away as is the case with negative photoresists. We will study the behavior of positive photoresists since that will be the main category of photoresists studied in this work for fabricating micro optic elements using additive lithography.

There are two technologies available for developing namely wet developing using solvents and dry developing which is similar to plasma etching. Wet developing can be done by spraying the developer on the wafer while spinning, forming a puddle on the wafer or immersing the wafer into the developer solution. Both processes utilize exposure induced changes in the photoresist which could be either variation in molecular weight of the polymers by chain scission or chain formation also called cross linking during the exposure and reactivity or polarity change due to exposure. The disadvantages of wet developing are swelling of the photoresist, loss of adhesion to the wafer and the enormous amounts of toxic solvents needed in this process. Due to these advantages dry developing is replacing wet developing slowly in the industry.

The first step in the developing process is to calculate the dissolution rate 'R' based on the final PAC concentration after exposure and post exposure processing. Post exposure processing involves delay effects and PEB, e.g. thick photoresists like AZ 4903 that have to be allowed to absorb ambient moisture for the reaction to occur; usually for a minimum of half an hour before exposure and chemically amplified photoresists that also need a bake to amplify the exposure through reactions into the photoresist bulk. We will not discuss these processes here except to mention that these are diffusion processes where the acid released during exposure diffuses to smoothen out the profile and/or start a chain of reactions to change the polymer dissolution properties through the bulk [62].

There are many models for the calculation of the dissolution rate of the photoresist but we will look at the Mack 4- parameter and 5-parameter models. The parameters needed

for these models were supplied by the vendor and are very specific to the processing conditions, developer used and the concentration of this solution.

This model is also called the kinetic development model since it involves proposing a reasonable mechanism for the development reaction and then applying standard kinetics to this mechanism to derive the rate equation. There are assumed to be three processes occurring: diffusion of developer from the bulk solution to the surface of the photoresist, reaction of the developer with the photoresist and diffusion of the byproducts back into the solution.

The photoresist is formed by a base resin and the photo active compound. The resin itself easily dissolves in the developer but the presence of the photo active compound acts as an inhibitor to this dissolution process. The reduction of PAC after exposure increases the dissolution rate of the resin in the developer for the positive photoresist. With this in mind the rate equation from Mack's 4-parameter model is given as

$$r = r_{max} \frac{(a+1)(1-m)^n}{a+(1-m)^n} + r_{min} \qquad \text{A.16}$$

where

$$a = \frac{(n+1)}{(n-1)}(1-m_{th})^n \qquad \text{A.17}$$

where n is a selectivity parameter defining sensitivity of exposed photoresist to the developer, mth is a threshold inhibitor concentration and is the value of m at the

159

inflection point in the dissolution curve. The parameters rmin and rmax are the dissolution rate of the photoresist when m=1 and m=0 respectively.

This model is based on dissolution enhancement due to the formation of carboxylic acid during the exposure. The effect of the PAC in inhibition is not included in this model. Mack proposed a new enhanced 5-parameter model to include this effect. The rate equation from this model is given as

$$r_{enh} = r_{re\,sin} \frac{1 + k_{enh}(1 - m)^n}{1 + k_{inh}m^l} \qquad\qquad A.18$$

where rresin is the dissolution rate of the resin alone, kinh is the rate constant for the inhibitor mechanism, kenh is the rate constant for the enhancement mechanism, n is the enhancement mechanism and l is the inhibition reaction order.

For m=1 corresponding to no exposure we have

$$r_{min} = \frac{r_{re\,sin}}{1 + k_{inh}} \qquad\qquad A.19$$

and for m=0 corresponding to full exposure we have

$$r_{r\,max} = r_{re\,sin}(1 + k_{enh}) \qquad\qquad A.20$$

Thus we are now equipped with the dissolution rate depending on the PAC at each point inside the photoresist bulk. Now we need to perform an actual developing model where the photoresist is etched away to form the final profile on the photoresist depending on the bulk PAC distribution after exposure. There are various models that are routinely used to study such problems in lithography or etching and deposition.

The idea is to track the advancement of the surface as the developer removes photoresist from the surface. One of the first attempts was made by Robert Jewett using the String algorithm where the surface is approximated by a series of points joined by straight line segments forming a string. Each point advances along the angle bisector of the two adjoining segments according to the local value of the development or etch rate. Another popular method is the cellular automata based on a cellular material representation of the underlying geometry. This could be of two types the cell removal algorithm which can be very computation intensive hence slow. The other cellular method called the structuring algorithm introduced by Ernst Strasser et al is based on structuring and dilation and gets rid of the problems with the cell removal algorithm. Other methods such as the level set methods introduced by Stanley Osher and James Sethian based on solving a Hamilton Jacobi type equation for a level set function is also widely used. Fast marching algorithms using level set methods are highly efficient and accurate.

In this work we have used a simple volume removal algorithm to study the developing of the exposed photoresist. A cross section of the structure of the problem domain is shown in Figure A- 3. The volume of each cell V is updated during each time increment during

the simulation. The time increment is chosen such that it is small enough to consider the higher dissolution rate in the matrix. The developer is in contact with this cell if the cells around this cell have zero volume so that the developer has filled in. Thus the cell (i,j) is affected by the adjacent cells (i,j-1), (i,j+1), (i-1,j-1), (i-1,j), (i-1,j+1). The exposure is top down and hence we use this simple model and do not consider the cells below. In complex exposure techniques where structures are formed with the bulk this method will lead to looping problems and the more advanced models mentioned above have to be used.
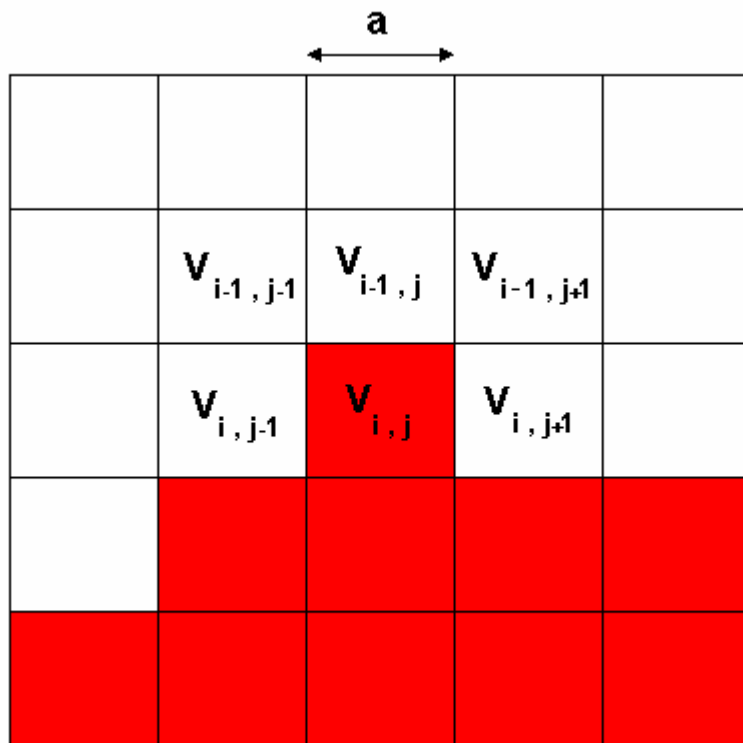
Figure A- 3 Volume removal algorithm showing cross section and interaction of cells

The dissolution time of each cell is given as,

$$t_{dis} = \frac{a}{r}$$ A.21

The incremental time for each cell is calculated as

$$t_{loop} = t_{top}(V_{i-1,j}) + t_{side}(V_{i,j-1} + V_{i,j+1}) + t_{diag}\left[\frac{V_{i-1,j-1} + V_{i-1,j+1}}{2}\right]$$ A.22

where ttop=tinc a/b and tside=tinc b/a ; tdiag = tinc(a/b+b/a)/4.

Now we update the time on each cell by considering the above increment on each cell. When the time equals tdis the volume is set to one. Otherwise the volume is a fraction of the actual time on each cell and the dissolution time needed for that cell. The loop is continued till the set develop time is reached to get the final volume of each of the cells. This will give us the final profile on the resist obtained by exposing a photoresist coated wafer through a mask on a projection system.

REFERENCES

1. M. Kufner and S. Kufner, Micro-Optics and Lithography Vub press, Belgium, 1997.

2. Hans Peter Herzig, "Micro-Optics, Elements, systems and applications", Taylor & Francis Inc, 1997.

3. Nicholas F Borelli, "Micro Optics Technology Fabrication and applications of lens arrays and devices", Optical Engineering Series, Marcel Dekker Inc, 1999.

4. "Diffractive Optics and Optical Microsystems", S. Martellucci and A.N. Chester, ed. Plenum Press, 1997.

5. K. Iga, Y. Kokubun, M. Oikawa, "Fundamentals of microoptics: Distributed index microlens and stacked planar optics", Academic Press Inc. 1984.

6. Jurgen Jahns, Karl-Heinz Brenner, "Microoptics: From Technology to Applications", Springer Series in Optical Sciences, 2004.

7. Manouchehr E. Motamedi, Ed., "MOEMS: Micro-Opto-Electro-Mechanical Systems", SPIE 2005.

8. Ming-Hsien Wu, George. M. Whitesides, "Fabrication of two dimensional arrays of microlenses and their applications in photolithography", J. Micromech. Microeng. Vol 12, 2002, pp. 747-758.

9. G. Poleshchuk, "Techniques for formation of the surface profile of diffractive optical elements", Optics and lasers in Engg. (Elsevier Science Ltd.), Vol 29, 1998, pp. 289-306.

10. W. B. Veldkamp, G. J. Swanson, "Developments in fabrication of binary optical elements", Proc. SPIE 437, 1983, pp 54-59.

11. M. B. Stern, "Fabricating Binary Optics: An overview of binary optics process technology", Conference on Binary Optics, NASA conference publication 3227, 1993, pp 153-166.

12. M. B. Stern, "Pattern transfer for diffractive and refractive microoptics", Microelectronic Engineering, Vol. 34, 1997, pp 299-319.

13. Chuck Wu, S. H. Lee, "General aspheric refractive micro-optics fabricated by optical lithography using a high energy beam sensitive glass gray-level mask", J. Vac. Sci. Tech. B, Vol 14, No. 6, Nov/Dec 1996, pp. 3730-3733.

14. W. Daeschner, P. Long, R. Stein, C. Wu, S. Lee, "One step lithography for mass production of multilevel diffractive optical elements using high energy beam sensitive (HEBS) glass grey-level mask", Proc. SPIE 2689, 1996, pp. 153-155.

15. Y. Oppliger, P. Sixt, J. M. Stauffer, J. M. Mayor, P. Regnault, G. Voirin, " One step 3D shaping using a gray tone mask for optical and microelectronic applications", Microelectronic Engg. Vol 23, 1994, pp 449-545.

16. T. J. Suleski, D. C. O'Shea, "Gray scale masks for diffractive optics fabrication: 1. Commercial slide imagers", Appl. Opt. Vol. 34, No. 32, Nov. 1995, pp 7507-7517.

17. D. C. O'Shea, W. S. Rockward, "Gray-scale masks for diffractive optics fabrication: II. Spatially filtered halftone screens", Appl. Opt. Vol. 34, No. 32, Nov. 1995, pp 7518-7526.

18. D. Purdy, "Fabrication of complex micro-optics components using photo-sculpting through halftone transmission masks", Pure Appl. Opt. Vol 3, pp 167-175

19. W. Henke, W. Hoppe H. J. Quenzer, P. Staudt-Fischbach, B. Wagner, "Simulation and experimental study of gray tone lithography for the fabrication of arbitrarily shaped surfaces", Proc. IEEE MEMS, Japan, 1994, pp 205-210.

20. Jinwon Sung, Mahesh Pitchumani, Jeremiah Brown, Heidi Hockel and Eric G Johnson, "Analog micro-optics fabrication by use of a binary phase grating mask", Proc. SPIE. Int. Soc. Opt. Eng. 5347, 62 (2004).

21. T. Fujita, H. Nishihara, J. Koyama, "Blazed gratings and Fresnel lenses fabricated by electron beam lithograph", Opt. Lett. Vol. 7, 1982, pp 578-580.

22. M. T. Gale, K. Knop, "The fabrication of fine lens arrays by laser beam writing", Proc. SPIE, Vol 398, 1983, pp. 347-535.

23. Andreas Schilling, hans Peter Herzig, Laurent Stauffer, Urs Vokinger, Markus Rossi, "Efficient beam shaping of linear, high power diode lasers by use of micro-optics", Applied Optics, Vol. 40, 2001, pp. 5852-5859.

24. C D Popovic, R A Sprague, and G A Neville Connell, "Techniques for monolithic fabrication of microlens arrays", Applied Optics, 27, 1988, pp 1281-1284

25. D Daly, R F Stevens, M C Hutley and N Davies, "The manufacture of microlens by melting photoresist", J Meas. Sci. Technology, Vol. 1, 1990, pp 759-766.

26. T. R. Jay, M.B. Stern, "Preshaping photoresist for refractive microlens fabrication", Optical Engg. Vol 33, 1994, pp. 3552-3555.

27. Ph Nussbaum, R. Volkel, H. P. Herzig, M. Eisner, S. Haselbeck, "Design, fabrication and testing of microlens arrays for sensors and microsystems", Pure Appl. Opt. Vol. 6, 1997, pp. 617-636.

28. Andreas Schilling, Roman Merz, Christian Ossmann, Hans Peter Herzig, "Surface profiles of reflow microlenses under the influence of surface tension and gravity", Optical Engineering, Vol. 39, 2000, pp. 2171-2176.

29. Yuh-Sheng Lin, Cheng-Tang Pan, Kun-Lung Lin, Shih-Chou Chen, Jauh-Jung Yang, Jei-Pin Yang, "Polymide as the pedestal of batch fabricated micro-ball lens and micro-mushroom array", Proc. IEEE MEMS, Switzerland, 2001, pp. 337-340.

30. U. Kohler, A. E. Guber, W. Bier, M. Heckele, "Fabrication of microlenses by plasmaless isotropic etching combined with plastic moulding", Sensors and Actuators A, Vol. 53, 1996, pp. 361-363.

31. Edgar Pawlowski, Herbert Engel, "Multilevel diffractive optical elements fabricated with a single amplitude-phase mask", Pure Applied Optics, Vol. 6, 1997, pp. 655-662.

32. D. W. de Lima Monteiro, O. Akhzar-Mehr, P. M. Sarro, G. Vdovin, "Single-mask microfabrication of aspherical optics using KOH anisotropic etching in Si", Optics Express, Vol. 11, 2003, pp. 2244-2252.

33. Man-Lyun Ha, Jae-Ho Kim, Sung-Ku Yeo, Young-Se Kwon, "An oxidized porous silicon (OPS) microlens implementation on thick OPS membrane for a silicon-based optoelectronic multichip module (OE-MCM)", IEEE. Photonics Tech. Letters, Vol. 16, No. 6, June 2004, pp. 1519-1521.

34. P. Merz, H. J. Quenzer, H. Brent, B. Wagner, M. Zoberbier, "A novel micromachining technology for structuring borosilicate glass substrates", IEEE. Proc. Conf. on Solid state sensors, actuators and Microsystems, 2003, pp. 258-261.

35. Bernard Kress, Patrick Meyrueis, "Digital Diffractive Optics: An introduction to planar diffractive optics and related technology", John Wiley and sons Ltd., 2000.

36. Victor A. Soifer, Ed. "Methods for computer design of diffractive optical elements", Wiley series in lasers and applications, 2002.

37. Fred M. Dickey, Scott C. Holswade, Ed., "Laser beam shaping: Theory and techniques", Marcel Dekker Inc., 2000.

38. Thomas Hessler, Markus Rossi, Rino E. Kunz, Michael T. Gale, "Analysis and optimization of fabrication of continuous relief diffractive optical elements", Applied Optics, Vol. 37, No. 19, July 1998, pp. 4069-4079.

39. W. B. Veldkamp, "Laser beam profile shaping with interlaced binary diffraction gratings", Applied Optics, Vol. 21., No. 17, September 1982, pp. 3209-3212.

40. E.G. Johnson, Jared Stack, and Charles Koehler, "Light Coupling by a Vortex Lens into Graded Index Fiber", Journal of Lightwave Technology, Vol. 19, No. 5, May 2001, pp. 753-758,

41. R. W. Gerchberg and W. O. Saxton, "A practical algorithm for the determination of the phase from image and diffraction plane pictures", Optik Vol. 35, No. 2, 1972, pp. 237-246.

42. Marc J. Madou, "Fundamental of Microfabrication, The science of miniaturization", CRC press, 2nd edition.

43. Mahesh Pitchumani, Heidi Hockel, Waleed Mohammed, Eric. G. Johnson, "Additive Lithography for fabrication of diffractive optics", Applied Optics, Vol. 41, No29, Oct 2002, pp.6176-6181

44. Mahesh Pitchumani, Jeremiah Brown, Waleed Mohammed, and Eric G. Johnson "Micro-Optic Fabrication using Sub-domain Masking", Applied Optics, Vol. 43 Issue 8 March 2004 pp 1676

45. Mahesh Pitchumani, Waleed Mohammed, Heidi Hockel Eric G Johnson, "Presculpting of photoresist using additive lithography", Proceedings of SPIE January 2004, Vol. 5347, p. 85-94

46. Mahesh Pitchumani, Heidi Hockel, Jinwon Sung, Waleed Mohammed, Laurent Vaissie, and Eric G Johnson, "Additive lithography for Micro-optics Fabrication", OSA Trends in Optics and Photonics (TOPS), Vol. 75,Diffractive Optics and Micro-optics, OSA Technical Digest, pp.158-160 June 2002

47. Mahesh Pitchumani, H Hockel, J. Brown, W. Mohammed, E. Johnson, "Additive lithography for refractive micro-optics", Proceedings of SPIE Volume: 4984, January 2003.

48. S. Traut, H. P. Herzig, "Holographically recorded gratings on microlenses for a miniaturized spectrometer array", Optical Engg, Vol 39, No. 1, Jan 2000, pp. 290-298.

49. Arthur W Adamson, "Physical Chemistry of Surfaces", John Wiley & Sons, 1982

50. W Neumann, Jan K Spelt, " Applied Surface Thermodynamics", Surfactant Science Series volume 63, Marcel Dekker Inc, 1996.

51. P.G.de Gennes, "Wetting: statics and dynamics", Rev. Mod. Phys., Vol. 57, No3, PartI, July 1985 pp 828-863.

52. S. Haselbeck, H. Schreiber, J. Schwider, N. Streibl, "Microlens fabricated by melting photoresist on a base layer," Opt Eng. 32(6), 1993, pp1322-1324.

53. L.Erdmann, D. Efferenn, "Technique for monolithic fabrication of silicon microlenses with selectable rim angles," Opt. Eng. 36(4), 1997, 1094-1098.

54. Ed. Dennis M Manos and Daniel L Flamm, "Plasma Etching : An introduction", Plasma Material Interactions, Academic Press Inc, 1989.

55. W.N.G. Hitchon, "Plasma processes for semiconductor fabrication", Cambridge studies in semiconductor physics and microelectronic engineering, Cambridge university press, 1999.

56. Michael Kohler, "Etching in microsystem tehnology", Wiley-VCH, 1999.

57. Shen Ronggui, Giancarlo C. Righini, "Characterization of reactive ion etching of glass and its applications in integrated optics", J. Vac. Sci. Tech. A, Vol. 9, No. 5, Sep/Oct 1991, pp. 2709-2712.

58. Ph. Nussbaum, K. J. Weible, M. Rossi, H. P. Herzig, "Potential of dry etching for the fabrication of fused silica micro-optical elements", SPIE Conference on Micromachine technology for diffractive and holographic optics, Vol. 3879, September 1999, pp. 63-70.

59. G. S. Oehrlein, Y. Zhang, D. Vender, O. Joubert, "Fluorocarbon high-density plasmas. II. Silicon dioxide and silicon etching using CF4 and CHF3", J. Vac. Sci. Tech. A, Vol. 12, No. 2, Mar/Apr 1994, pp. 333-344.

60. Deepak Bose, M. V. V. S. Rao, T. R. Govindan, M. Meyyappan, "Uncertainty and sensitivity analysis of gas-phase chemistry in a CHF3 plasma", Plasma sources science and technology, Vol. 12, April 2003, pp. 225-234.

61. James. R. Sheats, Bruce. W. Smith, Eds., "Microlithography Science and Technology", Marcel Dekker Inc., 1998.

62. Alfred Kwok Kit Wong, "Resolution Enhancement techniques in optical lithography", SPIE tutorial texts in optical Engineering, 2001.